Impairement Aware Network Planning

Venkata Virajit Garbhapu

INSTITUT POLYTECHNIQUE DE PARIS

NNT : 2024IPPAT026

Thèse de doctorat

Impairment Aware Optical Networks

Thèse de doctorat de l'Institut Polytechnique de Paris
préparée à Télécom Paris

École doctorale n°626 École doctorale de l'Institut Polytechnique de Paris (ED IP Paris)
Spécialité de doctorat : Information, communications, électronique

Thèse présentée et soutenue à Palaiseau, le 18/07/2024, par

VENKATA VIRAJIT GARBHAPU

Composition du Jury :

Christelle Aupetit-Berthelemot Professor, University of Limoges, Limoges, France	Présidente/Examinatrice
Christine Tremblay Professor, École de technologie supérieure	Rapporteur
Nicola Calabretta (absent) Professor, Technical University of Eindhoven	Rapporteur
Massimo Tornatore Professor, Politecnico di Milano, Milano, Italy	Examinateur
Nicolas Fabre Maître de Conférences, Télécom Paris, Palaiseau (LTCI)	Examinateur
Cédric WARE Professeur, Télécom Paris, Palaiseau (LTCI)	Directeur de thèse
Mounia Lourdiane Maître de Conférences, Télécom SudParis, Palaiseau	Co-directeur de thèse
Yvan Pointurier Optical Networking Research Team Leader, Huawei Technologies, Paris Research Center	Invité

Abstract

The exponential growth in global data traffic and the increasing demand for high-speed, reliable communication networks have pushed optical networks to their limits, resulting in a capacity crunch. Additionally, as consumers and businesses seek more secure and efficient networks, there is an urgent need to address the inherent challenges in managing energy consumption, reducing latency, and ensuring robust security. These twin challenges of capacity and security form the core of this thesis.

Expanding the capacity of optical networks traditionally involves deploying new fiber, upgrading transponders, or extending the spectrum to the S and L bands, all of which come at a significant cost. Instead, this thesis explores a cost-effective alternative: managing per-channel power levels in such a way that linear and dominant non-linear impairments are mitigated. We propose a per-channel power allocation to maximize the worst service's SNR network-wide or capacity. This technique, rooted in the Gaussian noise model but accounting for all transmission effects, is validated on a testbed with commercial, real-time equipment on an example tandem network. The proposed network-heuristics demonstrate enhancements in network capacity and reliability, ensuring high-quality transmission over longer distances and reducing capital expenditure.

Current SDN management tools and network planning tools often overlook the physical layer, making it vital to develop a network planning simulator that integrates these aspects. We developed a new optical network simulator, PyFIOA, that aims to take into account physical layer impairments and eventually handle future optical functionalities in a generic way. The simulator is designed to accurately evaluate the QoT by modeling precisely the physical degradations affecting the transmitted signals. The QoT encompasses physical layer impairments and is used in the RWA decision-making at the network level. Simulation results for network planning on different topologies show the impact of accurately evaluating physical impairments on traffic blocking probability compared to results obtained without the QoT input.

Building on the advantages of impairment aware network planning, the thesis also focuses on different optical functionalities that have struggled to transition from research labs to commercial deployment, such as optical packet switching, wavelength converter, etc. Demonstrating the impact of these functionalities could facilitate their integration.

Among the functionalities explored, the thesis highlights the integration of QKD, underscoring its potential to revolutionize data security while addressing compatibility challenges with existing infrastructure and potential impairments. We investigate the coexistence of classical and QKD channels. By accurately calculating the Raman noise affecting QKD and optimizing its wavelength placement, we can significantly reduces the blocking probability of WDM channels with minimal impact on the QKD SKR. This highlights the potential of integrating advanced security functionalities into existing optical networks.

Through this holistic approach, the research ensures that optical networks can meet future demands with enhanced performance, efficiency, and security.

Résumé

La croissance exponentielle du trafic de données mondial et la demande croissante de réseaux de communication fiables et à haute vitesse ont poussé les réseaux optiques à leurs limites, entraînant une saturation de la capacité. De plus, alors que les consommateurs et les entreprises recherchent des réseaux plus sécurisés et plus efficaces, il est urgent de relever les défis inhérents à la gestion de la consommation d'énergie, à la réduction de la latence et à la garantie d'une sécurité robuste. Ces deux défis, capacité et sécurité, constituent le cœur de cette thèse.

L'expansion de la capacité des réseaux optiques implique traditionnellement le déploiement de nouvelles fibres, la mise à niveau des répéteurs ou l'extension du spectre aux bandes S et L, ce qui a un coût important. Au lieu de cela, cette thèse explore une alternative rentable : gérer les niveaux de puissance par voie de manière à atténuer les dégradations linéaires et non linéaires dominantes. Nous proposons une allocation de puissance par canal pour maximiser la capacité SNR du pire service à l'échelle du réseau ou de la capacité. Cette technique, ancrée dans le modèle de bruit gaussien mais prenant en compte tous les effets de transmission, est validée sur une plateforme d'essai avec du matériel commercial en temps réel sur un réseau tandem d'exemple. Les heuristiques de réseau proposées démontrent des améliorations de la capacité et de la fiabilité du réseau, garantissant une transmission de haute qualité sur de plus longues distances et réduisant les dépenses en capital.

La gestion optimale de la puissance par voie permet d'exploiter pleinement les ressources existantes tout en minimisant les coûts associés à l'expansion du réseau, offrant ainsi une alternative plus durable à l'ajout de nouvelles fibres ou à la mise à niveau du matériel. L'utilisation d'une allocation de puissance différenciée par canal, axée sur l'optimisation de la SNR du pire service, permet d'équilibrer les performances globales du réseau, garantissant ainsi une transmission de données plus fiable et plus efficace, même sur des distances plus longues. En intégrant cette technique dans les réseaux commerciaux actuels, les opérateurs peuvent tirer parti des infrastructures existantes tout en améliorant leur efficacité, ce qui est crucial dans un contexte où les besoins en bande passante augmentent exponentiellement.

Les outils de gestion SDN et les outils de planification de réseau actuels négligent

souvent la couche physique, d'où la nécessité de développer un simulateur de planification de réseau qui intègre ces aspects. Nous avons développé un nouveau simulateur de réseau optique, PyFIOA, qui vise à prendre en compte les dégradations de la couche physique et à terme gérer les futures fonctionnalités optiques de manière générique. Le simulateur est conçu pour évaluer avec précision la qualité de service en modélisant précisément les dégradations physiques affectant les signaux transmis. La QoT (Quality of Transmission) englobe les défaillances de la couche physique et est utilisée dans la prise de décision RWA (Routing and Wavelength Assignment) au niveau du réseau. Les résultats de simulation pour la planification du réseau sur différentes topologies montrent l'impact de l'évaluation précise des dégradations physiques sur la probabilité de blocage du trafic par rapport aux résultats obtenus sans l'entrée QoT.

Le simulateur PyFIOA développé dans cette thèse offre un outil puissant pour modéliser et prédire l'impact des dégradations physiques sur la qualité de service des réseaux optiques. Ce simulateur se distingue des outils de planification de réseau conventionnels en intégrant une évaluation précise des dégradations physiques, notamment les effets de dispersion, de diffusion non linéaire et les bruits qui affectent la transmission des signaux. En améliorant la précision de la planification RWA, PyFIOA permet de réduire les probabilités de blocage des services, contribuant ainsi à une meilleure utilisation des ressources réseau. L'implémentation de ce simulateur dans des scénarios réels a permis de valider son efficacité et son potentiel à devenir un outil clé dans la gestion des réseaux optiques du futur, particulièrement dans des contextes où la haute fiabilité et la performance sont essentielles.

S'appuyant sur les avantages de la planification de réseau sensible aux défaillances, la thèse se concentre également sur différentes fonctionnalités optiques qui ont eu du mal à passer des laboratoires de recherche au déploiement commercial, telles que la commutation optique de paquets, le convertisseur de longueur d'onde, etc. Démontrer l'impact de ces fonctionnalités pourrait faciliter leur intégration dans les réseaux commerciaux. En particulier, l'intégration de la QKD (Quantum Key Distribution) est soulignée comme une solution de sécurité prometteuse, capable de révolutionner la protection des données dans les réseaux de communication.

Enfin, la coexistence des technologies classiques et de QKD dans un même réseau optique ouvre la voie à une sécurité des données sans précédent, tout en préservant la compatibilité avec les infrastructures actuelles. L'analyse approfondie des interactions entre les canaux WDM et QKD, notamment par l'optimisation de la longueur d'onde et la réduction du bruit Raman, démontre que ces deux technologies peuvent coexister sans altérer significativement les performances globales du réseau. Cette approche favorise non seulement une sécurité accrue, mais elle jette aussi les bases d'une intégration harmonieuse des innovations futures dans les réseaux de communication optiques. En combinant des

avancées technologiques en matière de gestion de la capacité, d'efficacité énergétique et de sécurité, cette thèse propose des solutions concrètes pour les réseaux de demain, répondant aux besoins croissants des consommateurs tout en anticipant les défis futurs.

Grâce à cette approche holistique, la recherche garantit que les réseaux optiques peuvent répondre aux demandes futures avec des performances, une efficacité et une sécurité améliorées.

Dedicated to those who guide and inspire us—like light through optical networks, leading the way through darkness towards discovery

Acknowledgements

First and foremost, my profound gratitude goes to Prof. Cedric Ware, my thesis director and main supervisor. His unparalleled guidance, wisdom, and patience have been pivotal in sculpting both this thesis and my growth as a researcher. I am equally thankful to my co-supervisor, Dr Mounia Lourdiane, whose insightful feedback and support have been invaluable.

My appreciation extends to my industrial co-supervisors from Huawei— Dr. Yvan Pointurier, Dr. Alessio Ferrari and Dr. Gabriel Charlet. Their industry insights and collaborative spirit have been crucial in bridging the gap between academia and the practical field, enriching my research significantly.

A special acknowledgment to my mother, whose endless love, support, and belief in me have been my cornerstone. Her sacrifices and encouragement are the bedrock of my perseverance. Equally, I am indebted to my wife Meghana, for her steadfast faith in me.

Finally, my gratitude to Prof Massimo Tornatore for enriching my academic journey and personal development. His guidance and enlightening discussions have not only shaped my research but also fortified my resolve in the field of optical networks.

I extend my sincere appreciation to the reviewers, reporters, and examiners of this thesis for their critical insights and constructive critiques. Their thorough evaluations and thoughtful feedback have significantly contributed to the refinement and depth of this research. Their expertise and dedication to academic excellence have not only challenged me to elevate my work but have also been instrumental in guiding this thesis to its fruition.

Contents

List of Figures

List of Tables

Acronyms

B92 Bennett 1992 (a QKD protocol)

BB84 Bennett-Brassard 1984 (a QKD protocol)

BBM92 Bennett-Brassard-Mermin 1992 (a QKD protocol)

BtB Back-to-back

CAPEX capital expenditure

CD chromatic dispersion

COW Coherent One-Way (a QKD protocol)

CV-QKD Continuous Variable Quantum Key Distribution

DKRT-RKA Distributed Key Resource Time-Resource Key Assignment

DP-16QAM Dual-Polarization 16-Quadrature Amplitude Modulation

DP-QPSK Dual-Polarization Quadrature Phase Shift Keying

DPR-QKD Distributed Phase Reference Quantum Key Distribution

DPS Decoy-State Protocol (a QKD protocol)

DSKRT-SM Dynamic Secret Key Recycling and Time-Resource Management

DSP digital signal processing

DV-QKD Discrete Variable Quantum Key Distribution

DWDM Dense Wavelength Division Multiplexing

E91 Ekert 1991 (a QKD protocol)

EDFA Erbium Doped Fiber Amplification

EGN Enhanced Generalized Nonlinearity

EON Elastic Optical Networks

FOA Fiber optic amplifier

FWM Four Wave Mixing

GMCS Gaussian-Modulated Coherent States

GN Generalized Nonlinearity

GNPy Generalized Nonlinear Propagation Python Library

HR/LR High raman/ low raman

ILP Integer Linear Programming

IPTV Internet Protocol Television

ISI Inter-Symbol Interference

ISRS-GN Impulse Scattering Raman Spectral-Global Noise

ITUR International Telecommunication Union Radiocommunication Sector

KRT-RKA Key Resource Time-Resource Key Assignment

LI/nLI Linear / nonLinera impairments

LOGO Local Optimum Global Optimum

MMF multi-mode fibers

MRN Multicast Routing Node

NFV Network Function Virtualization

NLT Non-Linear Threshold

NMS network managements systems

OA Optical Amplifier

OEO optical-to-electrical-to-optical

OFs Optical Functionalities

OMS Optical multiplexing section

ONC Optical Network Capacity

ONs Optical Networks

OOK On-Off shift keying

OPEX operational expenditure

OPS optical packet switching

OSA Optical Spectrum Analyzer

OSaaS Optical Spectrum as a Service

OSNR Optical Signal to Noise Ratio

OTU Optical Termination Unit

PASE Amplifier Spontaneous Emission Noise Power

PDL Polarization dependent loss

PIC Photonic integrated circuits

PICh Public Information Channel

PMD Polarization mode dispersion

PNLI Nonlinear Noise Power

PON Passive Optical Network

pre-FEC BER pre-Forward Error Correction Bit Error Rate

PSCF Polarization-Sensitive Correlated Fiber

PyFIOA Python Fiber Impairment & Optical Analysis

QAWA Quantum Aware Wavelength Assignment (not in acrnm list but used in dov)

QKD Quantum Key Distribution

QoS quality of service

QoT Quality of Transmission

QSCh Quantum Signal Channel

RN Raman noise

RNM Raman noise model

ROADM Reconfigurable Optical Add-Drop Multiplexers

RSA Raman spontaneous absorption

RWA Routing and Wavelength Assignemnt

RWFA Routing and Wavelength/Fiber Allocation (not in the acrnm list but used in doc)

RWTA routing and wavelength time assignment

SARG04 Scarani-Acín-Ribordy-Gisin 2004 (a QKD protocol)

SBPP Secret Key Blockage Probability Protocol

SDM space division multiplexing

SDN Software-defined networking

SKFM Secret Key Failure Model

SKR Secure Key Rate

SMF single mode fibre (not in acrnm list but used in document)

SNR Signal to Noise Ratio

SNRB2B Back-to-Back Signal-to-Noise Ratio

SNRLin Linear Signal-to-Noise Ratio

SNRNL Non-Linear Signal-to-Noise Ratio

SNRo Back-to-Back Signal-to-Noise Ratio

SNU Shot Noise Units

SPM Self-Phase Modulation

SpRS Spontaneous Raman Scattering

SRS Stimulated Raman Scattering

SSMF Standard Single-Mode Fiber

SSP Six-State Protocol (a QKD protocol)

Tbps Terabits per second

VOA Variable Optical Attenuator

WC wavelength converters

WDM Wavelength Division Multiplexing

WSS Wavelength Selective Switch

x-QAM Various levels of Quadrature Amplitude Modulation

XPM Cross-Phase Modulation

Introduction

Optical networks have played a crucial part in enabling the global communication revolution that has brought the planet together, enabled rising nations to join the digital world economy, and enhanced people's quality of life all over the world. They are seen as the foundation of the future internet, particularly with applications like as Internet Protocol Television (IPTV), video on demand, cloud computing, and grid computing.

This sustained increase in the information bandwidth achieved on a single fiber is a result of continuous device invention and system innovation and introductions of new technologies. An excellent example is the invention and development of the fiber optic amplifier that, together with wavelength multiplexing technologies, enabled the cost-effective commercialization of wavelength division multiplexed transmission. Innovation of wavelength add/drop, and optical cross-connects systems together with automated control software subsequently enabled fully reconfigurable optical networks. That enables flexible bandwidth management and restoration capability in today's global networks.

Nowadays, optical fiber networks form the physical infrastructure of the access, metro and core networks. This induces an increase in optical network capacity while ensuring that existing end-user services become more cost-effective. Aside from addressing capacity requirements, consumers want secure, low-latency, and energy consumption optimized optical networks. These requirements have prompted the research community to address several issues in parallel. One critical area is overcoming the constraints and limits imposed by the optical physical layer and its new functionalities, while another key focus is the optimization of network performance.

The growth in the demand for high data rates has led to a capacity crunch [1]. To meet this demand, rather than solely increasing the capacity on a single fiber, one could deploy multiple parallel fiber transmission systems as in Spatial Division Multiplexing (SDM) or extend the spectrum by using additional bands such as O, E, S, and L bands as in multiband transmissions in addition to the conventional C band. SDM and multiband transmissions are viewed as contemporary approaches to increase the capacity, but more commercial solutions have been developed and realised for the multiband transmissions [2, 3]. However, these approaches come with significant costs (4 times more than the C Band), including the need for new equipment such as different band Reconfigurable Add-Drop Mul-

tiplexer (ROADM), amplifiers, and the fibers themselves as studied in [4]. Consequently, the network cost would grow roughly at the same rate as capacity. Until fairly recently, the approach was based on increasing the number of wavelength division multiplexing channels, creating Dense Wavelength Division Multiplexing (DWDM), and using higher bit rates. However, more complex modulation formats, while increasing spectral efficiency, also require higher power levels for transmission. This higher power consumption makes the transmission more sensitive to impairments such as noise and non-linear effects, significantly impacting the transmission reach and quality. Therefore, optimizing the power for different modulation formats becomes crucial. It has been shown that a remarkable saving in capital expenditure (CAPEX) can be obtained by power optimization for different modulation formats [5] while using the DWDM systems. By managing the power levels effectively, one can minimize the negative impacts of these impairments, thus maintaining high-quality transmission over longer distances and reducing overall costs.

As mentioned earlier, the challenges of the ever-growing traffic in optical networks are not only limited to capacity but also include the management of energy consumption and the ability to handle new functionalities without imposing changes to the existing optical infrastructure. Traditionally, networks operated in an opaque mode using optical-electrical-optical (OEO) signal conversion to improve signal quality (signal regeneration 3R) or to switch the path to the destination. However, the development of all-optical amplifiers and all-optical switching aimed to create transparent optical networks in which the signal is maintained in the optical domain, thereby lowering both CAPEX and operational expenditure (OPEX) [6].

Many optical functionalities are currently being explored in research labs such as space division multiplexing, optical packet switching, etc. Optical packet switching, for instance, allows for more efficient handling of data by enabling the network to dynamically route packets based on current network conditions, thereby improving bandwidth utilization and reducing latency. However, the commercialization of optical packet switching is not yet fully realized due to various technical and operational challenges. These innovations hold promise, but their integration into existing networks poses challenges, particularly regarding their seamless operation alongside established infrastructure.

One critical area of focus for new optical functionalities is security. Quantum Key Distribution (QKD) is an emerging technology that leverages the principles of quantum mechanics to provide unprecedented security for data transmission. Integrating QKD into optical networks offers significant advantages in terms of security but also presents challenges in terms of potential impairments and compatibility with existing infrastructure. If the impacts of integrating such advanced functionalities are not thoroughly studied and addressed, their commercialization could be significantly delayed, as has been the case with other optical functionalities. Therefore, a comprehensive understanding and

mitigation of these impacts are crucial for the timely and effective deployment of new optical functionalities, ensuring they enhance network performance without introducing additional complexities or costs.

To encapsulate, the future of optical networks entails strategies that reduce CAPEX and OPEX by

1. Implementing per-channel power optimization techniques that enhance the capacity of DWDM optical networks and make them more reliable by efficient use of network resources.

2. Studying the impact of new optical functionalities to reduce end-to-end latency, energy consumption, spectral occupancy, and to increase security.

Thesis Contributions

The core of this thesis focuses on advancing impairment-aware network planning, which is essential for the efficient operation of future optical networks. By understanding and mitigating physical layer impairments, it is possible to design and operate network and control plane functionalities that do not disrupt the data layer. This holistic approach ensures that advancements in network technologies and functionalities are seamlessly integrated, maintaining the reliability and performance of optical networks. This approach involves:

- Detailed modeling of physical layer impairments: Accurate modeling of impairments such as noise, non-linear effects, and dispersion is crucial. Understanding these impairments allows for the development of techniques to counteract them, ensuring that network performance is optimized.

- Integration with network and control plane operations: By incorporating physical layer awareness into network or control plane operations, it is possible to make informed decisions about routing, wavelength assignment, and power levels. This integration ensures that changes at the network or control plane do not adversely impact the data layer.

- Adaptive and predictive optimization techniques: Implementing adaptive techniques that respond to real-time network conditions and predictive models that anticipate future impairments can significantly enhance network resilience and efficiency. For example, power optimization algorithms can adjust the transmission power in response to varying network conditions, dynamically mitigating the effects of impairments.

- Enhancing network reliability and security: Incorporating advanced functionalities like QKD within an impairment-aware framework ensures that these new technologies

are deployed without compromising the network's capacity. This approach not only enhances security but also maintains the overall performance and reliability of the network.

In summary, impairment-aware network planning is about creating a synergy between understanding physical impairments and optimizing network operations. By doing so, it ensures that optical networks can meet the growing demands for higher data rates, enhanced security, and advanced functionalities while maintaining robust and reliable performance.

The specific contributions of this thesis towards these goals are detailed in the following chapters.

Chapter Organization

Chapter 1 sets the foundation by introducing optical networks and their significance in global communication. It covers the theoretical background of impairments in the physical layer (data plane) and discusses the network functionalities at the control plane essential for network planning activities.

In Chapter 2, we propose per-channel power optimization techniques that account for both linear and non-linear impairments in scenarios involving multi-modulation formats and flexible grids. These algorithms aim to either increase the overall network capacity or enhance the performance of the worst-performing channels. While this work primarily focuses on tandem networks, it can be extended to more complex network structures. Additionally, we develop network-wide heuristics that are impairment-aware, addressing both linear and non-linear impairments. This research, conducted at the Huawei Paris Research Center, showcases the design of optimum launch power algorithms to enhance network capacity and reliability without increasing the CAPEX.

Chapter 3 details the development of a network planning simulator that includes all physical layer impairments and optimization techniques for routing and wavelength allocation. The simulator is designed to easily integrate new optical functionalities and study their impacts quickly.

In Chapter 4, QKD is introduced as an advanced optical functionality aimed at enhancing network security. After theoretically modeling QKD, we investigate its coexistence with classical optical channels. A key focus of this chapter is the accurate calculation of Raman noise, which can significantly affect QKD performance. Raman scattering, a nonlinear effect where optical power from classical channels is transferred to QKD channels, introduces noise that can degrade the quantum signals, particularly because QKD relies on single photons or weak coherent states that are highly susceptible to even minimal noise levels. The impact of Raman noise on QKD channels is particularly critical when compared to other impairments like loss, polarization effects, chromatic dispersion, and other

nonlinear effects. While optical loss and chromatic dispersion generally reduce the overall signal strength and can cause temporal spreading of the quantum signal, they do not introduce additional noise into the quantum channel in the same direct manner as Raman scattering. Nonlinear effects like Four-Wave Mixing (FWM) and Cross-Phase Modulation (XPM) also impact QKD channels, primarily by causing crosstalk and phase noise. While these non-linear effects can not be completely eliminated, it can be reduced through the use of advanced filtering techniques [7]. Given its significant impact [8], mitigating Raman scattering through optimized wavelength placement of QKD channels within WDM systems is crucial.

We propose a network-wide heuristic for wavelength assignment that can significantly reduce the blocking probability of WDM channels while maintaining minimal impact on the QKD channels. This study provides critical insights into the integration challenges and practical solutions for incorporating QKD into existing optical networks, ensuring enhanced security without compromising network capacity and performance.

This work has been conducted at Télécom Paris, focusing on realizing optical functionalities that have not yet been materialized outside research labs. The main goal is to develop a practical impairment-aware optical network simulator that can add and evaluate these optical functionalities, providing insights and suitable abstractions for real-time implementation in networks.

Finally, the general conclusion summarizes the key findings of the thesis, highlighting the advancements made in impairment-aware network planning, per-channel power optimization, and the integration of advanced optical functionalities such as QKD. Additionally, this section identifies potential perspectives for future research that involve continued integration of emerging technologies to address evolving network demands and challenges.

List of Publications

The work presented in this manuscript has led to 4 conference publications and 1 workshop poster.

Conferences

1. V. V. Garbhapu, C. Ware and M. Lourdiane, "Minimal Impact Network-Wide Heuristics for the Coexistence of Classical and CV-QKD Signals in the C-Band," 2024 European Conference on Optical Communication (ECOC), Frankfurt, Germany.

2. V. V. Garbhapu, C. Ware and M. Lourdiane, "Physical-layer-aware network simulator for future optical functionalities," 2023 14th International Conference on Network of the Future (NoF), Izmir, Turkiye, 2023, pp. 28-36, doi: 10.1109/NoF58724.2023.10302753.

3. A. Ferrari, V. V. Garbhapu, D. L. Gac, I. F. de Jauregui Ruiz, G. Charlet and Y. Pointurier, "Demonstration of AI-Light: an Automation Framework to Optimize the Channel Powers Leveraging a Digital Twin," 2022 Optical Fiber Communications Conference and Exhibition (OFC), San Diego, CA, USA, 2022, pp. 1-3.

4. V. V. Garbhapu, A. Ferrari, I. F. de Jauregui Ruiz, D. Le Gac, G. Charlet and Y. Pointurier, "Network-Wide SNR-based Channel Power Optimization," 2021 European Conference on Optical Communication (ECOC), Bordeaux, France, 2021, pp. 1-4, doi: 10.1109/ECOC52684.2021.9605942.

Poster

1. V. V. Garbhapu, C. Ware and M. Lourdiane, "Network-Wide Heuristics for the Coexistence of Classical and CV-QKD Signals in the C-Band," Quantum Secure Networks Partnership (QSNP) General Assembly. 6 June 2024. ICFO, Castelldefels, Spain.

CHAPTER 1

General Introduction to Optical Networks

1.1 Organization of an optical network

Optical networks, often unrecognized yet pivotal in our digital era, have transformed global communications through a robust and unseen lattice of light. This network seamlessly links continents together, fostering a surge in technological breakthroughs. Serving as the backbone of the internet, these networks facilitate the swift flow of extensive data, propelling human advancement and molding our way of living, working, and interacting in the modern world. According to TeleGeography, the worldwide internet bandwidth reached 1217 Tbps in 2024, witnessing a compound annual growth rate of 59% from 2018 to 2024 [9]. Furthermore, Erricson anticipates that by 2029, the global internet traffic will exceed 313 Exabytes monthly [10].

To support the escalating demands for data transmission and keep in stride with emerging innovations like the Internet of Everything, ONs must undergo constant enhancements. Since their initial commercial deployment in the late 20th century, the volume of data these networks need to handle has increased exponentially, surpassing a growth of four orders of magnitude in transmission system capacity, and three orders in switching capacity [11]. ONs are categorized into access, metro, and core segments, each distinguished by their reach, capacity, equipment complexity, etc. Continuous updates in these segments are crucial to boost bitrates for users, as evidenced by GFiber's recent achievement of offering download speeds up to 2 Gbps during 2021 and pushing towards 20.2 Gbps in the near future [12].

As shown in Fig. 1.1, the ONs can be represented by a data plane and a control plane. The optical data plane forwards traffic in the form of optical circuits or lightpaths. Hence the data plane as shown in Fig. 1.1 comprises of the active and passive elements. With the evolution of WDM technology and EDFA, the capacity and the reliability of long-haul transmissions have improved dramatically. This has been sustained by different technological advancements in the data plane such as

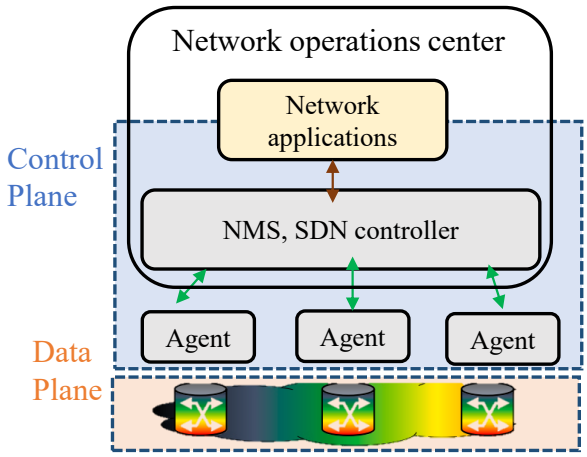

Figure 1.1: Optical Network Infrastructure Overview: Data Plane & Control Plane [13]

1. Fiber Technology: Low-loss optical fibers have enabled high-speed, long-distance data transmission.

2. Ultra-Wide band WDM: Expands on the traditional WDM concept by using a wider portion of the optical spectrum to accommodate more wavelength channels, leading to an increased overall network capacity [14].

3. Complex Modulation and Coherent Detection: Improving the modulations formats from OOK to advanced ones, such as QPSK, x-QAM [15] and probabilistic shaping constellation modulations, increases the number of symbols being transmitted. Coherent detection has enabled the use of advanced modulation formats and DSP techniques for better network performance.

4. Photonic Devices and Integration: Device-level photonic improvements have enhanced performance, efficiency, and miniaturization of ONs equipments through developments in lasers, modulators, and detectors. PICs have integrated multiple photonic components onto a single chip for improved performance, reduced size, and lower power consumption [16].

In addition to that, there are multiple emerging technologies, such as SDM and MMF, to further improve the network capacity.

The control plane governs the data plane elements (Fig. 1.1). It includes software agents, embedded in the optical elements that exchange messages with NMS and SDN controllers running in the network operations center. The exchanges between these controllers dictate the data plane behaviour.

Over the years, the control plane, much like the data plane, has seen numerous technological advancements. These innovations have significantly transformed the perception of

optical communications, shifting away from the outdated view of them as mere 'dumb optical pipes'. Concepts such as SDN and NFV have brought programmability and flexibility to optical networks, enabling more efficient network management and resource allocation [17].

1.2 Data Plane

The data plane, also known as the forwarding plane, is a critical component of optical networks responsible for the actual transmission of data packets between nodes. It encompasses all the elements and technologies that handle the direct flow of user data through the network. In optical networks, this includes the physical transmission of light signals across optical fibers, the multiplexing and demultiplexing of wavelengths, and the amplification and switching of optical signals.

Having pointed out the significant advancements in the data plane, including the introduction of cutting-edge fiber technology, ultra-wideband WDM, and sophisticated modulation schemes, we now consider the practical implementation of these technologies within the framework of typical WDM links. WDM stands as a cornerstone of modern optical networking, enabling the simultaneous transmission of multiple data channels over a single optical fiber. This multiplexing capability not only maximizes the efficiency and capacity of the optical data plane but also introduces complexities in design and operation that demand detailed examination. The following section delves into the typical elements of a WDM link, including the Optical Multiplexing Section (OMS), to provide a comprehensive understanding of how these technologies are applied in practice. We will also explore the critical role of SNR calculations in ensuring the reliability and performance of these links, thereby highlighting the intricate interplay between technological advancements and the practical challenges of their implementation.

1.2.1 Theoretical background

A typical WDM system consists of multiple optical components, such as the Optical Termination Unit (OTU), Multiplexer/ Demultiplexer (MUX/DMUX), Wavelength Selective Switch (WSS), Variable Optical Attenuator (VOA), Optical Amplifier (OA), and long distance fibers, as shown in Fig. 1.2. A single optical segment between two WSS is often called an OMS.

With the continuous need for more data transmission, optical networks become increasingly complex, and the number of wavelengths keep reaching the limits of the available spectrum. Therefore, it is more and more challenging to ensure the quality performance of WDM systems. The performance of an optical signal determines the maximum transmission distance over a given route, influencing the type and amount of equipment required

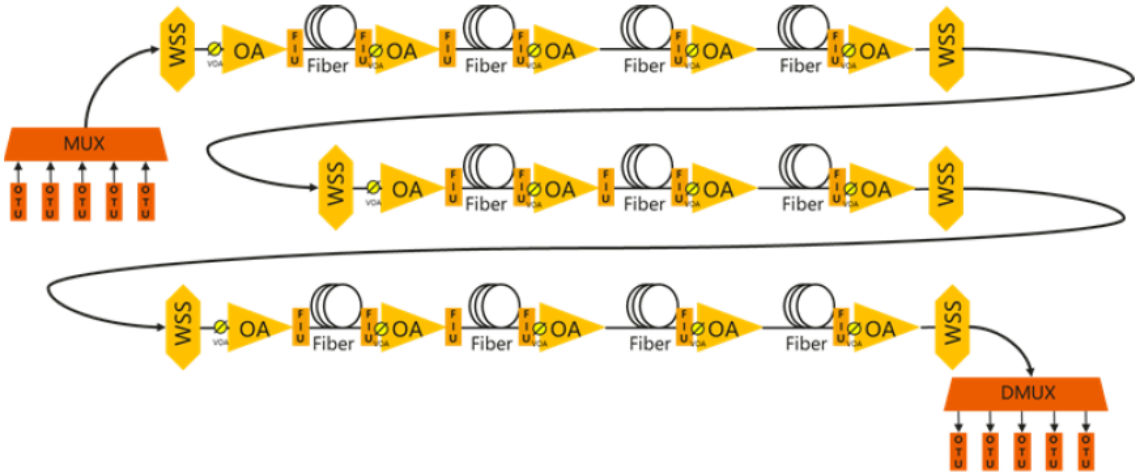

Figure 1.2: Typical WDM optical Point-to-Point link

in the network, such as optical amplifiers or regenerators. In a WDM network, multiple optical signals are transmitted over the same fiber. For instance, consider two wavelengths in a transmission network that traverse the same route, use the same coding modulation format, and are received by the same receiver. Despite these similarities, these optical signals might not perform identically. This discrepancy can be attributed to various factors such as the ripples in optical amplifiers like EDFAs and non-linear effects such as SRS.

Ripples in optical amplifiers, particularly in EDFAs, refer to small variations in the gain spectrum of the amplifier. These gain ripples are caused by the uneven spectral response of the amplifier's components, such as the erbium-doped fiber and the wavelength-dependent losses within the amplifier. The physical phenomenon causing these ripples includes the inhomogeneous broadening of the erbium ions' energy levels and the interference effects within the optical cavity of the amplifier. In our simulations, these ripples are accounted for by collecting experimental data on the gains and noise figures of the EDFAs and mapping this data into our simulator models. This approach ensures that the experimental characteristics of the amplifiers are accurately reflected in the simulations, providing a realistic representation of their performance.

Theoretically, to mitigate the impact of gain ripples, gain flattening filters are often employed in practical systems. These filters are designed to equalize the gain across the amplifier's bandwidth, thereby ensuring more uniform amplification of all wavelengths. Additionally, the heuristic strategies discussed later in this thesis consider these gain variations to ensure robust and reliable network performance.

Understanding the varying performance of optical signals within a WDM network underscores the necessity of meticulous performance measurement and management. Among the various metrics that can be employed to gauge the quality and integrity of optical signals, the Signal-to-Noise Ratio stands out as a critical indicator. SNR not only reflects

the clarity and quality of the signal by comparing the level of the desired signal to the level of background noise but also directly influences the network's data transmission capabilities and reliability. By rigorously measuring and analyzing the SNR of each wavelength, network engineers can pinpoint discrepancies in signal quality that may necessitate equalization. This precise identification and subsequent adjustment ensure that all channels perform optimally, thereby maximizing the overall efficiency and capacity of the WDM network. Thus, the measurement of SNR becomes a foundational step towards achieving uniform signal performance across the network, facilitating the identification of underperforming channels that require intervention to maintain the network's integrity and service quality.

Table 1.1 analyzes the different penalties and these factors together determine the SNR value. The most important factors that affect the WDM system performance are:

- OSNR: With other conditions unchanged, a higher OSNR at the receiver generally leads to better transmission performance. The OSNR is predominantly influenced by the amplified spontaneous emission (ASE) noise introduced by optical amplifiers. ASE noise is typically the dominant noise source in long-haul and amplified systems, as it accumulates with each amplification stage, degrading the signal quality. However, the OSNR is also affected by wavelength-dependent nonlinear interference (NLI) factors, which become increasingly significant in dense WDM systems with high power levels and closely spaced channels. In scenarios where the system operates near the nonlinear regime, NLI can significantly contribute to the overall noise, competing with or even surpassing ASE noise, particularly in the presence of strong co-propagating signals as in a typical WDM systems. Hence the quest to increase the OSNR by increasing the powers might result in a worse NLI.

- Other Factors: The performance of the WDM system is also influenced by back-to-back (BtB) transponder tolerance, fiber nonlinear penalties (NLI), filtering penalties, polarization dependent loss (PDL) penalties, chromatic dispersion (CD) penalties, and polarization mode dispersion (PMD) penalties. Among these, fiber nonlinear penalties (NLI) are especially important in high-power, long-distance, or densely packed WDM systems. NLI becomes more prominent in such contexts, as the interaction between multiple channels can lead to effects like Four-Wave Mixing (FWM) and Cross-Phase Modulation (XPM), which degrade the signal quality. On the other hand, ASE noise tends to dominate in systems with multiple amplification stages, especially when the channel power is low to moderate, as the cumulative effect of ASE can overshadow the nonlinear effects. In practical systems, the relative impact of NLI and ASE is often a trade-off: as channel power increases to improve OSNR, NLI becomes more significant, requiring careful balance to optimize overall system

Table 1.1: Factors affecting the WDM system performance

Factor	Impact (Coherent System)	Source of Influence	Description
OSNR	Top 1	ASE noise of the OA	Result of the noise generated by OAs, a major contributor to limiting the transmission distance of a WDM system
Transponder BtB tolerance	Top 2	Transmit coding and modulation rate, and receiving mode	Optimizes coded modulation at the transmit end and reduces the BtB OSNR tolerance by using coherent reception, digital signal processing equalization, etc.
Nonlinearity	Top 3	Line transmission optic fiber	The power of the signal is affected by all the co-propagating signals. If the incident optical power is designed within a proper range it will reserve a certain SNR margin
PDL	Top 4	Optical Components	Cannot be ajusted. A certain SNR margin should be reserved
Optical filtering	Top 5	MUX/DMUX/WSS	The filter bandwidth should be optimized and a certain SNR margin should be reserved
CD	None	Line transmission optical fiber	Fully compensated by the DSP
PMD	None	Line transmission optical fiber	Fully compensated by the DSP

performance.

While evaluating the SNR at the receiver end of the optical channel the top 3 penalties contributions are summed up as follows [18]:

$$\frac{1}{SNR} = \frac{1}{OSNR} + \frac{1}{SNR_{BtB}} + \frac{1}{SNR_{NL}} \tag{1.1}$$

Many efforts have been made to estimate correctly the SNR [19]. Fast and accurate closed-form models derived from the Gaussian Noise (GN) model and its enhanced version (EGN), were proposed and used in building QoT models such as GNPy developed by V. Curri in [20]. Assuming P_{sig} is the lightpath's launch power and P_{ASE} is the accumulated ASE noise originating from the amplifiers. It can be calculated as the cumulative sum of all the amplifiers (number of fiber spans (n) +1) the lightpath traverses as shown in Eq (1.2) obtained from [21]. Each amplifier is characterized by its noise figure (NF), its gain (G), and output power (P) profile. h is the Planck's constant, f is the optical frequency of the lightpath (determined by its wavelength) and B being the resolution bandwidth of the ASE measurement.

$$\frac{1}{OSNR} = \sum_{i=1}^{n+1} \frac{hf(G_i - 1)NF_iB}{P_i} \tag{1.2}$$

Power evolution along the OMS i.e., P_i can be computed to include Inter-channel Stimulated Raman Scattering (ISRS) effect along the fiber by solving the continuous-wave Raman equations using the triangular approximation proposed in [22] in addition to the fiber loss and compensating amplifier's gain. The lightpath's non-linear noise power SNR_{NL} at the end of each OMS is dependent on the channel frequency and is calculated as a sum of the SPM and XPM effects that include the impact of the powers of the M co-propagating signals on the OMS as done by the authors in [23].

$$\frac{1}{SNR_{NL}} = \sum_{j=1}^{M} (\eta_{SPM} + \eta_{XPM})_j P_J^2 \tag{1.3}$$

Now from Eq (1.2) and Eq (1.3) we can compute the OSNR (linear) and the non-linear components of the lightpath's SNR for each OMS. When calculating the total SNR for a lightpath that crosses various OMSs, we must aggregate both the linear and non-linear components of the SNR from each OMS. Additionally, the BtB SNR, derived from experimental characterization, must be incorporated into this total (Eq 1.1). Apart from this the lightpaths would traverse different filters when they hop over different OMS's. Unlike the previous effects, in-line filtering introduces coloured ASE noise causing inter-symbol-interference (ISI).

In the realm of WDM design, the SNR margin emerges as a pivotal indicator of system robustness. It is defined as the difference between the measured SNR and the predefined SNR threshold necessary to achieve a certain pre-Forward Error Correction (pre-FEC) Bit Error Rate (BER). This threshold is critical as it represents the minimum BER required for the system to decode the optical signal with an acceptable error rate before any error correction is applied. To relate BER to SNR, the following formula is commonly used:

$$\mathrm{SNR} = 10\log_{10}\left(\frac{E_c}{N_0}\right) \tag{1.4}$$

where E_c is the constellation energy and N_0 is the noise power spectral density. Eq (1.4) is derived based on the modulation format and other system parameters. Specifically, the relationship between BER and SNR can be calculated using:

$$\mathrm{SNR} = 10\log_{10}\left(\mathrm{constellation\_energy} \times \left(\frac{\mathrm{erfcinv}\left(\frac{\mathrm{BER}}{g\times\frac{\mathrm{nb\_mean}}{2\times\mathrm{nb\_bits}}}\right)^2}{2}\right)\right) \tag{1.5}$$

In the Eq (1.5), the parameters are calculated as follows:

- **constellation_energy**: The energy of the constellation points.
- **erfcinv**: The inverse complementary error function, which is used to relate the BER to the Q-factor.
- **BER**: The target Bit Error Rate.
- **g**: A factor that depends on the modulation format and source entropy.
- **nb_mean**: The average number of neighboring constellation points.
- **nb_bits**: The number of bits per symbol in the modulation format.

Determining the SNR threshold is a meticulous process, often derived from empirical studies that scrutinize the performance of various transponders across different modulation formats. The resulting SNR margin thus serves as a buffer, quantifying the extent to which the SNR can degrade before the system's error performance exceeds acceptable levels. It is a measure of the system's capacity to withstand noise and other signal impairments, ensuring reliable data transmission over the optical network. The computation of the SNR margin is integral to system design and performance optimization. For different transponders, each tailored to its modulation format, the SNR threshold is established through rigorous experimentation. Therefore, the transmission performance metric SNR margin may be simply expressed as:

$$SNR_{Margin}[dB] = SNR_{received}[dB] - SNR_{Threshold}[dB] \tag{1.6}$$

1.2.2 Challenges in the Data Plane

The ongoing surge in global data traffic has driven the need for innovative solutions to expand network capacity. SDM and multiband transmission have emerged as promising approaches to address this capacity crunch. SDM involves deploying multiple parallel fiber

transmission systems, while multiband transmission extends the spectrum by utilizing additional bands such as O, E, S, and L, alongside the conventional C band. While both methods can significantly enhance capacity, they come with considerable costs, particularly due to the need for new equipment like different band ROADMs, amplifiers, and additional fibers. In fact, expanding beyond the C band can result in costs that are up to four times higher, as detailed in recent studies [2–4].

Amid these high-cost solutions, WDM has been the cornerstone of optical network expansion for years. The evolution from WDM to DWDM allowed for a substantial increase in the number of channels and data rates, making it the go-to method for scaling network capacity. However, as DWDM systems have become saturated, they face their own set of challenges. The use of more complex modulation formats to improve spectral efficiency requires higher power levels for transmission. This increase in power exacerbates the sensitivity of the system to impairments such as noise and nonlinear effects, which can degrade transmission reach and quality.

One consequence of these challenges is the need for optical regenerators, particularly Optical-Electrical-Optical (O-E-O) regenerators, which convert degraded optical signals into electrical signals for regeneration before converting them back into optical form. While necessary for maintaining signal quality over long distances, the frequent need for regenerators adds significant cost and complexity to the network. This underscores the importance of achieving equal transmission performance across all channels to minimize the need for such interventions.

In light of these challenges, power optimization within DWDM systems emerges as a highly effective alternative. By intelligently managing power levels across the network's channels, it is possible to mitigate the negative impacts of impairments, thereby enhancing the SNR and overall network performance. This approach offers significant CAPEX savings compared to the more infrastructure-intensive methods like SDM and multiband transmission [5]. Power optimization leverages existing infrastructure more efficiently, reducing the need for costly expansions while ensuring that the network can meet growing demands without sacrificing performance.

1.2.2.1 Technical Hurdles in Per-Channel Power Optimization

Implementing per-channel power optimization, however, is fraught with technical complexities. The process requires precise calibration of power levels across a myriad of channels, each potentially utilizing different modulation formats that vary in their sensitivity to signal impairments. These impairments, if not properly managed, can significantly impact the transmission reach and network reliability.

The quest for optimal network performance through power optimization must not overshadow the imperative for reliability. Managing SNR margins is critical in this balancing

act, as it involves fine-tuning the signal quality to mitigate noise while avoiding excessive power levels that could lead to nonlinear effects detrimental to the network. As the thesis ventures deeper into the nuances of per-channel power optimization in Chapter 2, a detailed literature survey will shed light on the state-of-the-art techniques and their implications for OMS design and operation.

The first part of the thesis focuses on proposing a per-channel power optimization heuristics to select the power of each channel, on each OMS, intending to either enhance the capacity by improving the SNR margin of all the channels or to improve the worst channels' SNR margin among all the other established services, thereby improving the network's robustness.

1.3 Control Plane

In the intricate world of optical networking, the seamless interconnection of OMSs forms the backbone of modern telecommunications infrastructure. These connections, ranging from straightforward point-to-point links to complex mesh and ring networks, underpin the vast and interconnected networks that facilitate global communication. As we have shown in the Data Plane section, the physical infrastructure and technological advancements in OMS significantly enhance network capacity and reliability. However, the efficient operation and optimization of these interconnected networks necessitate a sophisticated management layer – the Control Plane.

Central to the Control Plane's functionalities are the processes of RWA and Routing and Wavelength/Fiber Allocation (RWFA). These processes are pivotal in planning the traffic across the network's complex topology, ensuring that each optical signal is transmitted over the optimal path and wavelength, and, when necessary, through the appropriate fiber. The Control Plane's ability to efficiently manage these resources is crucial for maximizing network performance, minimizing congestion, and ensuring the reliable delivery of data. As optical networks evolve, becoming more complex and integral to our digital lives, the role of the Control Plane has never been more critical. Its advancements, particularly in leveraging concepts such as SDN, and NFV, have revolutionized optical communications. No longer viewed as mere conduits for data, optical networks are now dynamic, intelligent systems capable of self-optimization and real-time management, thanks to the sophisticated capabilities of the Control Plane.

Currently, the use of optics in performing advanced network operations like switching, routing, regeneration, or wavelength conversion remains somewhat limited. However, a range of OFs including wavelength converters and optical packet switching have been investigated for direct application within the optical domain [24]. These OFs ambition to be part of an all-optical network [6], which conduct signal processing and switching entirely in

the optical domain. This approach has been demonstrated to significantly reduce energy consumption and decrease end-to-end latency [25].

1.3.1 Challenges in the Control Plane

Enhancements or additional functionalities within the control plane have direct repercussions on the data plane's operations, necessitating seamless communication between the two. This interplay is fundamental, as decisions made at the control level regarding routing, wavelength assignment, or network configurations directly influence the efficiency, capacity, and reliability of the data transmission paths. Unlike in traditional network architectures, where the control and data planes operated more independently, contemporary designs underscore the necessity of continuous feedback between these planes. This feedback mechanism ensures that adjustments in the control plane translate into optimized performance in the data plane, reflecting a departure from past practices towards a more integrated and responsive network infrastructure. The evolution towards such a synergistic approach highlights the importance of the control plane not just as a managerial entity, but as a critical component that dynamically shapes the data plane's functionality to meet the ever-growing demands of network performance and efficiency.

Considering the numerous technologies emerging from research labs, for both data and control plane, their commercialization will remain a significant challenge unless they can prove to have a substantial impact on ONs. When the ONs undergoes a state change by integrating any of the above-mentioned advancements, the overall ONs performance should be analysed to evaluate the incidence of the new approach and decide if it is worth to upgrade the existing network.

As an example, QKD [26], can be viewed as a new function in the ONs. It would provide physics-based security to the network. However, with the existing simulation tools, we are not able to integrate this function in both the control and data plane to evaluate its effects on the existing WDM network.

A variety of simulators have been developed independently to study the impact of different technological advancements and provide valuable insights about their effects on network behavior. However, at this stage, either they focus on the detailed physical layer impairments but do not blend in with a broad network planner [20, 27, 28], or we get tools with good network traffic management but poor accuracy on the QoT [29–31]. On top of that, the current simulators do not offer an agile way to add on new OFs.

The second part of this thesis introduces a novel simulator specifically designed for impairment-aware network planning (PyFIOA - Python Fiber Impairment & Optical Analysis). This tool seamlessly integrates comprehensive insights into the QoT with robust capabilities for managing network traffic. What sets this simulator apart is its remarkable flexibility, particularly in accommodating new OFs, which ensures its relevance and

efficacy amidst the rapidly evolving landscape of network technologies and demands. By overcoming the limitations inherent in existing simulation tools, our simulator marks a significant leap forward in the field. It provides a more accurate and comprehensive solution for modeling and optimizing the performance of optical networks. In Chapter 3 we describe the existing simulators and their functionalities in detail.

In a significant enhancement to the proposed simulator, we have successfully integrated QKD as a key optical functionality. This integration not only extends the simulator's capabilities but also enables us to explore the nuanced impacts of QKD on network performance and security. By incorporating QKD as an OF, PyFIOA offers a unique platform for analyzing how quantum security mechanisms interact with traditional optical network infrastructures and how they can be optimized alongside conventional data traffic.

Furthermore, our work in integrating QKD stands out as a pioneering effort in the field of optical network simulation. We propose a detailed model of the impairments specific to QKD within a network planning tool, addressing a critical gap in existing simulation methodologies. The detailed modeling of these impairments is discussed in depth in Chapter 4, accompanied by a comprehensive literature review that situates our contributions within the broader context of QKD research and optical network development. Through this innovative integration, the proposed simulator not only advances the state of the art in network planning tools but also lays the groundwork for future explorations of quantum communications within optical networking.

1.4 Summary

In conclusion, this chapter has provided a comprehensive overview of the fundamental components and advancements in optical networks, emphasizing the significant roles of both the data and control planes. The discussion on physical layer impairments and their impact on network performance underscores the necessity for meticulous impairment-aware network planning. As we delve deeper into specific topics in subsequent chapters, including per-channel power optimization and the optical functionalities such as QKD, this foundational understanding will inform our approach to developing innovative solutions that address the complexities and demands of modern optical networks.

CHAPTER 2

SNR-based Channel Power Optimization for Optical Networks

2.1 Introduction

In the quest to meet the ever-growing demand for higher data rates and increased network capacity, efficient management of optical signal power becomes paramount. This chapter focuses on per-channel power optimization, a critical technique for enhancing the performance and capacity of DWDM systems. By leveraging SNR-aware equalization, we aim to optimize the power levels of individual channels, thereby improving the overall network performance. Equalization stands out as a pivotal strategy, championing the judicious distribution of power among the channels of a network to elevate its overall efficacy. This approach is aimed at boosting the SNR, an essential factor influencing the quality of data transmission, thus significantly enhancing both the network's capacity and its dependability. Through the meticulous reallocation of power to bolster channels that perform poorly, equalization effectively mitigates performance imbalances across the network, promoting a more consistent and streamlined operational framework.

2.1.1 Literature Survey

Optical-layer Commissioning is the WDM network-wide task where we adjust the channel powers in the fiber using OA, VOA, and WSS, to maximize the performance. A typical approach for commissioning is to use constant launch powers for all the channels to equalize the performance of all the optical channels. The field channel powers may be far from the target resulting in non-equalized performance.

Current commissioning methods consist in either equalizing powers at the input of each OMS or equalizing OSNR at the output of each OMS. With power equalization, all channels at a given OMS have the same power after the last WSS of the node prior to the OMS or equivalently before the booster at the beginning of the OMS. With the relevant

assumptions, in particular, amplifier gain flatness and no Stimulated Raman Scattering (SRS) effect, the Gaussian Noise model [19] yields the following per-channel power in the fixed grid case, which optimizes the capacity of the line:

$$P_{ch,opt} = \sqrt[3]{\frac{hfNF(G-1)R_s}{2\eta_{NLI}}} \tag{2.1}$$

where h is the Planck constant, NF is the amplifier's noise figure, G is the amplifier's gain, R_s is the symbol rate and η_{NLI} is the nonlinear efficiency:

$$\eta_{NLI} = \frac{16}{27\ \pi}\ \gamma^2 \frac{\alpha_e L_{eff}^2}{|\beta_2| R_s^2}\ \log_e\left(\frac{\pi^2}{2}\frac{|\beta_2|}{\alpha_e} R_s^2 N_{ch}^{2\frac{R_s}{\Delta f}}\right) \tag{2.2}$$

where γ is the fiber nonlinear coefficient, β_2 is the dispersion coefficient, α_e is the electric field attenuation coefficient in linear unit, Δf is the channel spacing and L_{eff} is the effective length of the fiber:

$$L_{eff} = \frac{1 - e^{-2\ \alpha_e\ L_s}}{2\alpha_e} \tag{2.3}$$

where L_s is the fiber length.

The power allocation strategy is denoted by Local Optimum Global Optimum (LOGO) by their authors [19].

For a flexible grid with uneven spacing, power spectral density rather than power is equalized, i.e.:

$$G_{ch,opt} = \sqrt[3]{\frac{hfNF\,(G-1)}{2\ \eta_{PSD,NLI}}} \tag{2.4}$$

where $\eta_{PSD,\ NLI}$ is the power spectral density nonlinear efficiency:

$$\eta_{PSD,\ NLI} = \frac{16}{27\ \pi}\ \gamma^2 \frac{\alpha_e L_{eff}^2}{|\beta_2|} \log_e\left(\frac{\pi^2}{2}\frac{|\beta_2|}{\alpha_e} B_{tot}^2\right) \tag{2.5}$$

where B_{tot} is the total optical bandwidth.

The LOGO strategy is not optimal for capacity maximization in the general case, where wavelength dependence (attenuation, amplifier ripples, SRS) exists; however, due to its simplicity, we will use LOGO as a baseline. LOGO accounts for both linear and nonlinear effects. Other effects are either not power-dependent or only weakly so, thus acting as offsets in the SNR formula and not impacting power equalization.

On the other hand, typically in the industries OSNR equalization [32] is performed to equalize the OSNR of all channels on a given OMS; it usually requires sending a technician on the field to measure OSNR at the end of the OMS for all channels, while power is being adjusted at the beginning of the line. OSNR equalization only accounts for linear noise.

From the preceding points, we can observe that the low powers degrade the linear part of the SNR (OSNR) and the higher powers degrade the non-linear part of the SNR. Therefore, we need to set the power of each channel in the WDM comb to balance both.

Current equalization methods as mentioned earlier equalize powers at the input of the OMS. With power equalization, all channels at a given OMS have the same power after the last WSS of the node prior to the OMS or equivalently before the booster at the beginning of the OMS. With the relevant assumptions, in particular, OA gain flatness and no Stimulated Raman Scattering (SRS) effect, the Gaussian Noise model [19] yields a per-channel power strategy that would optimize the performance.

For example, let us consider a system that is composed of a single OMS (described in Figure 2.1 (a)) with EDFA's and 5 Single Mode Fiber (SMF) fiber spans. Implementing the power allocation strategy as described in Eqn. 2.1 for 80 co-propagating channels with different modulation formats would result in the SNR as shown in Figure 2.1 (b). We have used a commercial flex-rate transponder that can handle both 400G 16QAM and 200G QPSK. The amplifier design was transparent, meaning that the mean gain of the amplifier is equal to the span loss, and the gain and noise figure were collected from the lab, thus they exhibit wavelength dependency. The SNR was calculated using the QoT tool at the Paris research center, which will be explained further. This power allocation strategy has resulted in channels operating close to the $SNR_{threshold}$ (FEC limit). In addition, the $SNR_{margins}$ obtained are shown in Figure 2.1 (c), indicating that the system is not robust to unforeseen circumstances. This practical experience has led us to understand that output SNRs are different when the signal of different wavelengths passes through multiple OAs contrary to the flatness assumption made in [19] the general optical networks always suffer from wavelength dependence (OA, fiber attenuation, SRS effect of the fibers). This unflattens the optical power of each signal that enters the OA. The unflattened signal would also be affected by the OA gains and noise figure which would be wavelength dependent, resulting in an unequalized performance at the receiver end.

The SNR threshold, as shown in Table 1.1 and Eq 1.5, depends on many factors including the modulation format. Therefore, any non-SNR-based equalizing strategy would result in channels operating close to the threshold as seen in Figure 2.1 (c).

However, during the life of a network, some parameters may change, such as the fiber loss (e.g., due to fiber cuts and splices) and accordingly amplifiers' gains, resulting in performance degradation for all services. The main performance metric is the pre-FEC BER i.e. the SNR, which should remain above a predefined limit, and is intrinsically needed to ensure a given quality of service (SNR includes all degradations: linear and nonlinear noise, transponder back-to-back penalties, filtering ...). The relationship between SNR and BER can be expressed in terms of the Q-factor (Q). Specifically, the SNR can be expressed as the ratio of energy per bit to noise power spectral density (SNR = $\frac{E_b}{N_0}$), and

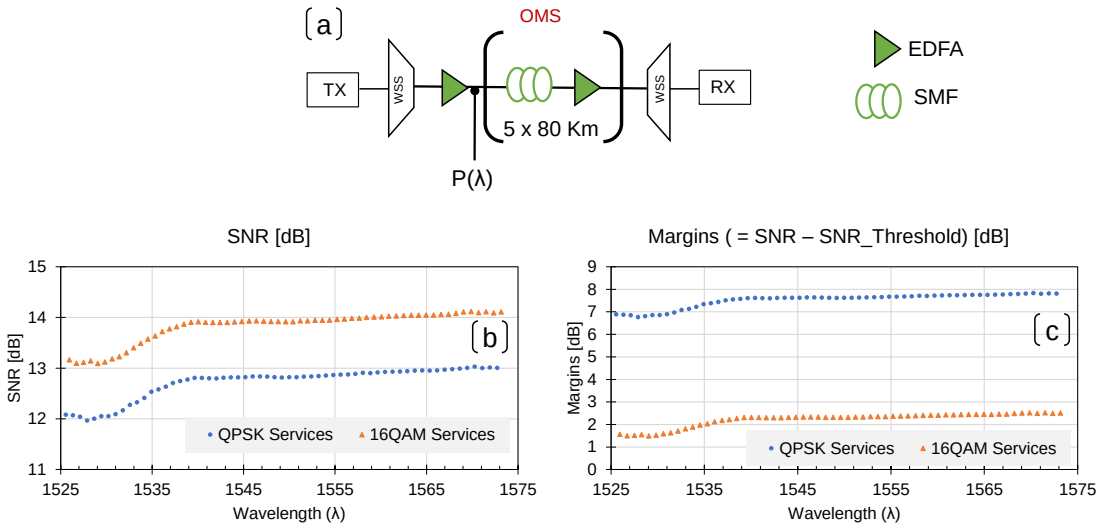

Figure 2.1: (a) OMS Setup for 80 channels; (b) SNR vs Channel Number ; (c) Margins vs Channel Number

the BER can be approximated by the complementary error function (erfc) of the Q-factor. A higher SNR, therefore, results in fewer errors in the transmitted data before FEC is applied. Thus, maintaining an adequate SNR is crucial for ensuring a low BER and, consequently, high-quality data transmission. As network parameters change, the service already close to the FEC limit may be disrupted. For this reason, we propose to optimize the margin of the SNR of services in a network; in particular, we propose to maximize the SNR margin of the worst service in the network in order to make the network more robust to unforeseen impairments such as aging. This will be done through per-OMS, per-channel power allocation. Note that, in case several power allocations return the same worst service margin, the capacity of the system will be optimized as a secondary goal to avoid wasting it. In a word, the aim of our equalization strategy is to maximize the robustness of the network as a primary goal and its capacity as a secondary goal. We also propose an equalization strategy, whose goal is to optimize capacity only.

In Figure 2.2 we try to encapsulate the novelty of our proposed equalization strategy compared to the existing strategies. As shown in Figure 2.2 we start by grouping them under the wavelength dependence categories. It should be noted here that capacity maximization and margin maximization through power allocation have been investigated through formal, convex optimization-based techniques in [33]; however, the main system parameters (fiber attenuation, amplifier gain) are assumed to be flat, and deviation from this assumption breaks the convexity of the original problems such that the convex optimization solutions proposed in [33] are actually sub-optimal. SRS is accounted for in a further paper from the same team [34] but again the flatness assumption remains. No optimal solution is known for the general case, and heuristics were proposed in [35] in the

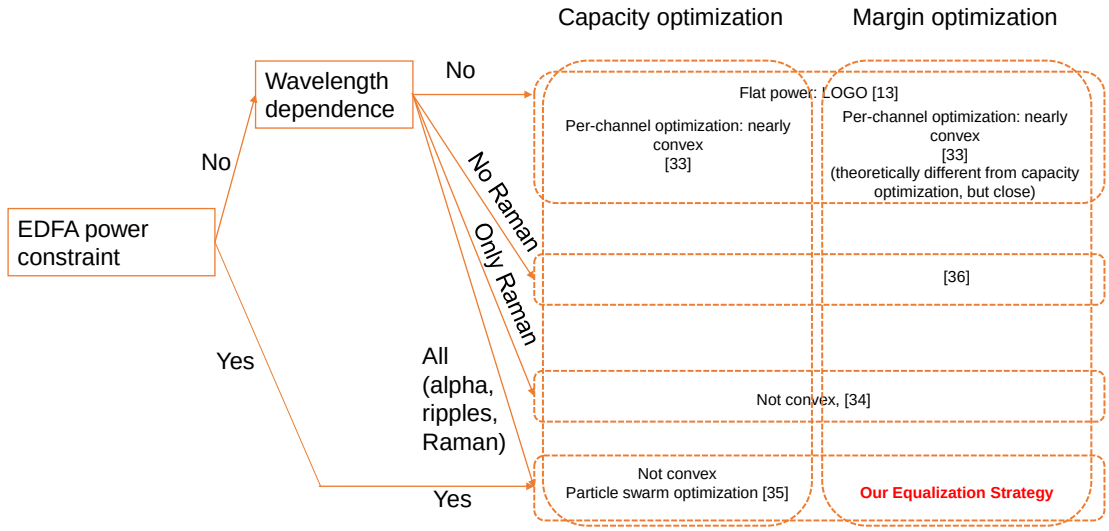

Figure 2.2: Literature survey of different power optimization strategies

context of submarine links with EDFA power constraints to optimize capacity, and in [36] for more general systems without EDFA power constraints for robustness optimization and without Raman effect. To the best of our knowledge, no existing work addresses the general case of robustness optimization for systems impaired by SRS and constrained by EDFA power limitations, hence we placed ourselves in the block (**Our Equalization Strategy** in Figure 2.2) where both the EDFA power constraints and the wavelength dependence is considered.

In the following sections, we would propose per channel power allocation strategies that would be considering the wavelength dependent SRS, fiber attenuation and the EDFA power constraints as shown in Figure 2.2. It is important to note that a portion of the content presented in this chapter has been previously presented at the ECOC 2021 and is cited as [37]. The insights and findings from the ECOC 2021 paper provide a foundational basis for the discussions and analyses presented herein. Also we have demonstrated in real time at OFC 2022 an automation framework using the proposed per channel optimization strategy. The OFC 2022 demo paper is cited as reference [38].

2.1.2 Proposed Equalization Strategy for a point-to-point link

We propose the following strategy in the case where all services start at the same node and terminate at the same node, i.e., a point-to-point scenario. This work later can be extended to multipoint-to-multipoint or meshed scenarios.

A sample OMS is depicted in Fig. 2.3. The problem consists in optimizing the SNR margin through proper allocation of the launch power spectrum $P(\lambda)$, i.e., the launch power for each service/optical channel mapped to channel λ. [19] dictates that the SNR of the worst channel is maximized when ratio $\rho = P_{ASE}/P_{NLI}$ between the amplifiers

spontaneous emission (ASE) noise power P_{ASE} and the nonlinear noise power P_{NLI} is $3dB$ (Non-Linear Threshold, NLT). In those conditions, we have $d\rho/dP = 3$, while, in the linear regime, $dSNR/dP = 1$. We have verified these assumptions across the sample OMS shown in Fig. 2.3 using 120 channels spaced at 50 GHz (using the complete 6 THz super-C band) with 32 GBaud DP-QPSK modulation format. We use EDFAs with a max gain of 21 dB in the simulations. In Table 2.1, we have detailed the changes observed from our simulations, with a particular emphasis on the effects of different impairments. Specifically, we have documented the changes in the SNR and the relative changes in the ratios for the two extreme wavelengths among the 120 channels. These variations correspond directly to adjustments in the power levels per channel, with each iteration fine-tuned by 1 dB.

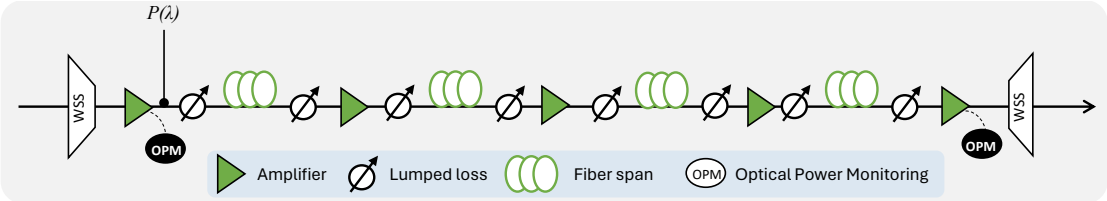

Figure 2.3: Sample OMS to Equalize

Table 2.1: Correspondence of $d\rho$ and $dSNR$ with dp

Impairments			$d\rho$ [dB]		dSNR [dB]	
SRS	Attenuation	EDFA Ripple	$1 \rightarrow 2$	$2 \rightarrow 3$	$1 \rightarrow 2$	$2 \rightarrow 3$
✓	✗	✓	2.1, 3.8	2.2, 2.8	-0.6, -1.4	-0.78, -1.2
✗	✓	✓	2.9, 3	2.7, 2.2	-1, -1	-1, -1
✗	✗	✓	3,3	2.8, 2.1	-1, -1	-1, -1
✗	✓	✗	3, 3	2.8, 2.4	-1, -1	-1, -1
✗	✗	✗	3, 3	2.8, 2.4	-1, -1	-1, -1

The results of the first three iterations are reported in Table 2.1, capturing the dynamic response of both SNR and channel ratios to modifications in power values. These results highlight the nuanced response of the system's performance to incremental power variations, particularly between iterations 1 to 2 and 2 to 3, with each iteration involving a 1 dB increase in power. The differential impact on channel ratios ($d\rho$) showcases a nonlinear behavior with a range from 2.1 to 3.8. This data is indicative of a substantial rate of change ($d\rho/dP$) in the channel ratios amounting to approximately 3 dB across these iterations. Simultaneously, the $dSNR$ demonstrates a more subdued fluctuation, with the minimum and maximum changes spanning -0.6 to -1.4 dB for iteration 1 to 2, and -0.78 to -1.2 dB for iteration 2 to 3. This pattern denotes a linear rate of change ($dSNR/dP$) of about

1 dB, evidencing a consistent SNR shift per unit power increment. These observations conclusively affirm the hypothesis that while the channel ratio exhibits a threefold change per dB in a nonlinear progression through the iterations, the SNR reflects a proportional and linear change rate of 1 dB per dB of power.

We use those rules of thumb as an approximation within our optimization process in the more general case where the system is not flat and SRS is present. However, while optimizing, we leverage our more generic SNR computation tool that accounts for non-flatness and SRS, such that the system SNR margin is indeed maximized. This SNR computation tool accounts for the ISRS GN model proposed in [22] along with the SPM and XPM effects that include the impact of the powers of the co-propagating signals on the OMS. When calculating the total SNR for a lightpath that crosses various OMSs, we must aggregate both the linear and non-linear components of the SNR from each OMS. Additionally, the BtB SNR, derived from experimental characterization, must be incorporated into this total 1.1. Apart from this the lightpaths would traverse different filters when they hop over different OMSes. The influence of this filtering penalty has been analytically modeled using the estimation theory proposed by Ivan et al in [39]. This lays the foundation for the proprietary SNR estimation tool developed at the Huawei Paris Research Center.

Our proposed equalization strategy follows the schematic in Figure 2.4. Given an OMS, monitoring information (e.g., power per channel at the start/end of OMS, total EDFA output powers, ...) is stored in the physical layer database of the SDN controller. This database feeds the equalizer, which is described next. The equalizer relies on a QoT estimator, which itself uses the data in the physical layer database to perform accurate QoT estimation. Once the equalizer has computed a power allocation, this allocation is pushed to the WSS at the start of the OMS to set the desired per-channel powers. This process can be done only once, or, in case there is a discrepancy between the desired metrics (e.g., powers or SNR) and the corresponding measured metrics, the process can be iterated as shown by cycle ❶ in Figure 2.4: at each iteration, new monitoring information is collected such that QoT estimation is improved and the monitored equalization metrics converge to the desired values. In the following, we will consider a single iteration of cycle ❶.

The equalizer (Figure 2.5) is initialized with a power allocation $P_0(\lambda)$ for each channel λ, e.g., using the LOGO formula in 2.1. We estimate the SNR for all services in the OMS using an SNR estimation tool. A cost function is evaluated, using one of the cost functions (metrics) defined in Equations of Figure 2.5(a). If the difference between the cost at the current iteration j and the cost at the previous iteration $j-1$ is sufficiently small, the equalizer returns the current power allocation $P(\lambda) = P_j(\lambda)$ and sends it to the SDN controller, which can then tune the per-channel attenuation on the WSS located immediately prior to the considered OMS. Otherwise, the optimizer is executed to update the new power allocation $P_{j+1}(\lambda)$, and the method loops from there.

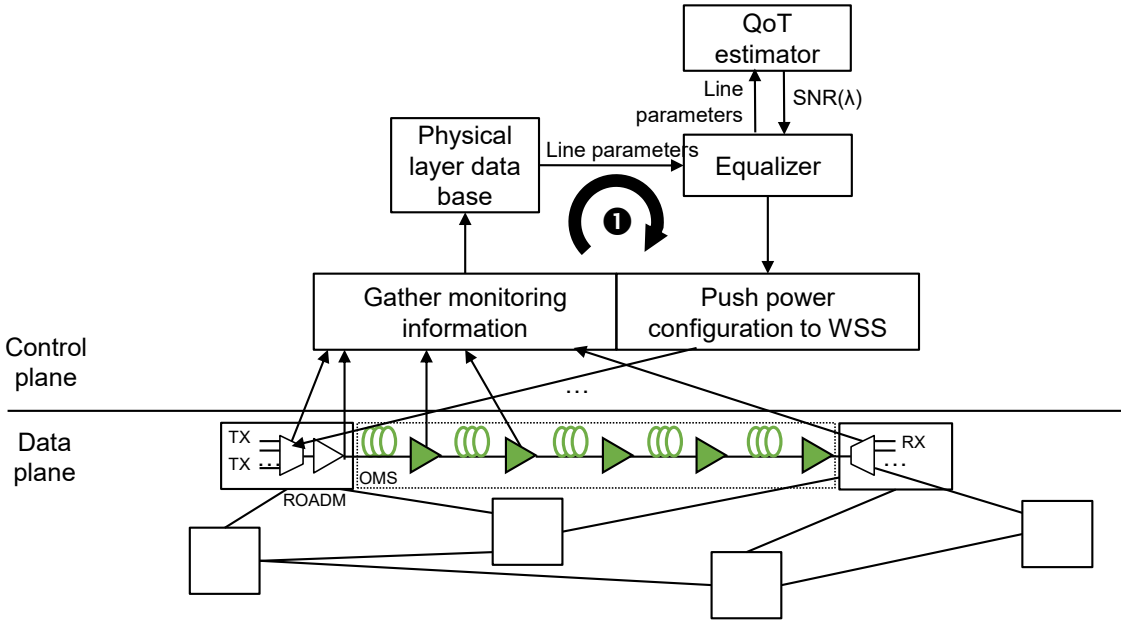

Figure 2.4: Equalization Strategy

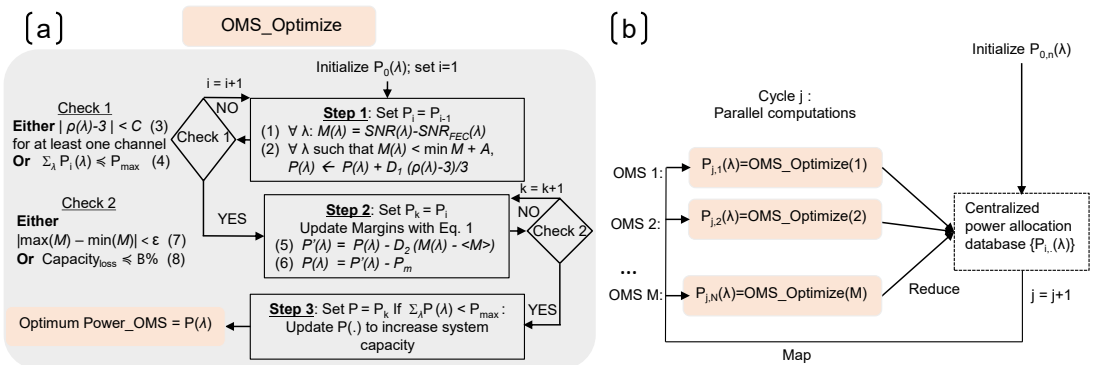

Figure 2.5: (a) Point to Point; (b) network Heuristic

This process can be extended to the more generic meshed network case (Figure 2.5(b)). The iterative method relies on cycles indexed by j, each cycle consisting of a "map" and a "reduce" step, as in distributed computing. $P_{j,n}(\lambda)$ is the power at Cycle j for the n-th OMS on the service going though channel λ; $P_{0,n}$ is initialized using LOGO for each OMS. A centralized database contains all power allocation $P_{j,n}(\lambda)$. In the "map" step, each OMS is optimized using OMS_Optimize, independently of the other OMS: each OMS is optimized in parallel, assuming that the data from other OMS are known (from the global database) so that the margins of all the services going through a given OMS can be computed. After this step, the power allocation for each OMS is known. Then, in the "reduce" step, each OMS shares its power allocation with all the other OMS through the global database. Cycles are iterated until convergence of the desired metric, e.g., SNR margin. If a single cycle is run, the optimization is OMS-local as each OMS can compute

its power allocation independently by simply assuming that all other OMS use the LOGO procedure. When several cycles are run, the optimization is global as the OMS exchanges information through the centralized database.

The algorithm can optimize network capacity or worst channel SNR (margin maximization), with or without power constraints on the EDFAs. We first present the margin maximization algorithm with power constraint i.e., the total output power of the first (booster) amplifier should not exceed P_{max}.

The insight behind the proposed algorithm is that equalization, i.e., changing the power of each channel, only changes the quantity of linear ASE noise and nonlinear noise of the services crossing a given OMS, while other sources of penalty (filtering, TRX back-to-back, PDL, ...) are power invariants i.e., they are left unchanged. Hence, the algorithm will strive to balance the linear and nonlinear noise given the target metric. It is known from the GN model that the SNR of the worst channel is maximized when the ratio ρ between the ASE noise power P_{ASE} and the amount of nonlinear noise power P_{NLI} is $\rho = P_{ASE}/P_{NLI} = 3dB$. In addition, the GN model dictates that $d\rho/dP = -3$ (ρ, P in dB scale). Finally, in the linear regime, $dSNR/dP = 1$ (SNR, P in dB scale).

Given that, we propose the following 3-step algorithm. The starting point is in the highly linear regime, for instance, using a flat power allocation:

$$P_{in} = \min(P_{LOGO}, P_{max}) - 3dB \tag{2.6}$$

All 3 steps are implemented in the OMS_Optimize box shown in Figure 2.5(a). The first step drives the SNR margin up. The second step flattens the SNR margins while the third step allocates any left-over power to increase capacity without impacting (decreasing) the SNR margin of the worst channel. Note that, in the second step, it may happen that we start losing capacity to have more gain in margins of the worst performing channels. The trade-off between the margin gain and capacity loss is a design choice and is quantified by the parameter B below.

Step 1: SNR margin maximization

$$\text{Compute margins: } \forall\lambda : M(\lambda) = SNR(\lambda) - SNR_{FEC}(\lambda), \tag{2.7}$$

where $SNR_{FEC}(\lambda)$ is the FEC limit for the service using channel λ.

For each channel λ such that $M(\lambda) < min(M) + A$ (where A is a parameter that impacts the number of channels to be impacted in the step): set powers closer to NLT, using a damping factor $D_1 < 1$ to avoid oscillations:

$$P(\lambda) \leftarrow P(\lambda) + D_1(\rho(\lambda) - 3]/3)[P, \rho \text{ in } dB] \tag{2.8}$$

Repeat Eq 2.8 until either $|\rho(\lambda) - 3| < C(\rho \text{ in } dB)$ for at least one channel λ, or the

EDFA power constraint is met. Parameter C defines the lower and upper bounds that can be accepted as closeness to NLT as a stopping criterion.

Step 2: SNR margin flattening

Compute per-service margins $M(\lambda)$ and average margin $< M >$:

$$\forall \lambda : M(\lambda) = SNR(\lambda) - SNR_{FEC}(\lambda), \tag{2.9}$$

Set the power of each service such that its margin is closer to $< M >$ using damping factor $D_2 < 1$:

$$P'(\lambda) = P(\lambda) - D_2(M(\lambda) - < M >)[\text{in } dB] \tag{2.10}$$

$$\text{Normalize powers:} \qquad P(\lambda) = P'(\lambda)/P_m[\text{linear}] \tag{2.11}$$

Where, $P_m = P_{step1}$ (where P_{step1} is the total output power of Step 1) if after the last iteration of Step 1 we have a channel with $\rho =$ NLT; $P_m = P_{max}$ otherwise.

Perform Eq 2.10 until convergence ($|\max(M) - \min(M)|$ small enough or does not change over iterations) or we have $B\%$ (design parameter for the tradeoff between capacity and margins) loss in the capacity.

Step 3: Capacity maximization

If there is any leftover power that is at the last iteration of Step 2 if we meet the condition $\sum P(\lambda) < P_{max}$

We set powers closer to NLT, using a damping factor $D_3 < 1$:

$$P'(\lambda) = P(\lambda) + D_3(\rho(\lambda) - 3]/3)[P, \rho \text{ in } dB] \tag{2.12}$$

Note that the proposed algorithm can be also used to maximize the system capacity without optimizing the worst-channel SNR, by simply skipping Steps 1 and 2 and running Step 3 only.

In the next sections, we would be implementing the proposed equalization strategy for the full load and partial load tandem networks. We would compare it against with the state of the art strategies such as LOGO in terms of accuracy and the computation time. At the same time we also experimentally validate the proposed strategy using the commercial transponders and line set-up at Huawei Paris Research center.

2.2 Validation of the Proposed Equalization Strategy for Full Load

2.2.1 Point-to-Point Link Assesment

We evaluated the equalizer for 2 types of OMS. Unless otherwise specified, the setup is:

- OMS1: 5 × 80km SMF (20 dB span loss including VOAs before/after the fiber), "power unconstrained" (the working region is below the booster EDFA maximum output power of $P_{\max} = 24dBm$);
- OMS2: 5 × 100km PSCF (22 dB span loss including VOAs before/after the fiber), "power constrained" ($P_{\max} = 22.5dBm$).

There is no filtering on those OMS. The effects that are modeled are: linear noise (based on real EDFA gain shapes measured in the lab for their nominal gain, and NF characterized in the lab), nonlinear noise (GN model), SRS, TRX back-to-back penalties. All results are generated with simulations based on Hauwei SNR estimation tool, which was experimentally validated. The lines are fully loaded with modulated signals.

OMS1 equalization (SMF), single rate, single FEC limit

For this scenario, we loaded OMS1 with 120 Channels modulated at 34 GBaud with 50 GHz spacing in the C120 band (6 THz C-Band). We assumed DP-QPSK modulation for the 120 channels.

We show in Figure 2.6: (a) the per-channel power after the OMS booster, (b) ratio ρ, and (c) the SNR margin at the end of the OMS, for the following 4 strategies: LOGO (flat power before the booster), margin maximization, capacity maximization and OSNR Loss Equalization (OLE). The x-axis corresponds to channels ordered by increasing wavelength. Figure 2.6(d) depicts the evolution of the capacity and minimum margin obtained during the iterations.

Table 2.2: Summary table on the performance of each equalization strategy for an SMF OMS, single FEC limit

Method	**Total power [dBm]**	**Capacity (average) [b/s/Hz]**	**Margin (min, max, range) [dB]**	**#iterations**
LOGO	21.8	9.8	8.7, 9.8, 1.1	1
Capacity	22.4	10	9.5, 10, 0.5	6
Margin (S1-S2)	21.3	9.8	9.5, 9.7, 0.2	5(3+2)
OLE	22.5	9.9	9.5, 9.9, 0.4	2

The capacity and margin maximization algorithms converge to the same solution and return the same capacity, which is slightly larger than the LOGO and OLE capacity Figure 2.6(d). We report the total power, capacity, margin, and number of iterations for each step as well as the sum in Table 2.2. In particular, we report results for the margin heuristic when stopping at Step 2 (S1-S2), and when completing all 3 steps (S1-S2-S3). A large

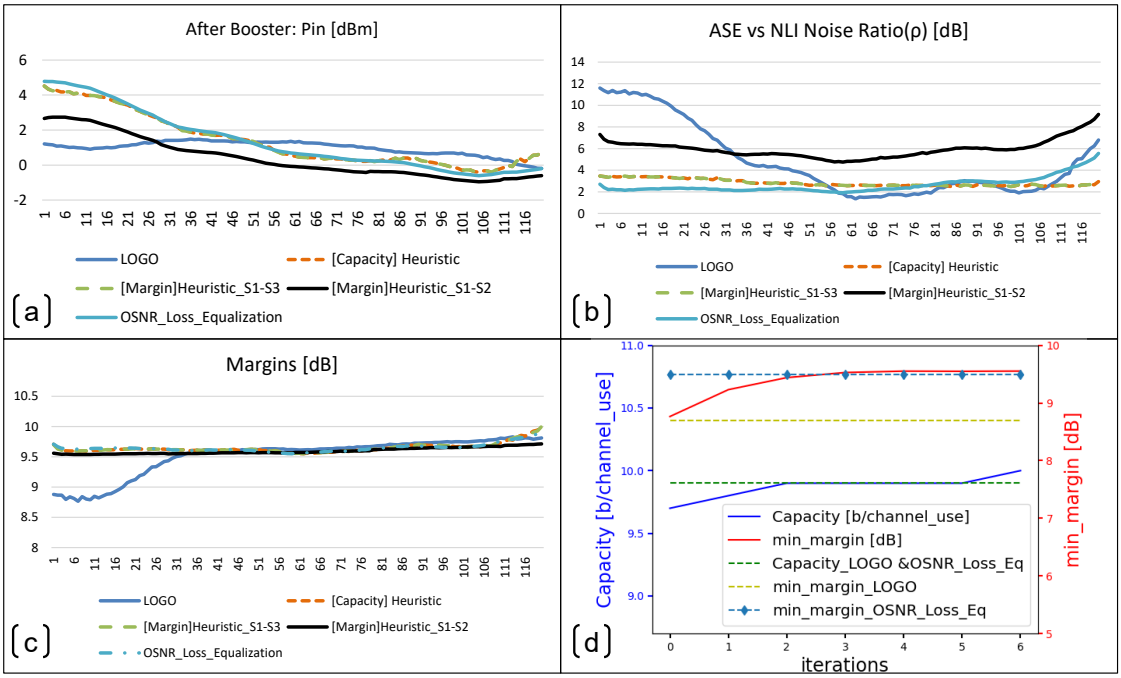

Figure 2.6: Equalization for an SMF OMS, single FEC limit

ripple of the C120 EDFA in the short wavelengths area strongly degrades the quality of the channels in this area (Figure 2.6(c)) and the SNR margin ranges between 8.7-9.8 dB (range: 0.9 dB) with LOGO.

Our algorithms are able to remove this wavelength-dependent margin and all services now have an SNR margin of at least 9.5 dB (with a variation of only 0.5 dB over the whole C120 band, even after Step 3 which allocates leftover power). When we stop our margin maximization at Step 2, the variation is 0.2 dB, at the expense of a slightly reduced capacity, see the black and green lines in Figure 2.6(c). In either of the cases, we have a 0.8 dB gain over flat power allocation. Compared with the OLE, the heuristic does not improve the minimum margin as the nonlinear threshold is reached for all techniques when using $P_{max} = 22.4$ dBm and no margin improvement is possible. The line operates in the power-unconstrained regime, i.e., the total power is below the EDFA limitation power of 24 dBm. As a result, it is possible to operate the system close to the nonlinear threshold, as can be seen in Figure 2.6(b): ratio ρ is close to 3 dB across the band. The running time of the margin equalizer is 5 iterations, i.e., it needs to run the SNR estimation tool 5 times. This would result in an increased computation time compared to LOGO (5 iterations vs 1 iteration), but results in 0.8 dB of increased worst-case SNR-margin.

OMS2 equalization (PSCF), single rate, mixed FEC limits

For this scenario, we loaded OMS2 with 80 Channels modulated at 68 GBaud with 75 GHz spacing in the C120 band. We assumed DP-QPSK modulation with a FEC limit

of $SNR_{FEC,1}$ ='x' dB for half of the channels and $SNR_{FEC,2}$ ='$x+1$' dB for the other half. This choice of FEC limits was made to demonstrate the capability of our equalizers to actually reduce margins in a multi-modulation format or multi-FEC limit context.

A "good" wavelength allocation strategy would allocate services with $SNR_{FEC,2}$ in the long wavelengths where propagation impairments are lower, however, this may not always be feasible depending on the availability. Hence, for the sake of generality and to avoid any wavelength allocation-dependent effect, we interleaved the services with different FEC limits. The booster is limited to 22.5 dBm.

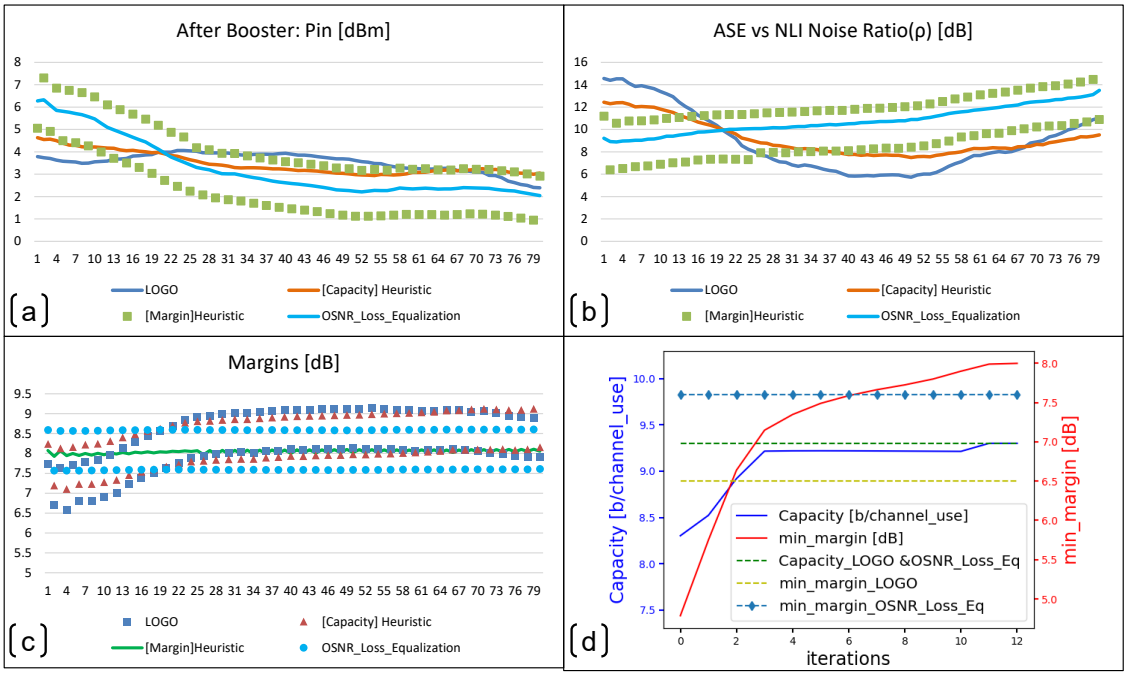

Figure 2.7: Equalization for a PSCF OMS, two FEC limits

Table 2.3: Summary table on the performance of each equalization strategy for a PSCF OMS, two FEC limits

Method	**Total power [dBm]**	**Capacity (average) [b/s/Hz]**	**Margin (min, max, range) [dB]**	**#iterations**
LOGO	22.5	9.4	6.5, 9.1, 2.6	1
Capacity	22.5	9.4	7.1, 9.1, 2	4
Margin (S1-S3)	22.5	9.4	8.0, 8.2, 0.2	13(5+8+0)
OLE	22.5	9.3	7.6, 8.6, 1	2

All 4 methods consume the total power budget of the booster EDFA and yield the

same system capacity (Figure 2.7(d)). The margin heuristic improves the worst channel margin from 6.5 to 8.0 dB (gain: 1.5 dB) and the range from 2.6 to 0.2 dB within 13 iterations (SNR estimator tool calls) when compared with LOGO. Compared with OLE the worst channel margin improves from 7.6 to 8.0 dB (gain: 0.4 dB). As can be seen in Figure 2.7(b), the system operates in the highly linear regime ($\rho > 3dB$).

OMS1 equalization (SMF), flexgrid/flexrate

We loaded OMS1 with 96 channels with a single modulation format over a flexible grid: 48 channels modulated with DP-16QAM/34 Gbaud in a 50 GHz grid (TRX: 8061) and 48 channels modulated with DP-16QAM/68 Gbaud in a 75 GHz grid (TRX: 8017). The 50 GHz and 75 GHz grids were interleaved. The services occupy the full C120 band.

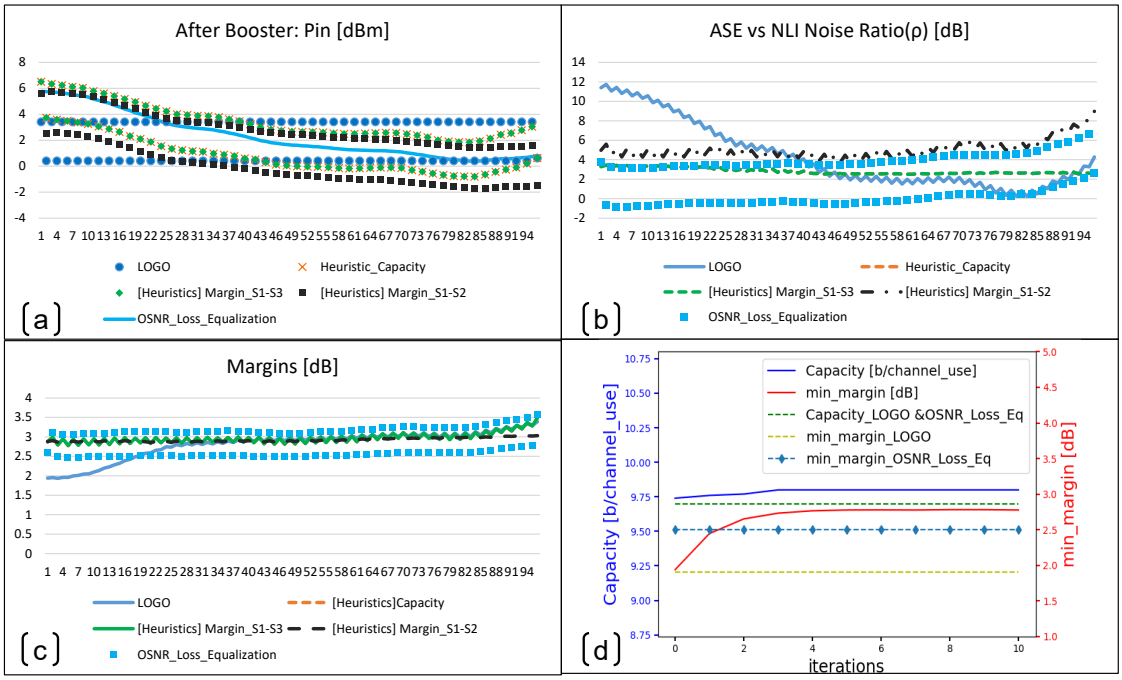

Figure 2.8: Equalization for an SMF OMS, two baudrates, and two grid spacings

In this scenario, the power constraint is not reached. Both margins and capacity optimizations converge and both drive the line to the nonlinear threshold (Figure 2.8(b)). The capacity is maximized and slightly higher than with LOGO and OLE. The SNR margin improves from 1.9 to 2.8 dB and the SNR margin range decreases from 1.5 to 0.7 dB compared with LOGO.

When we stop the margin equalization at Step 2 we have the same SNR margin improvement but the SNR margin range decreases to 0.2 dB compared to margin equalization executed till Step 3 at an expense of slightly reduced capacity (green and black lines in Figure 2.8(c)). The SNR margin improves from 2.5 to 2.8 dB (gain: 0.3 dB) when compared to OLE, we have a lower gain because the nonlinear threshold is reached for $P_{\max} = 22.5dBm$.

Table 2.4: Summary table on the performance of each equalization strategy for an SMF OMS, two baudrates, and two grid spacings

Method	**Total power [dBm]**	**Capacity (average) [b/s/Hz]**	**Margin (min, max, range) [dB]**	**#iterations**
LOGO	22	9.7	1.9, 3.4, 1.5	1
Capacity	22.4	9.8	2.8, 3.5, 0.7	11
Margin (S1-S3)	22.4	9.8	2.8, 3.5, 0.7	11(3+7+1)
Margin (S1-S2)	21.7	9.6	2.8, 3.0, 0.2	10(3+7)
OLE	22.5	9.7	2.5, 3.5, 1	2

OMS2 equalization (PSCF), flexgrid/flexrate

We loaded OMS2 with 96 channels with a single modulation format over a flexible grid: 48 channels modulated with DP-16QAM/34 Gbaud in a 50 GHz grid and 48 channels modulated with DP-16QAM/68 Gbaud in a 75 GHz grid. The 50 GHz and 75 GHz grids were interleaved. The services occupy the full C120 band.

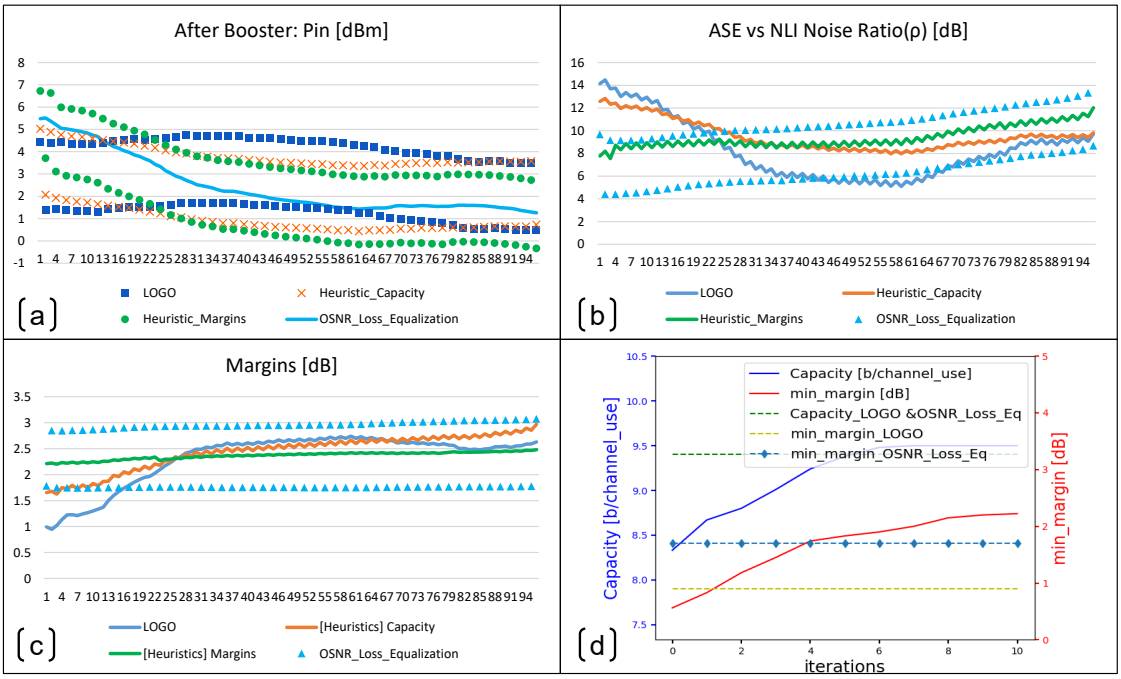

Figure 2.9: Equalization for a PSCF OMS, two baudrates and two grid spacings

In this scenario, the line operates in the linear regime. All methods again return approximately the same capacity but the margin equalizer returns, in 11 iterations, the highest

Table 2.5: Summary table on the performance of each equalization strategy for a PSCF OMS, two baudrates and two grid spacing

Method	**Total power [dBm]**	**Capacity (average) [b/s/Hz]**	**Margin (min, max, range) [dB]**	**#iterations**
LOGO	22.5	9.4	0.9, 2.7, 0.8	1
Capacity	22.5	9.5	1.6, 3.0, 1.4	5
Margin (S1-S3)	22.5	9.5	2.2, 2.5, 0.3	11(3+9+0)
OLE	22.5	9.4	1.7, 2.0, 0.3	2

minimum margin (2.2 dB) and all SNR margins are within 0.3 dB. This would result in an increased computation time compared to LOGO (5 iterations vs 1 iteration), but results in 0.8 dB of increased worst-case SNR-margin.

OMS2 equalization (PSCF), flexgrid/flexrate/mixed modulation format

We loaded OMS2 with 96 channels with 2 modulation formats over a flexible grid: 48 channels modulated with DP-QPSK/34 Gbaud in a 50 GHz grid and 48 channels modulated with DP-16QAM/68 Gbaud in a 75 GHz grid. The DP-QPSK and DP-16QAM channels were interleaved, to avoid any wavelength allocation-dependent effect. The services occupy the full C120 band.

Table 2.6: Summary table on the performance of each equalization strategy for a PSCF OMS, two baudrates, two FEC limits, and two grid spacings

Method	**Total power [dBm]**	**Capacity (average) [b/s/Hz]**	**Margin (min, max, range) [dB]**	**#iterations**
LOGO	22.5	9.4	0.9, 9.1, 8.2	1
Capacity	22.5	9.4	1.5, 9.2, 7.7	9
Margin (S1-S3)	22.5	7.7	2.7, 3.0, 0.3	13(4+9+0)
Margin (S1-S3) @iteration 6	22.5	8.4	2.5, 5, 2.5	6(4+2+0)
OLE	22.5	9.4	1.7, 9.5, 7.7	2

In this scenario, the line operates in the linear regime. OLE, LOGO, and capacity

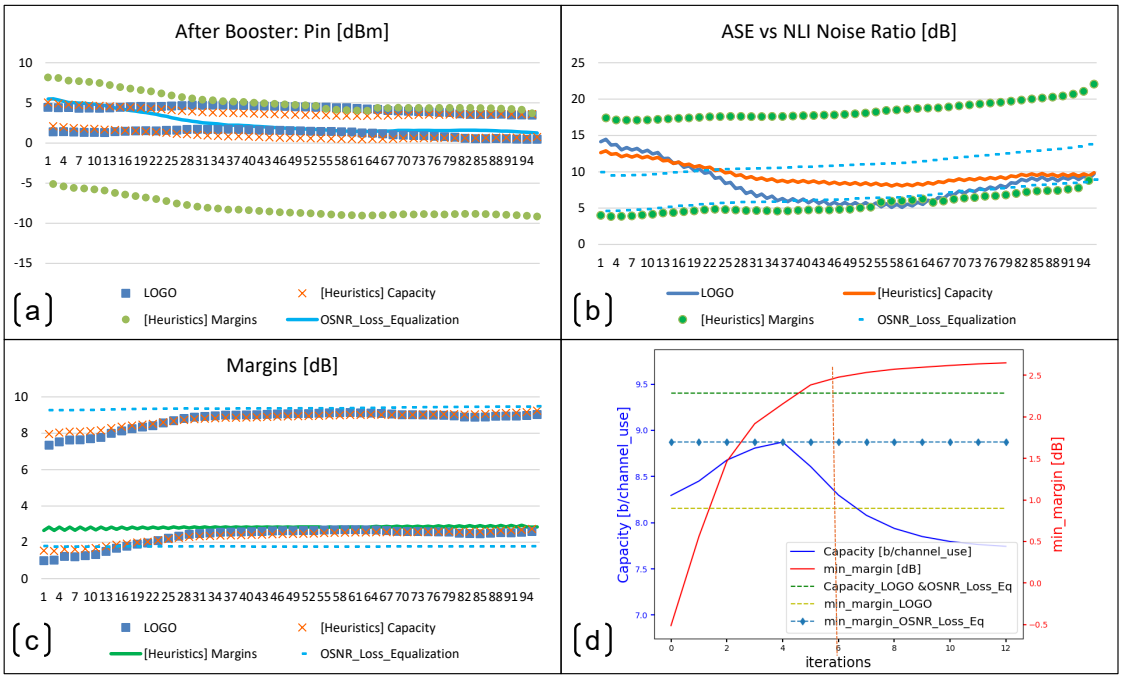

Figure 2.10: Equalization for a PSCF OMS, two baudrates, two FEC limits, and two grid spacings

heuristics return approximately the same capacity, but the margin equalizer returns lower capacity with the highest minimum margin (2.7dB) and all margins are within 0.2 dB. From Figure 2.10(d) the trade-off between the capacity and minimum margins can be seen. If we are not constrained by the capacity loss (18%) then we have a gain of 1 and 1.8 dB for the worst channel SNR margins when compared to the OLE and LOGO respectively (Figure 2.10(c)).

We defined parameter B (=10%) in the earlier section, which defines the amount of capacity that can be lost when optimizing margin. For this value of B, the algorithm stops at iteration 6 (identified with vertical dotted lines in Figure 2.10(d)), where the SNR margin is 2.5dB, i.e., 0.8dB higher than the OLE and 1.6dB than LOGO with only 10% capacity loss. Also after iteration 6, we have a minimal improvement in the minimum margins due to the fact that we are limited by the back-to-back SNR ceiling (BER floor). If the target is capacity then our capacity optimizer achieves the same capacity as LOGO but with a minimum margin improved by 0.6dB (from 0.9 to 1.5dB).

2.2.1.1 Application: robustness to aging

In this section, we show how our margin maximization technique makes OMSs more robust to aging. The SMF OMS was loaded with 120 channels at 34 Gbaud on a 50 GHz fixed grid (DP-16QAM) while the PSCF OMS was loaded with 80 channels at 68 Gbaud on a 75 GHz fixed grid (DP-16QAM).

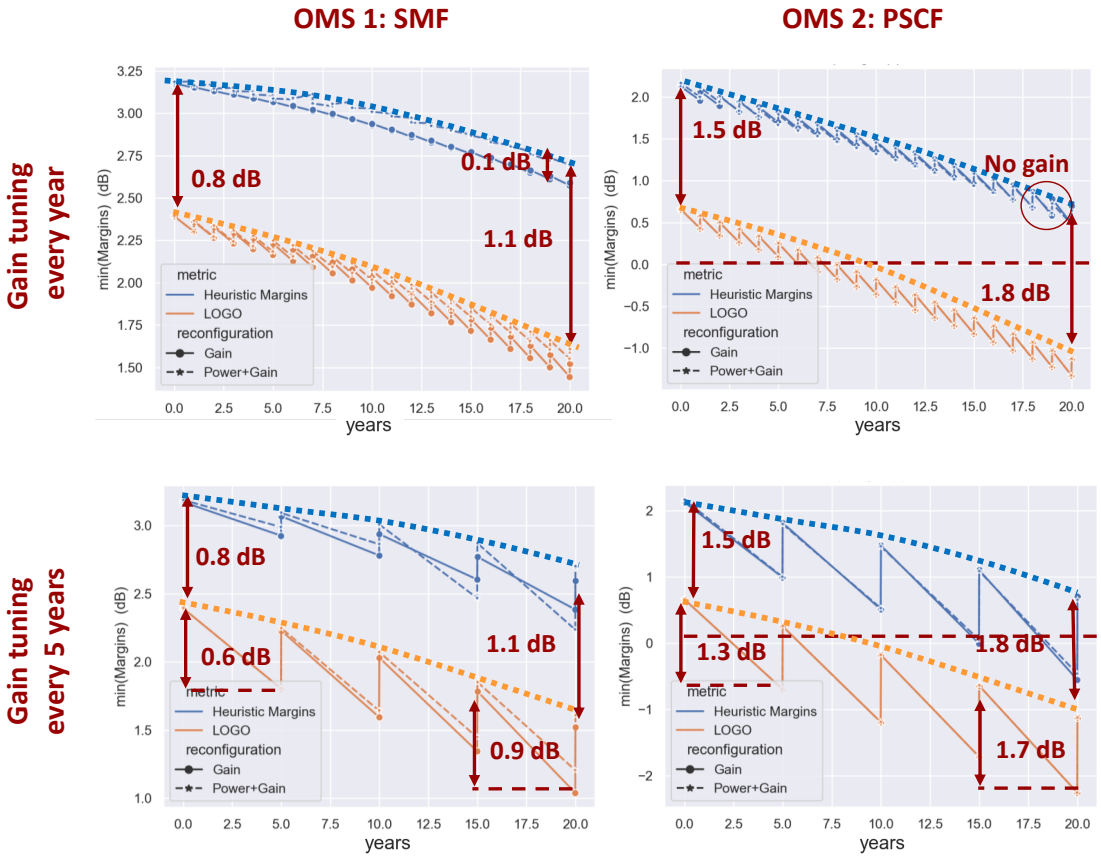

Figure 2.11: Robustness of the OMSs (SMF and PSCF) with SNR margin maximization

We emulated the aging of both OMS(lines) over 20 years by increasing the linear attenuation coefficient of the fibers by 0.0015dB/km/year yielding an extra attenuation of 2.4dB (resp. 3dB) for each 80km (resp. 100km) span over 20 years for the SMF line (resp. PSCF line). We periodically (every 1 or 5 years) adjusted the gains of the amplifiers to compensate for those losses. In addition, we optionally re-equalized the powers of the lines, and at the same time we reconfigured the amplifiers. The results are reported in Figure 2.11. The dashed lines depict upper envelopes (i.e., trends) of the margins for the scenarios where both power and gain are periodically re-optimized. The baseline is LOGO depicted in orange and our proposed SNR equalizer is depicted in blue.

We equalize the line at deployment time with our SNR equalizer. There is essentially no need to re-optimize the line later if the only impairment is attenuation degradation, as the line maintains its SNR margin throughout its life. The gain of additional periodic power re-equalization is at best 0.1dB with our method. Hence, we will consider only amplifier periodic re-optimization. At the beginning of life, the gap between our equalizer and LOGO is 0.8dB for the SMF line and 1.5dB for the PSCF line, as already seen. After 20 years, the gaps slightly increase, to 1.1dB (SMF) and 1.8dB (PSCF), which means that the (relative) robustness of the lines actually increase with time with our technique compared

with LOGO. This is because we operate the lines closer to the nonlinear threshold.

Worst-channel margin decreases with time, to 2.8dB (SMF) and 0.7dB (PSCF) with our method, up from 1.7 and -1dB with LOGO. In particular, on the PSCF line, with LOGO, the margin of some channels falls below 0dB after 7 years even with yearly re-optimization (and after only 2 years if amplifier re-optimization is done every 5 years), while no channel falls below FEC limit with our method.

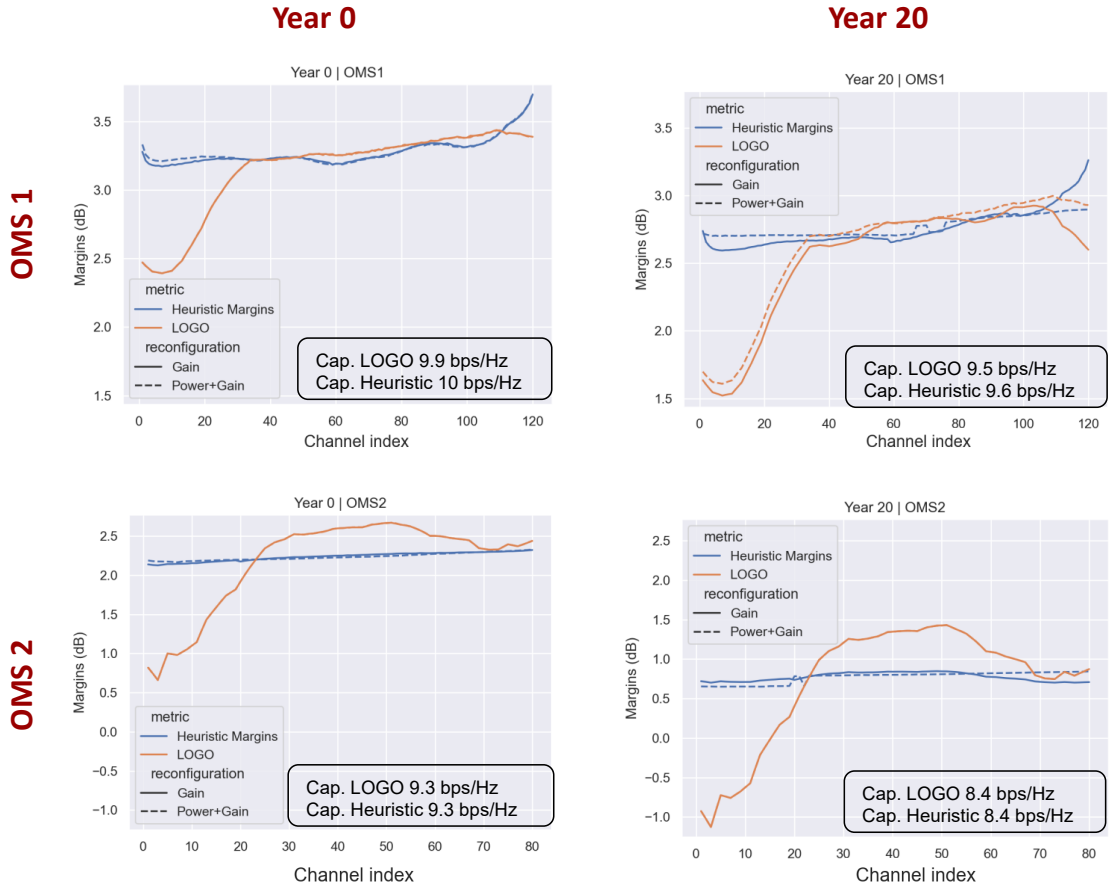

Figure 2.12: Margin spectra before and after OMSs aging and re-optimization

Figure 2.12 shows the spectra of the margins of the 2 OMSs before (Year 0) and after (Year 20) aging. After 20 years, a large ripple due to the combined effect of an EDFA gain ripple and SRS for the short wavelengths drive the SNR margin down for the LOGO flat power allocation, while the ripple completely disappears with our method. It can also be seen that with both power and gain periodic re-optimization, the margin with our technique is slightly flatter (blue curves, Figure 2.11 at Year 20).

2.2.1.2 Experimental validation

In this section, we report and describe the experimental validation of the equalization that we performed in the laboratory of the Huawei Paris Optics Lab. The goal of the experiment

is to validate and compare three equalization strategies: LOGO, OLE, and the heuristic algorithm.

Methodology

In order to set up the validation process, we first prepared the dummy light (DL) source to generate the desired WDM comb. This was accomplished by configuring the WSS of the DL source with the appropriate grid, interleaving odd and even channels into two different ports of the WSS. The generated DL comb was then transmitted along the OMS under analysis.

After this preliminary phase, we used an Optical Spectrum Analyzer (OSA) to probe the input and output ports of each EDFA in the OMS. The OSA measurements focused on two key aspects: the power levels and the spectral distribution of the optical signals. By placing the OSA at the input and output of each EDFA, we collected the total power and the power spectrum across all WDM channels. The OSA was set to a resolution bandwidth of 0.2 nm to ensure adequate spectral resolution while balancing the time required for data acquisition. These OSA measurements were cross-validated against the total power readings provided by the EDFA's internal monitoring system to ensure consistency and accuracy.

The process of probing with the OSA involved the following steps:

1. **Positioning the OSA:** The OSA was connected to the system at both the input and output ports of each EDFA, allowing us to capture the optical power levels and spectral data before and after amplification.

2. **Setting the Resolution Bandwidth:** A resolution bandwidth of 0.2 nm was selected to strike a balance between capturing sufficient spectral detail and maintaining a manageable acquisition time.

3. **Data Collection:** The OSA swept across the entire wavelength range of the WDM comb, recording the power levels and spectral distribution at each inline amplifier in the OMS. This provided a detailed view of how the power was distributed across different wavelengths and how it changed as the signals passed through each EDFA.

4. **Data Validation:** The collected data was validated against the total power readings from the EDFA's built-in monitoring system. This step ensured that the OSA readings were accurate and consistent with the expected power levels.

5. **Iterative Adjustment:** The data obtained from the OSA was used to compute the target power profile for each channel. The WSS attenuation profile was then adjusted accordingly, and the process was repeated to track any fluctuations in the line as the

gain of each amplifier changed with the input power spectral density. This iterative process continued until the desired power profile was achieved across all channels.

Once the OMS was properly configured, we probed each channel to measure the SNR by sweeping the WDM comb with an 8017 transceiver. For each spectral slot, the DL channel was removed and replaced with a modulated signal. The BER was measured and then converted into SNR. Afterward, the modulated channel was removed, and the DL channel was reinserted. This procedure was repeated for each spectral slot to ensure comprehensive coverage.

The use of an OSA in this experimental setup provides a detailed view of the power distribution across the WDM channels, making it a valuable tool for configuring and validating the system. However, there are inherent limitations associated with this method. The accuracy of OSA measurements can be influenced by factors such as the resolution bandwidth setting, the noise floor of the OSA, and the precision of the OSA's calibration. We used a resolution bandwidth of 0.2 nm for the data collection and the OSA can't be disclosed because of the propriety concerns. Additionally, the OSA itself may introduce variability due to slight changes in environmental conditions (e.g., temperature fluctuations) or inherent instrumental drift over time. To mitigate these issues, multiple measurements were taken, and the results were averaged to improve reliability.
Please observe that:

i) we are aware that probing all the inline amplifiers with an OSA is complicated and the operators do not intend to do it in the real field. Therefore, it is our intention in the future to replace this procedure with the integration of EDFA-AI (EDFA model that can calculate the wavelength-dependent gains and gain ripples based on the different loading conditions) with the optimization algorithms. In this way, the optimization will be able to track the fluctuations of the amlifiers without the need of any OSA measurement.

ii) In the WSS configuration we made use of the feedback from an OSA to achieve the target power profile and we are aware that OSAs are expensive and therefore, operators don't want to deploy them in their network. However, optical power monitors (OPM) are already deployed in commercial networks and they are used with the exact goal of replacing the OSAs in this kind of operation.

iii) While configuring the attenuation of the WSSs it was necessary to iterate the process in order to achieve the target profile. This happened because, while configuring the WSS, we targeted the power at the output of the booster and this changed the gain profile every time that the input changes. We operated this choice because it is expected to provide better performances since the ripple of one less amplifier is

involved in the propagation. However, by introducing EDFA-AI, we expect to reach the same performance by configuring either the input or the output of the booster amplifier.

Setup description

In our experiment, the transmitted comb is composed of 77 channels in the 75 GHz fixed grid, i.e. the C120 equipment has been used. The DL source has been realized by combining the EDFA 3.2, the EDFA 1-3.7, and the WSS 1.1 depicted in Figure 2.13. The filter width used for the DL channels is 68 GHz. To perform the validation we selected the OMS between the WSS 5.2 and the WSS 7.1 depicted in Figure 2.13. This OMS has five spans of 100 km PSCF fiber for a total covered distance of 500 km.

All the amplifiers can provide a maximum total output power of 22.5 dBm and, this scenario is power-constrained as the maximum output power is not enough to reach the NLT. Channels with different FEC limits were interleaved and assumed to be 'x' dB for the odd channels and 'x+1'dB for the even channels.

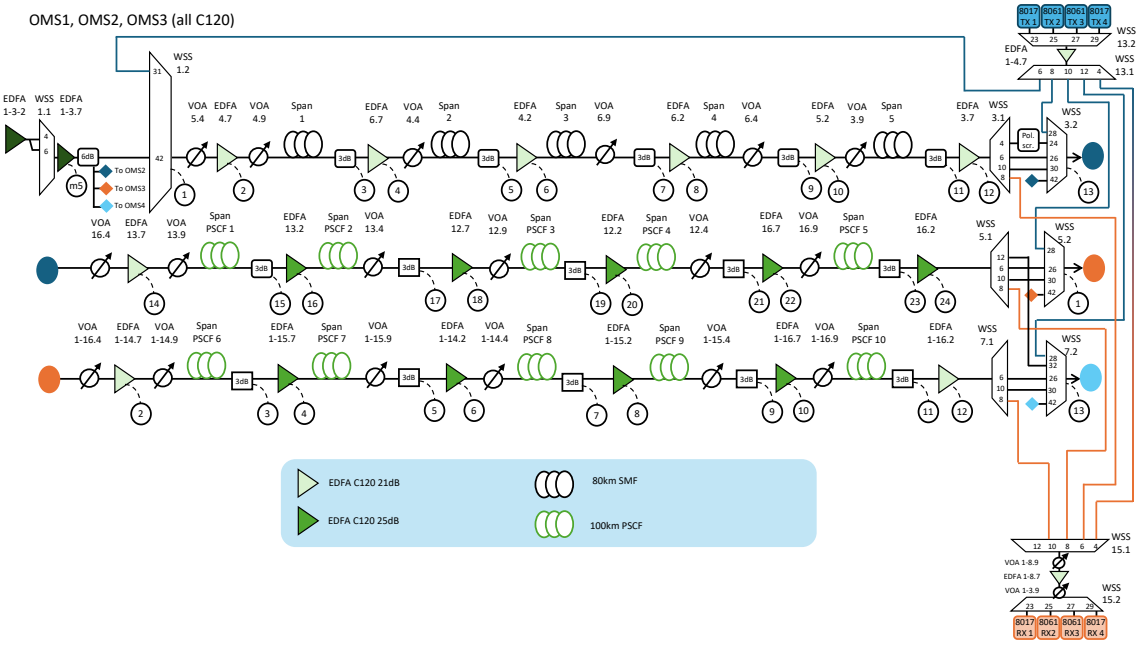

Figure 2.13: Expérimental Setup Description

Results

Figure 2.14 reports the target power profile (a), the measured SNR (b), and the margins (c) for the LOGO strategy (blue), the OSNR loss equalization (red), and the heuristic algorithm (green). Whereas, Table 2.7 reports the aggregated performance of each optimization strategy. We can observe that while using LOGO, the margins fluctuate between 6.1 dB and 9.1 dB for a variation of 3 dB which is the largest compared to the other two strategies. This limitation is mainly due to the neglection of all the frequency-dependent

effects such as the stimulated Raman scattering, the frequency variation of the attenuation, the amplifiers' ripple, and the dispersion slope.

On the contrary, the OSNR loss equalization is able to leverage the information on the signal power and the ASE noise power to properly adapt the transmitted power to the linear propagation impairments and the stimulated Raman scattering. The result is an improvement of 0.3 dB in the minimum margin with a very small loss in the average capacity with respect to LOGO. Finally, the heuristic algorithms leverage the knowledge of all the propagation effects plus the FEC limits. Because of this, the heuristic algorithm is able to improve the minimum margin by 1.1 dB with respect to LOGO and by 0.8 dB with respect to OSNR loss equalization. Moreover, the loss in average capacity is very small being only 0.2 b/s/Hz. This makes the heuristic algorithm the most robust solution in this case.

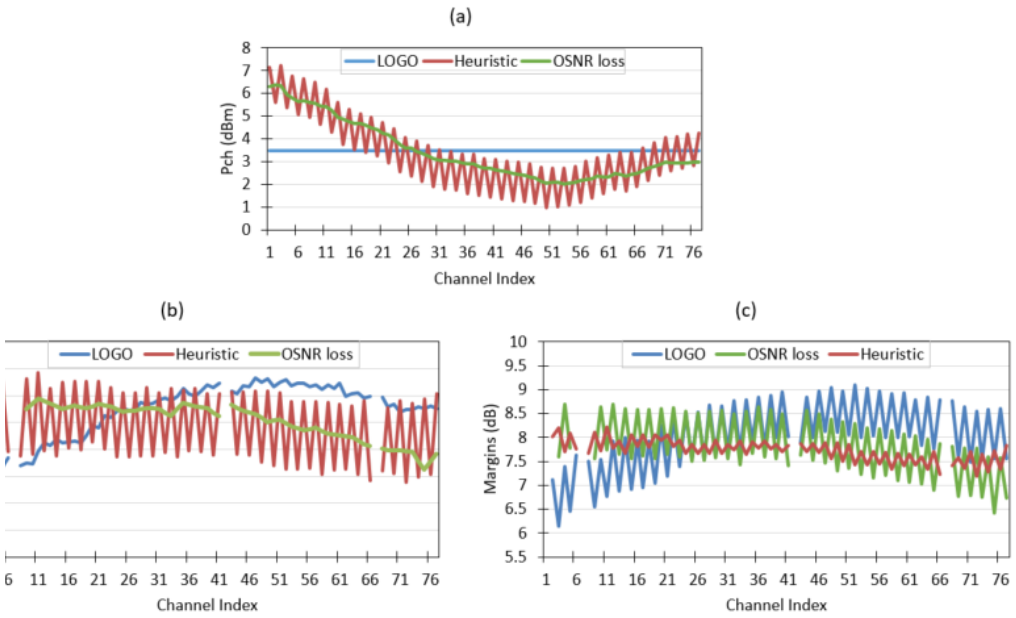

Figure 2.14: Target power (a), measured SNR (b) and Margins (c) of each equalization strategy.

Table 2.7: Summary table on the performance of each equalization strategy

Method	**Capacity (average) [b/s/Hz]**	**Minimum Margin [dB]**
LOGO	9.2	6.1
OLE	9.1	6.4
Margin Heuristic	9.0	7.2

2.2.2 Tandem Network Assesment

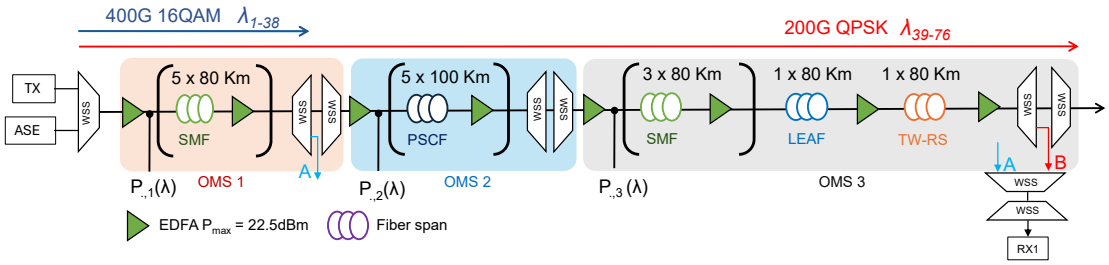

Figure 2.15: Tandem Network Setup

2.2.2.1 Simulations

In the intricate optical network architecture depicted in Figure 2.15, operational constraints are applied to the total output powers (Pmax) of the OMS1, OMS2, and OMS3, with values set at 18 dBm, 22.5 dBm, and 22.5 dBm, respectively. These constraints are essential for maintaining system integrity and performance. For the purposes of clear demonstration, a substantial back-to-back SNR (SNR_{B2B}) ceiling is employed. Table 2.8 catalogs key performance indicators such as capacity, margin, and computational efficiency—expressed in the number of calls to the QoT tool—across different operational cycles.

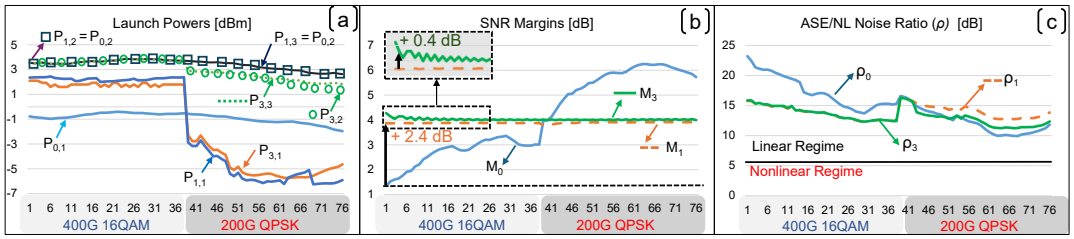

Figure 2.16: Simulations: equalization of a 3-OMS network (a) Launch power $P_{j,n}$ for all services (b) SNR margins M_j for all services at Cycle j. (c) Ratio ρ_j for all services at Cycle j on the n^{th} OMS

Figure 2.16(a) reveals a strategic underutilization of OMS2 and OMS3 during the initial cycle. This is attributed to the algorithm's prioritization, which results in all 16-QAM (Quadrature Amplitude Modulation) services being terminated post-OMS1, thereby maintaining the launch powers at the levels determined by the LOGO strategy ($P_{0,.}(\lambda) = P_{1,.}(\lambda)$). In stark contrast, Figure 2.16(b) elucidates the algorithm's power redistribution tactics in Cycle 1, which involve flattening the SNR margins (M1) on OMS1. Here, the generous SNR_{B2B} threshold facilitates the enhancement of SNR for the underperforming DP-16QAM services by re-distributing power from the more robust DP-QPSK services.

Proceeding to Cycle 2, the algorithm adopts a more inclusive approach by treating

Table 2.8: Simulation – cycles description

Cycles	**OMS 1**	**OMS 2**	**OMS 3**	**Capacity (Average) [bps/Hz]**	**Margins (min, max) [dB]**	**#Calls of QoT Tool (Step 1 + Step 2 + Step 3)**
LOGO	-	-	-	8.5	1.3, 6.2	N/A
Cycle 1	Improve margins	✗	✗	8.4	3.7, 3.9	14 (6+8+0)
Cycle 2	✗	Improve margins	Improve margins	8.5	3.8, 5.0	4 (2+2+0)
Cycle 3	Improve margins	✗	✗	8.5	4.1, 4.2	6 (2+4+0)

both DP-16QAM and DP-QPSK services as equally suboptimal, since the margins are equalized. Notably, the launch powers on OMS1 remain static, reflecting the algorithm's iterative optimization process, which has yet to address OMS2 and OMS3. It is during this cycle that improvements in the margins for DP-QPSK services on OMS2 and OMS3 are observed. Subsequently, Cycle 3 paves the way for the refinement of the previously lagging DP-16QAM services on OMS1, demonstrating the algorithm's capacity for sequential enhancement.

The comparative results delineated in Figure 2.16(b) are testament to the algorithm's efficacy. When juxtaposed with the baseline LOGO strategy, there is a significant increment in the minimum margin by 2.8 dB—an impressive gain realized through 2.4 dB in Cycle 1 and an additional 0.4 dB in Cycle 3. This optimization is achieved with a total expenditure of 24 calls to the QoT tool, underscoring the algorithm's operational efficiency. Such meticulous optimization serves not only to bolster system performance but also exemplifies the potential for sophisticated power management in contemporary optical networking, where each adjustment is meticulously calculated to enhance the overall Quality of Transmission.

2.2.2.2 Experiment

The proposed algorithm is validated using the experimental 3-OMS tandem network available in the Huawei Paris Research Center. The network consists of heterogeneous spans shown in Figure 2.15. 38 channels of 400Gbps each, using DP-16QAM (dropped after OMS1) and 48 channels of 200Gbps each, using DP-QPSK (dropped after OMS3) modulated services are allocated over a 75GHz fixed grid using a commercial 68GBaud 200/400 Gb/s (DP-QPSK/ DP-16QAM) transponder.

Lower wavelengths carry the 400G channels since they have the higher FEC limit. We can clearly visualize the advantage of the algorithm compared to the lower FEC limit channel. All the amplifiers gains and noise figures are experimentally measured and mapped into the QoT tool for the SNR calculation. The ASE noise has been loaded along the line to fill the empty portion of the spectrum for OMS 2 and OMS 3. We sweep a single transponder to obtain the SNR for all channels.

Figure 2.17(b) shows that after Cycle 1 we have improved the worst channel margin by 0.5dB. Margins cannot be flattened in Step 2 of Cycle 1 for OMS 1 because the 16QAM services are limited by the transponder SNR_{BtB} and the algorithm stops (Figure 2.17(c)). Further cycles would indeed re-allocate power to the BtB limited 16QAM services without any margin improvement, thereby degrading the overall capacity for no robustness gain. Furthermore, from Figure 2.17(a), we can observe that the launch power of OMS2 and OMS3 remains flat because the worst-performing channels are dropped after OMS1.

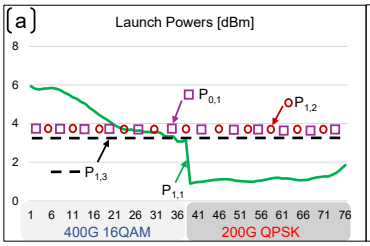

(c)

Cycles	OMS 1	OMS2	OMS3	Capacity (average) [bps/Hz]	Margins (min,max) [dB]	#Calls of QoT Tool
LOGO	-	-	-	8.7	1.9, 6.4	N/A
Cycle 1	Improve margins	×	×	8.7	2.4, 6.4	9 (7+0+2)

Figure 2.17: Experiment: (a) launch powers $P_{j,n}$ for all services on n^{th} OMS at Cycle j; (b) Margins M_j for all services at Cycle j; (c) Cycles

2.3 Validation of the Proposed Equalization Strategy for Partial Load

We have evaluated the proposed heuristics for the PSCF type of OMS for 4 loading configurations: 10 (deterministic and random), 40 (deterministic), and 80 (deterministic) **ON** channels respectively. Unless otherwise specified, the setup is as follows:

- OMS: 5×100km PSCF (24dB span loss including VOAs before/after the fiber), "power constrained" (P_{max} = 22.5dBm). This corresponds to the second (middle) OMS in Fig 2.13.

Similar to full load there is no filtering on those OMS. The effects that are modeled are: linear noise (based on real EDFA gain shapes measured in the lab for their nominal gain, and NF characterized in the lab), nonlinear noise (GN model), SRS, TRX back-to-back penalties. We first provide simulation results using the SNR estimation tool. We

compare our equalization heuristic with LOGO and OSNR loss equalization strategy. We then experimentally validate the simulation results.

2.3.1 Point-to-Point link Assesment

For each scenario, we show (a) the per-channel power after the OMS booster, (b) the ratio ρ, and (c) the SNR margin at the end of the OMS, for the following three strategies: LOGO, margin maximization, and OSNR loss equalization (OLE). The x-axis corresponds to channels ordered by increasing wavelength. We also report the total power, capacity, margin, and number of iterations for each step.

OMS equalization (PSCF), single rate, Multi FEC limit, 10 ch

For this scenario, we loaded OMS with 10 Channels modulated at 68 GBaud with 75 GHz spacing in the C120 band. We assume, there are 5 QPSK (high wavelengths) and 5 16QAM (low wavelengths) modulated channels respectively.

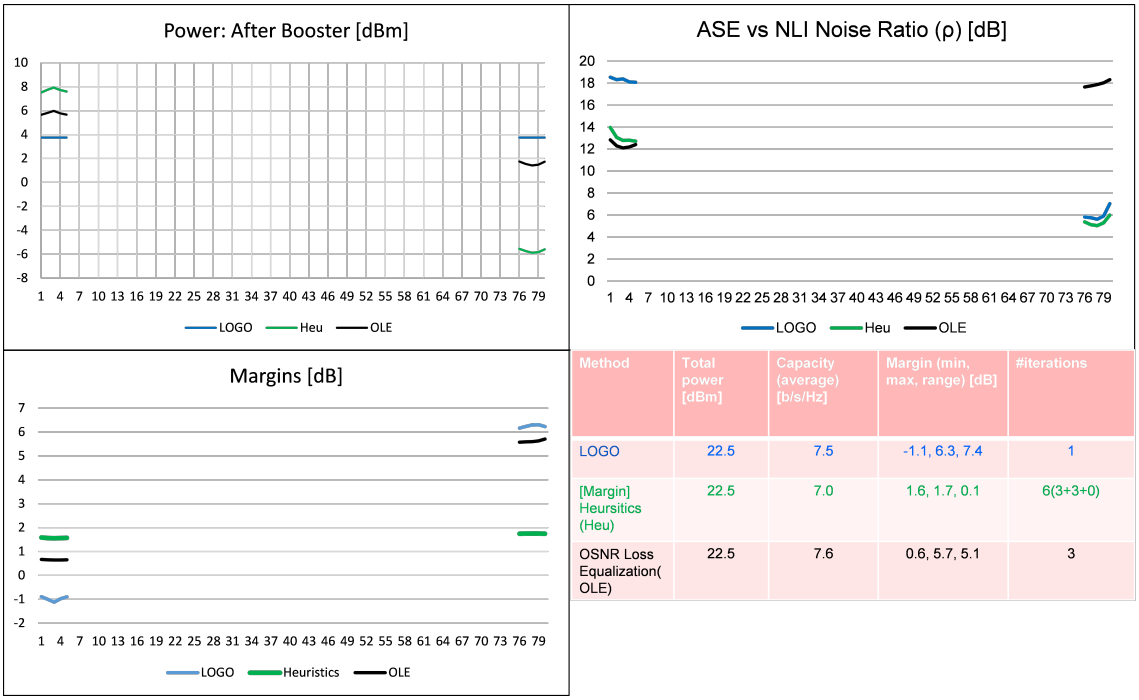

Method	Total power [dBm]	Capacity (average) [b/s/Hz]	Margin (min, max, range) [dB]	#iterations
LOGO	22.5	7.5	-1.1, 6.3, 7.4	1
[Margin] Heursitics (Heu)	22.5	7.0	1.6, 1.7, 0.1	6(3+3+0)
OSNR Loss Equalization(OLE)	22.5	7.6	0.6, 5.7, 5.1	3

Figure 2.18: Equalization for a PSCF OMS, multi FEC limit, 10 channels on

A large ripple of the C120 EDFA in the short wavelengths area strongly degrades the quality of the channels in this area (Figure 2.18(c)) and the SNR margin ranges between -1.1 to +6.3 dB (range: 7.4 dB) with LOGO. Our algorithms are able to remove this wavelength-dependent margin and all services now have an SNR margin of at least 1.6 dB (with a variation of only 0.1 dB over the whole C120 band). We have a 1 dB gain over OLE and 2.7 dB compared to the LOGO power allocation. The running time of the margin equalizer is 6 iterations, i.e., it needs to run the SNR estimation tool 6 times.

OMS equalization (PSCF), single rate, multi FEC limits, 40 ch

For this scenario, we loaded OMS with 40 Channels modulated at 68 GBaud with 75 GHz spacing in the C120 band. We assume, there are 20 QPSK (high wavelengths) and 20 16QAM (low wavelengths) modulated channels respectively.

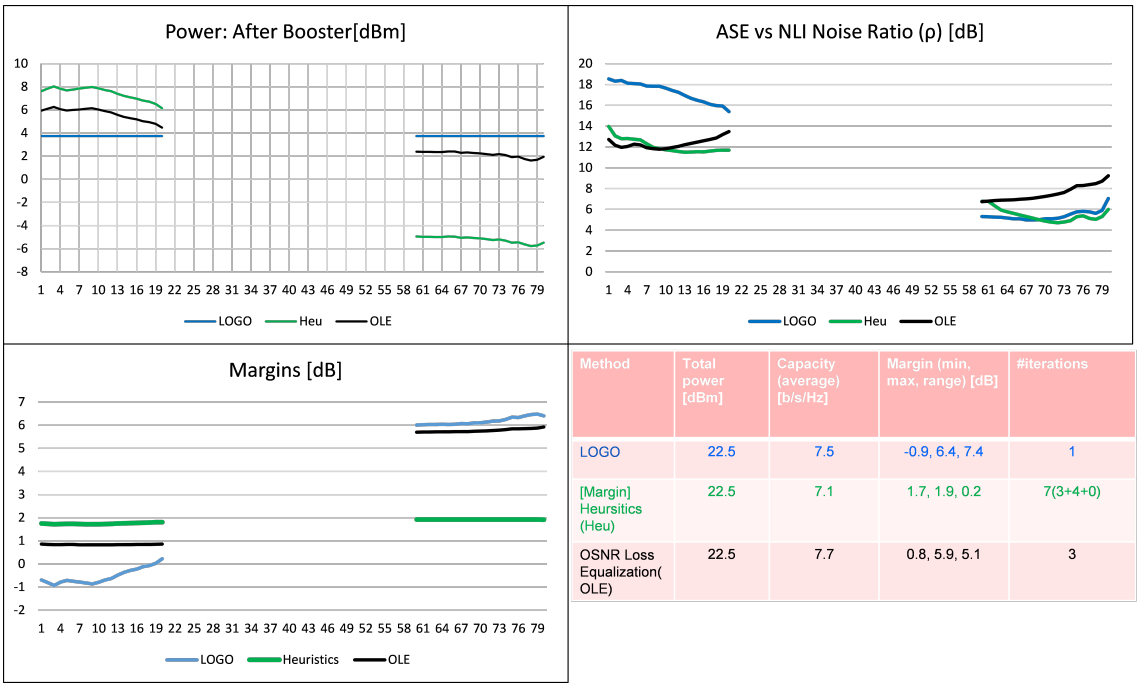

Method	Total power [dBm]	Capacity (average) [b/s/Hz]	Margin (min, max, range) [dB]	#iterations
LOGO	22.5	7.5	-0.9, 6.4, 7.4	1
[Margin] Heursitics (Heu)	22.5	7.1	1.7, 1.9, 0.2	7(3+4+0)
OSNR Loss Equalization(OLE)	22.5	7.7	0.8, 5.9, 5.1	3

Figure 2.19: Equalization for a PSCF OMS, multi FEC limit, 40 channels on

The C120 EDFA's ripple in the short wavelengths area strongly degrades the quality of the channels in this area (Figure 2.19(c)) and the SNR margin ranges between -0.9 to +6.4 dB (range: 7.3 dB) with LOGO. Our algorithms are able to remove this wavelength-dependent margin and all services now have an SNR margin of at least 1.7 dB (with a variation of only 0.2 dB over the whole C120 band). We have a 0.9 dB gain over OLE and 2.6 dB compared to the flat power allocation. The running time of the margin equalizer is 7 iterations, i.e., it needs to run the SNR estimation tool 7 times.

OMS equalization (PSCF), single rate, mixed FEC limits, full load

For this scenario, we loaded OMS with 80 Channels modulated at 68 GBaud with 75 GHz spacing in the C120 band. We assume, there are 40 QPSK and 40 16QAM modulated channels respectively. This scenario is not back-to-back limited.

The C120 EDFA's ripple in the short wavelengths area strongly degrades the quality of the channels in this area (Figure 2.20(c)) and the SNR margin ranges between -0.9 to +6.4 dB (range: 7.3 dB) with LOGO. Our algorithms are able to remove this wavelength-dependent margin and all services now have an SNR margin of at least 1.7 dB (with a variation of only 0.2 dB over the whole C120 band). We have a 0.9 dB gain over OLE and

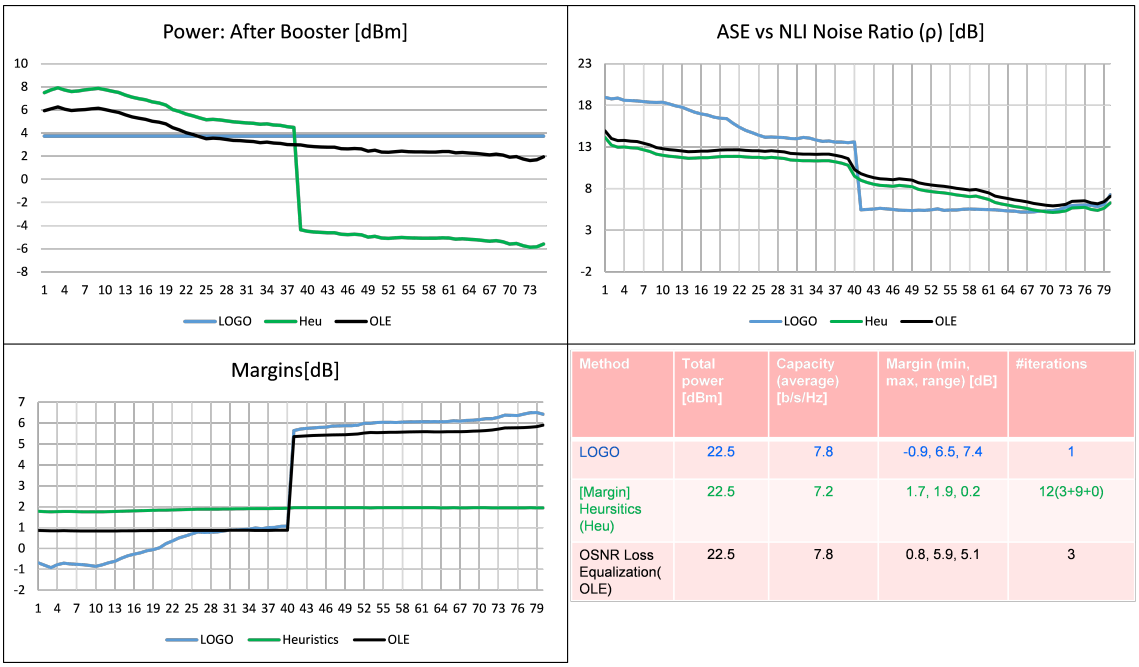

Method	Total power [dBm]	Capacity (average) [b/s/Hz]	Margin (min, max, range) [dB]	#iterations
LOGO	22.5	7.8	-0.9, 6.5, 7.4	1
[Margin] Heursitics (Heu)	22.5	7.2	1.7, 1.9, 0.2	12(3+9+0)
OSNR Loss Equalization(OLE)	22.5	7.8	0.8, 5.9, 5.1	3

Figure 2.20: Equalization for a PSCF OMS, multi FEC limit, 80 channels on

2.6 dB compared to the flat power allocation. The running time of the margin equalizer is 12 iterations, i.e., it needs to run the SNR estimation tool 12 times.

OMS equalization (PSCF), Random loading, mixed mod. format, 10 ch

For this scenario, we randomly loaded OMS with 10 Channels modulated at 68 GBaud with 75 GHz spacing in the C120 band. We assume, there are 6 QPSK and 4 16QAM modulated channels respectively.

We show in Figure 2.21, (a) the per-channel power after the OMS booster, (b) ratio ρ and (c) the SNR margin at the end of the OMS, for the following 3 strategies: LOGO, margin maximization and OSNR loss equalization (OLE). The x-axis corresponds to channels ordered by increasing wavelength.

The C120 EDFA ripple in the short wavelengths area strongly degrades the quality of the channels in this area (Figure 2.21(c)) and the SNR margin ranges between -0.9 to 6.4 dB (range: 7.3 dB) with LOGO. Our algorithms can remove this wavelength-dependent margin and all services now have an SNR margin of at least 1.6 dB (with a variation of only 0.1 dB over the whole C120 band). We have a 0.9 dB gain over OLE and 2.7 dB compared to the flat power allocation. The running time of the margin equalizer is 6 iterations, i.e., it needs to run the SNR estimation tool 6 times.

2.3.1.1 Experimental validation

We first acquire the line description by probing the input and output port of each EDFA by means of an OSA.

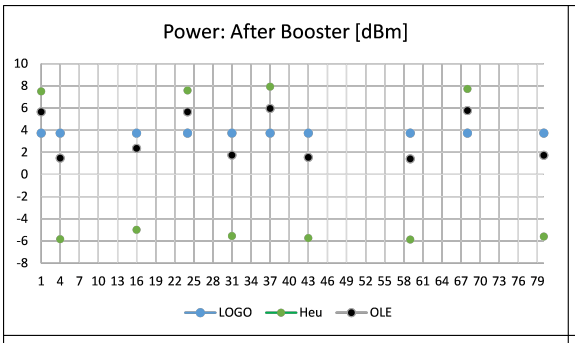

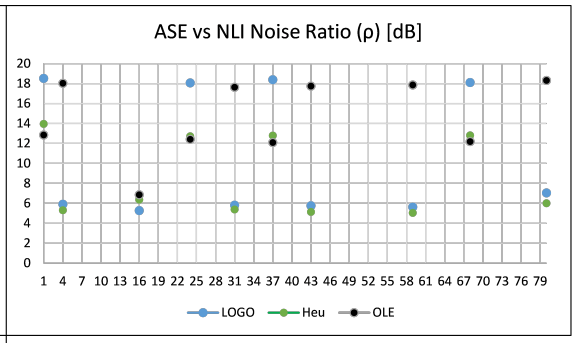

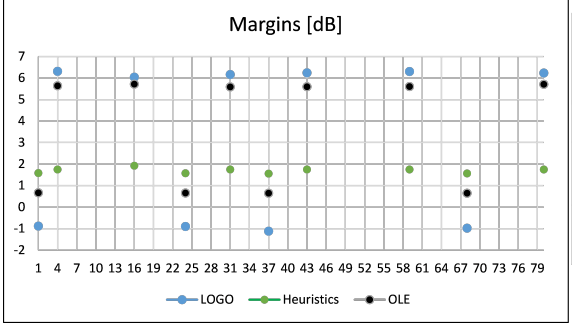

Method	Total power [dBm]	Capacity (average) [b/s/Hz]	Margin (min, max, range) [dB]	#iterations
LOGO	22.5	7.5	-1.1, 6.3, 7.4	1
[Margin] Heursitics (Heu)	22.5	7.0	1.6, 1.7, 0.1	6(3+3+0)
OSNR Loss Equalization(OLE)	22.5	7.6	0.6, 5.7, 5.1	3

Figure 2.21: Equalization for an PSCF OMS, multi FEC limit, 10 random channels on

Then, we used this measurement to compute the target power profile using each equalization strategy. After that, we configured the target profile by measuring the power spectrum with an OSA and by properly changing the attenuation profile of the WSS. Once the OMS had been properly configured, we probed each channel to measure the SNR by sweeping the WDM comb with a transceiver.

This initial probing step should be implemented with a spectrum estimation tool such as EDFA-AI in a commercial network, where the load changes with time. However, we observed that, once the gains were initially measured, they did not vary significantly when the heuristic was run and the channel powers were changed. This hints at a lack of need for EDFA-AI within the heuristic. EDFA-AI is needed to initialize the heuristic.

Setup description

In our experiment, the transmitted comb is composed of up to 80 channels in the 75 GHz fixed grid, i.e., the C120 equipment has been used. To perform the validation we selected the OMS between the WSS 5.2 and the WSS 7.1 depicted in Figure 2.13. This OMS has five spans of 100 km PSCF fiber for a total covered distance of 500 km. All the amplifiers can provide a maximum total output power of 22.5 dBm and, this scenario is power-constrained as the maximum output power is not enough to reach the NLT. Modulation formats are allocated as in the previous (simulations) section.

Results

Figure 2.22 reports SNR margins for each of the 4 considered loads the OSNR loss equalization (black) and the heuristic algorithm (green). Simulation results (plain lines or plain disk markers) are confirmed by the experiments (triangle markers).

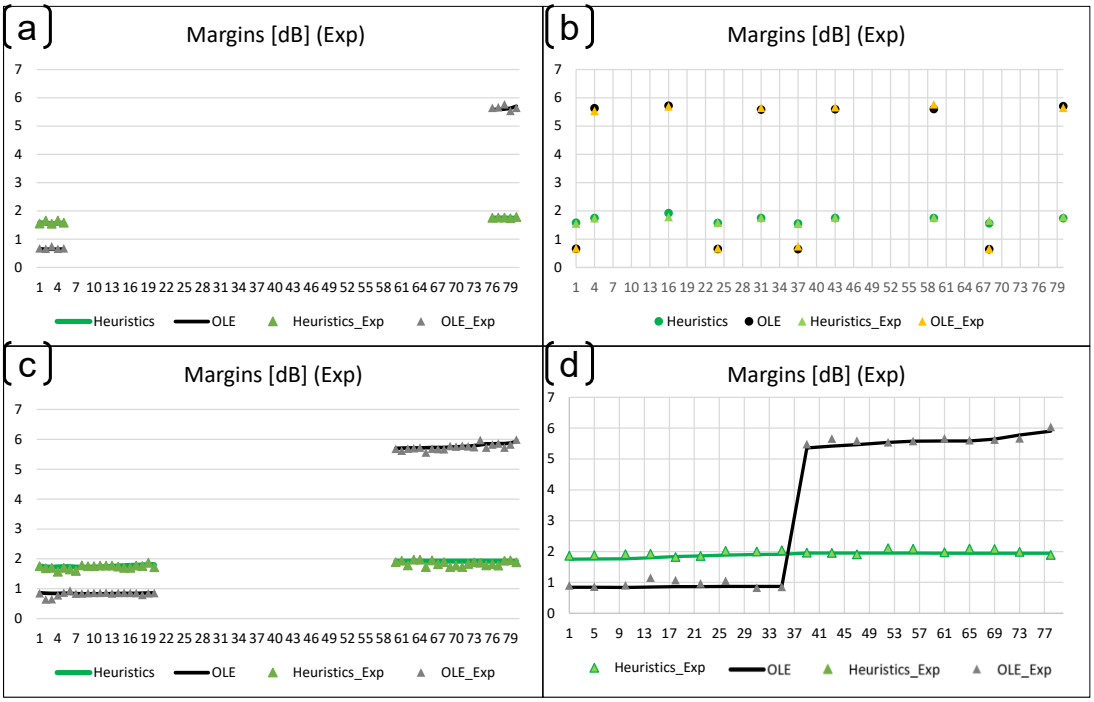

Figure 2.22: SNR Margins (a)10 channels (b) 10 random channels (c) 40 channels (d) 80 channels.

2.4 Conclusion

Traditional flat power allocation methods, such as LOGO, do not account for the SNR, resulting in unequalized SNR performance across all channels in the system. By focusing on SNR-aware methods, we equalize the performance of all channels, thereby boosting both the capacity and reliability in terms of SNR margins. We have proposed two optimization strategies: capacity optimization and margin optimization. These strategies take into account the SNR, as well as the ratio of ASE NLI noise, involving non-linear impairments to allocate per-channel power more effectively.

In our evaluation on a sample OMS, the SNR-aware equalization strategy demonstrated notable improvements: For different types of OMS, including those with single-rate and mixed modulation formats, the SNR-aware optimizations(capacity/margin) consistently enhanced performance. For example, on an OMS comprising of 5 SMF spans with 120 channels modulated at 34 GBaud with 50 GHz spacing, SNR margins improved by 0.8 dB compared to traditional methods like LOGO. Similarly on an OMS with 5 PSCF spans the minimum SNR margin has been increased by up to 1.5 dB compared to LOGO. The additional gain in the PSCF spans can be bounded to a lower non-linear threshold compared to the OMS with SMF fiber spans. In both cases using the capacity optimization, we have achieved an average capacity increase of approximately 0.2 b/s/Hz compared to LOGO. These results showcase the adaptability of the optimization strategies across various

configurations.

Similarly, for tandem networks with three OMSs comprising fiber spans of SMF and PSCF, the benefits of our equalization strategy were experimentally validated and the results are as follows:

- **Margin Optimization**: Improved the worst channel margin by 2.4 dB compared to the LOGO, enhancing the network's robustness and reliability.
- **Capacity Optimization**: Achieved an average capacity increase of approximately 0.2 b/s/Hz compared to LOGO, without extensive infrastructure changes.

We have tested our equalization strategies under partial load conditions (e.g., with 10, 40, and 80 channels), and the results maintained their efficacy with the experimental validations. For example, OMS comprising SMF spans with only 40 channels modulated at 68 GBaud, SNR margins improved by 2.6 dB compared to LOGO, demonstrating the robustness of the approach under varying traffic loads.

We have seen significant advantages by allocating power using the SNR-aware equalization approach, which considers all non-linear impairments such as wavelength-dependent fiber losses, SRS, SPM, and XPM, rather than using flat power allocations. This method not only improved network capacity but also enhanced reliability in terms of SNR margins. By using impairment-aware power allocations, we can achieve exact modeling and identify areas for optimization, thus avoiding the need for fixed margins for non-linearities and hence enabling more efficient resource utilization.

Looking ahead, we will extend this SNR-aware approach to complex network planning, incorporating advanced optical functionalities within an impairment-aware framework. This progression aims to further optimize network planning and performance, ensuring that optical networks can meet the growing demands of our digital era with greater efficiency and reliability. In the next chapter, we will introduce an impairment-aware network planning simulator that takes into account physical layer impairments during network planning. The dual-purpose simulator ensures that network-level optimizations do not adversely affect the physical layer. This capability will facilitate the integration of various emerging optical functionalities and allow us to study their impacts comprehensively. By addressing both physical layer impairments and network planning activities, the simulator aims to enhance the capabilities of optical networks.

CHAPTER 3

Impairment Aware Optical Network Planning Tool - PyFIOA

3.1 Introduction

To accommodate the rapid traffic growth and keep pace with technological advancements like the Internet of Everything, ONs must undergo constant upgrades. Since the first commercial deployments in the late 1970s and early 1980s, the traffic carried by telecommunication systems has increased by more than four orders of magnitude, with switching system capacity growing by three orders of magnitude. ONs are categorized into access, metro, and core segments, each defined by their reach, capacity, and equipment type. Continuous upgrades in these segments are essential to provide higher bitrates to end users. With advancements in WDM technology, EDFA, complex modulations, coherent detection, and photonic integrated devices, the capacity and reliability of long-haul transmissions have dramatically improved. Emerging technologies like SDM and MMF further enhance network capacity.

Technological innovations have significantly transformed the perception of optical fibers, moving away from the outdated view of them as mere 'dumb optical pipes'. Concepts such as SDN and NFV have introduced programmability and flexibility, facilitating efficient network management and resource allocation. Despite these advancements, optics currently play a limited role in executing higher-level network functions like switching, routing, regeneration, or wavelength conversion. Various OFs such as wavelength converters, ptical packet switching, etc.. have been explored to perform these functions directly in the optical domain. The development of all-optical networks to perform signal processing and switching within the optical domain has proven to reduce energy requirements and end-to-end latency. However, the commercialization of emerging technologies from research labs for both data and control planes remains challenging unless they demonstrate substantial impact on ONs. Therefore, any state change in ONs through the integration of new

advancements must be carefully analyzed to evaluate its overall performance and justify network upgrades.

A variety of simulators have been developed to study the impact of technological advancements at the physical and data plane on network behavior. However, existing tools either focus on detailed physical layer impairments without integrating broad network planning, or excel in network traffic management but lack accuracy in QoT. Moreover, current simulators do not provide an agile way to incorporate new OFs. For instance, integrating quantum key distribution for physics-based security remains challenging with existing tools, as they cannot evaluate its effects on both control and data planes within WDM networks. Our proposed simulator aims to address these gaps by integrating QoT estimation and verification at the core of the path computation process, while also offering a generic data model to seamlessly include new OFs. This integrated approach ensures comprehensive network planning and the ability to adapt to new technological advancements, providing a robust solution for future optical network challenges. It is important to note that a portion of the content presented in this chapter has been previously presented at the NoF 2023. The NoF 2023 paper is cited as reference [40]. The insights and findings from the NoF 2023 paper provide a foundational basis for the discussions and analyses presented herein.

3.2 Overview of existing ON simulation tools

There are several optical simulator tools on the market (Fig. 3.1): from the one focusing solely on optical components to the ones more network-oriented. OptSim [27] and OptiSystem [28] are both examples of such simulators. OptSim, developed by RSoft Design Group (now part of Synopsys), focuses on the design and analysis of single-mode fiber-optic. OptSim supports a wide range of modulation formats and includes advanced simulation capabilities for modelling optical components, signal propagation, and system performance. OptiSystem, on the other hand, is developed by Optiwave Systems and offers a comprehensive design environment for modelling, analysing, and optimising both single-mode and multimode fiber-optic communication systems.

The VPI Photonics Simulator [41] is a comprehensive tool widely used in optical communication systems for designing, analyzing, and optimizing photonic networks. It excels in detailed modeling of optical components and signal propagation, supporting advanced features like coherent transmission and WDM. However, VPI Photonics has limitations in network planning and the seamless integration of new OFs. It focuses primarily on component-level simulations and lacks advanced tools for holistic network planning, which involves optimizing network topology, routing, and resource allocation. Additionally, it struggles with the agility required to incorporate and evaluate emerging technologies.

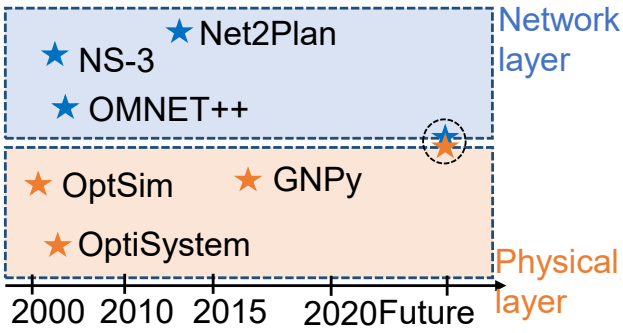

Figure 3.1: Illustrative timeline positions of various simulators

The evolution of the physical layer in ONs data-plane has led to enhanced flexibility and configurability in the photonic transmission medium. This progress gave rise to the development of Elastic Optical Networks (EON) [42] approximately ten years ago, a concept that has since matured and reached a consolidated state in the present day [43]. In this context, a plethora of ONs estimation models in ONs have been proposed in the last 30 years to assess optical signal performances. Their key challenge today is the ability to capture the nonlinear effects in the fibers, typically classified as either scattering effects (stimulated Brillouin and Raman scatterings) or caused by the Kerr effect that is the dependence of the refractive index on the signal power, producing impairments like self and cross-phase modulations, and four-wave mixing.

The introduction of the GN model in 2012 shook the field of QoT, by providing a simplified and manageable form for the nonlinear impairment estimation in the optical fibers, while retaining a very good accuracy. Multiple recent works employ GN-model extensions of classical calculations to study QoT performances of optical circuits, which are validated in lab testbeds [44–47]. In this context GNPy [20] is a relevant initiative in this regard given its open-source community-driven philosophy for QoT estimation based on the GN model. The QoT module is constantly updated to keep up with the transponder upgrades, to support EON. However, even though GNPy could perform the QoT estimation, it would need additional modules to perform the network planning and optimization, hence making it an incomplete tool.

Similarly for the network layer, a variety of simulators have been developed to perform the network operations. OMNeT++ [29] is an open-source modular, component-based simulation library particularly popular for modelling communication protocols, queuing networks, and evaluating the performance of various network types. While OMNeT++ can be extended to model optical networks, it does not provide built-in support for optical network simulations. Similarly, NS-3 [30] is an open-source, discrete-event network simulator primarily focused on the simulation of IP-based networks that can be extended to support ONs. In this context Net2Plan [31] was initiated in 2011 as a stand-alone tool for

the ON planning and optimization. The major drawback with Net2Plan is the absence of an QoT estimator.

Recently, an enhanced optical extension for Mininet has been suggested through the software-defined packet-optical network emulator [48]. This software suite, proposed by Lanz et al. [48], has the capability to emulate QoT performances at the optical data layer, such as Optical Signal-to-Noise Ratio (OSNR), and relay their impact to the Software-Defined Networking (SDN) controller. This emulation is achieved by enriching packets in conventional Mininet instances with wavelength/channel information, which is then used in adapted instances of Open vSwitch. Essentially, the entire Mininet-Optical emulation hinges on a software structure that triggers the Open vSwitch instances as sub-processes. However, this method deviates from practical deployment/production scenarios where optical systems are governed by their own lightweight software agent, housed within dedicated physical or virtual resources.

In today's context, the ideal situation for a network operator would be to have automated networks that can update, provision, and upgrade network capacities with minimal human intervention, drastically reducing deployment time and costs. To enable this, we need a stand-alone simulator that can capture the interactions of data layer elements when specific network operations are performed from the control plane. Such simulator could be designed to allow us to study the impact of emerging Optical Functionalities (OFs) like quantum key distribution (QKD), wavelength converters, and optical packet switching, etc...

By integrating OFs into the simulator, network operators can comprehensively evaluate the effects of these new technologies on existing infrastructures. This includes understanding how OFs influence network performance, capacity, latency, and energy consumption. For example, the integration of QKD can provide enhanced security by enabling quantum-based encryption, which is vital for protecting sensitive data in transit. A simulator that accurately models these effects helps operators make informed decisions about upgrading their networks to include such functionalities. Moreover, a simulator that integrates both physical and network layer interactions enables holistic network planning and optimization. This integration ensures that the simulator can account for real-world conditions, such as non-linear fiber impairments and dynamic changes in network topology. Consequently, operators can optimize resource allocation, improve quality of transmission (QoT), and increase overall network efficiency. This comprehensive approach reduces the risk of unforeseen issues during deployment and allows for more reliable and resilient network designs.

Additionally, the ability to simulate and validate new OFs within a cohesive tool accelerates the innovation cycle. Researchers and developers can test and refine their technologies in a virtual environment before physical deployment, saving time and reducing

costs associated with trial-and-error in real-world settings. This agility fosters a faster response to technological advancements and market demands, ensuring that networks remain competitive and capable of supporting the latest applications and services.

In summary, a stand-alone simulator with integrated OFs and robust physical and network layer modeling offers significant advantages. It supports automated, efficient, and cost-effective network management, facilitates the adoption of cutting-edge technologies, and enhances the overall performance and security of optical networks. This comprehensive tool is essential for advancing the capabilities and reliability of future optical communication system

3.3 Proposed Optical Network Simulator

3.3.1 Overview and Architecture

The objective of our work is dual. We first aim to build a simulator that merges both physical impairments (data plane) and network operations (control plane) to evaluate the network performance. We also consider the integration of OFs, eventually in a generic way, to be easily added and tested.

Different network operations can be performed with our proposed simulator. In this chapter, we focus on the network planning during the offline stage and explain the modular design of the simulator to easily integrate any OF and perform network planning. Network planning involves several key activities, such as determining the optimal network topology, routing and wavelength assignment (RWA), and accounting for physical layer impairments. These activities are essential for designing efficient, reliable, and cost-effective optical networks.

The proposed ON simulator is composed of different modules such as Network Topology, RWA and Physical layer as shown in Fig. 3.2. The different modules communicate among themselves for the network operations. In the following sections, we explain how these three modules have been integrated into a single tool for complex network planning operations.

3.3.1.1 Network Topology

The Network Topology (NT) module is responsible for defining the structure of the ON. It includes the nodes with their connectivity degree and the links with their spectral bandwidth. When describing the structure of the node, we are able to include all the node-related network element information such as transponders, wavelength selective switches (WSSs), reconfigurable optical add-drop multiplexers (ROADMs), etc. We can also add specific OFs such as wavelength converters (WCs), QKD sources to implement, etc. Similarly, for the links we include the number of spans, the fiber type and the fiber length of

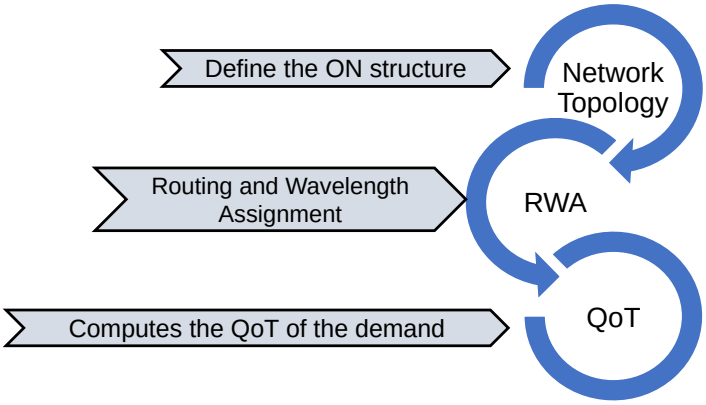

Figure 3.2: Architecture of the Proposed Simulator

each span along with the amplifier information. To provide the capacity of the links, we describe the number of slots and the available wavelengths on each link. This information can be used to control the spectral bandwidth of the links in the network. It allows to demonstrate the feasibility of both fixed and flexible grid ONs, hence implementing Elastic Optical Networks (EON).

Our simulator can read the topology from a file or create a new one when no file is provided. NetworkX is an open-source Python library [49]. We use it to initialize the topology, for the creation, manipulation, and analysis of complex networks as graphs. The NT module is used to represent the state of the network in our simulator.

Once we have defined the Network Topology (NT), any network planning activity requires a traffic matrix, which is composed of a list of connection requests that need to be served. The traffic matrix specifies the volume of traffic between each pair of source and destination nodes in the network. Connection requests in the traffic matrix are characterized by various parameters such as bandwidth requirements, latency, jitter, minimum Signal-to-Noise Ratio (SNR) requirements, priority, and other Service Level Agreements (SLAs). These parameters ensure that the network can meet different performance and quality requirements for various types of services.

To generate a traffic matrix, we can create connection requests randomly between different nodes. This random generation can be controlled to reflect realistic traffic patterns and network demands. For instance, bandwidth requirements can vary significantly between different connections, ranging from low-bandwidth connections for standard data transfers to high-bandwidth connections for video streaming or large data backups. Similarly, other parameters like latency and priority can be assigned based on the type of service being requested. This approach ensures that the traffic matrix accurately represents the diverse needs of the network's users.

In the context of our simulator, the traffic matrix can be generated using probabilistic

models or predefined distributions that reflect typical network usage. For example, we can use a Poisson distribution to model the arrival of connection requests or a uniform distribution to assign bandwidth requirements randomly. Additionally, real-world traffic matrices provided as files can be imported directly into the simulator, enabling it to process specific connection requests based on historical data or planned network expansions.

Once the traffic matrix is generated, it serves as the basis for network planning and optimization. The simulator processes the connection requests in the traffic matrix according to the Traffic Serving Order (TSO), which prioritizes the requests based on their SLAs and other criteria. As the simulator serves each request, it updates the traffic matrix to reflect the current state of the network, ensuring that all connection requests are handled efficiently and according to their specified requirements.

By using a traffic matrix that includes a variety of connection requests with different bandwidths and other SLAs, our simulator can thoroughly evaluate network performance under diverse conditions. This would enable network operators to optimize their networks for maximum efficiency, reliability, and quality of service, ensuring that they can meet the demands of modern optical communication systems.

3.3.1.2 RWA

In Wavelength Division Multiplexing (WDM) optical networks, a connection request is sent from a source node 's' to a destination node 'd' using a wavelength channel called a lightpath. To establish a lightpath, a route must be chosen, and a particular wavelength must be assigned to it. This process is known as the routing and wavelength assignment (RWA) problem, which is a critical aspect of network planning. The RWA problem involves two main tasks: selecting the best route from the source to the destination and assigning an available wavelength to the chosen route.

Routing Algorithms:

To determine the optimal route, various algorithms can be employed:

- **Shortest Path Algorithms**: Algorithms like Dijkstra's and Bellman-Ford are commonly used for finding the shortest path between two nodes. These algorithms minimize the total distance or cost between the source and destination.
- **k-Shortest Paths Algorithm**: This algorithm finds multiple paths between the source and destination, providing alternatives in case the shortest path is unavailable. It enhances network reliability and load balancing.
- **Constraint-Based Routing**: These algorithms consider multiple constraints such as bandwidth, latency, and QoT requirements to find the best path. Examples include Constrained Shortest Path First (CSPF) and Multi-Constraint Shortest Path (MCSP).

- **Load Balancing Algorithms**: These algorithms distribute traffic evenly across the network to prevent congestion and optimize resource utilization. Examples include Equal-Cost Multi-Path (ECMP) routing and load-adaptive routing.

- **Heuristic and Metaheuristic Approaches**: Algorithms like Genetic Algorithms, Ant Colony Optimization, and Simulated Annealing are used for more complex and dynamic routing scenarios.

For our simulator, we have chosen the k-shortest path algorithm from NetworkX for routing. This algorithm provides flexibility by offering multiple alternative paths, which is beneficial for maintaining network resilience and balancing traffic loads. However, it is important to note that our routing strategy also incorporates constraint-based path selection. Specifically, we take into account QoT metrics, bandwidth requirements, and other relevant constraints to ensure optimal network performance. These constraints are detailed in the physical layer impairments section, which explains how QoT and other factors influence path selection. While k-shortest path forms the basis of our routing approach, the integration of constraint-based criteria ensures that the selected paths meet the necessary performance standards. However, the choice of routing algorithms is arbitrary, and users can select other algorithms available in NetworkX or add more complex routing approaches as needed.

Wavelength Assignment Algorithms:

Once a route is determined, the next step is to assign a wavelength to the lightpath. Several algorithms can be used for wavelength assignment:

- **First-Fit Algorithm**: This algorithm assigns the first available wavelength to the lightpath. It is simple and fast but may not always yield the most efficient utilization of wavelengths.

- **Best-Fit Algorithm**: This algorithm selects the wavelength that best fits the current traffic load, aiming to optimize the use of available wavelengths.

- **Random-Fit Algorithm**: This algorithm randomly selects an available wavelength, which can help distribute traffic more evenly across the spectrum.

- **Least-Used Algorithm**: This algorithm assigns the least-used wavelength to balance the load across all wavelengths and prevent certain wavelengths from becoming congested.

- **Most-Used Algorithm**: Conversely, this algorithm assigns the most-used wavelength to pack traffic tightly and leave other wavelengths free for future connections.

For simplicity, we have initially implemented the first-fit algorithm for wavelength assignment in our simulator. This algorithm is straightforward and ensures that connection requests are processed quickly. However, more complex algorithms can be integrated at a later stage to enhance the efficiency and performance of the wavelength assignment process.

The design of our simulator allows users to customize both the routing and wavelength assignment processes. Users can choose from a variety of routing and wavelength assignment algorithms provided by NetworkX or implement their own. This flexibility ensures that the simulator can be adapted to different network scenarios and research requirements.

In future versions, we plan to include more sophisticated routing and wavelength assignment algorithms. These enhancements will provide better optimization, improved QoT, and more efficient resource utilization, making our simulator a robust tool for comprehensive network planning and performance evaluation.

3.3.1.3 Physical Layer Impairements (expressed as SNR)

For every connection request, followed by the route and the wavelength assignment we calculate by simulation the QoT associated to the physical layer. The performance of the coherent optical fiber system has been conventionally measured as OSNR which includes only signal distortions from the ASE noise. This approach becomes highly inaccurate for the modern WDM networks. A generalised SNR, that characterizes all the linear and non-linear impairments calculated at the end of the link, is a more accurate metric to use.

$$\frac{1}{\mathrm{SNR}} = \frac{1}{\mathrm{SNR_{Lin}}} + \frac{1}{\mathrm{SNR_o}} + \frac{1}{\mathrm{SNR_{NL}}} \tag{3.1}$$

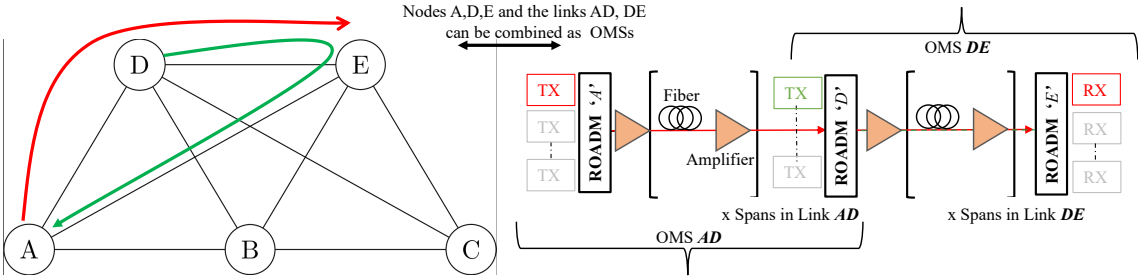

Figure 3.3: OMS formation from the NT information

To compute the SNR, once the route and the wavelength are selected, we must characterize the lightpath for the physical impairments. To compute this, we need to combine the information available from the NT to be aware of all the network elements that the request/lightpath is traversing. We combine the information of the nodes and the links under several Optical Multiplexing Sections (OMSs). For example, the red lightpath connection requested from Node A to Node E, shown in Fig. 3.3, goes through two OMSs: AD and DE. To calculate the SNR of this path, we have to include all the impairments

that accumulate when traversing different network elements such as ROADMs, fibers, amplifiers, and transponders (red TX & RX in the Fig. 3.3) of both OMSs. The impact of these different elements has been listed in Table 3.1 in the decreasing order of their impact on the WDM system's SNR.

Table 3.1: Factors impacting the WDM System Performance

Factor	***Source of Influence***	***Comments***
SNR_{Lin}	Amplified Spontaneous Emission (ASE) noise of the amplifier	Limits the transmission distance of a WDM system
Back-to-Back (BtB) SNR_o	Transmit coding and modulation rate, and receiving mode of the transponder	Impact can be reduced using coherent reception, digital signal processing (DSP) equalization, etc.
Non-linearity	Line transmission optical fiber	SNR of the signal is affected by all the co-propagating signals.
Optical filtering	ROADM	The filter bandwidth should be optimised, and a certain margin of SNR should be reserved.

Apart from these factors, there are several other physical impairments such as chromatic dispersion (CD) and polarization mode dispersion (PMD) that can be fully compensated by the DSP of a coherent receiver. In our simulator we focus on the coherent systems for now, but the modularity of the simulator will allow to use Intensity Modulation with Direct Detection (IM/DD) systems too (explained in Section 3.3.4). To take into account the polarization dependent losses (PDL) that arise from the components, we can reserve a certain SNR margin. Finally, the lightpath's SNR can be written as a sum of the linear Back-to-Back (BtB) and the non-linear factors respectively as they all can be modelled as additive Gaussian noises[50].

Many efforts have been made to estimate correctly the lightpath's SNR [19, 51, 52]. Fast and accurate closed-form models derived from the GN model and its enhanced version (EGN), were proposed and used in building QoT models such as GNPy developed by V. Curri in [20].

To model the SNR with accuracy, we chose to implement the closed-form approximation of the ISRS GN model proposed in [53]. This model reduces Eq (3.1) to

$$\frac{1}{\text{SNR}} = \frac{P_{\text{ASE}}}{P_{\text{sig}}} + \frac{1}{\text{SNR}_{\text{o}}} + \frac{\eta {P_{\text{sig}}}^3}{P_{\text{sig}}} \tag{3.2}$$

where P_{sig} is the lightpath's launch power and P_{ASE} is the accumulated ASE noise originating from the amplifiers. It can be calculated as the cumulative sum of all the ASE noises from the amplifiers (number of spans (n) +1) the lightpath traverses as shown in Eq (3.3). Each amplifier is characterized by its noise figure (NF), its gain (G), and output power (P) profile. h is the Planck's constant, f is the optical frequency of the lightpath (determined by its wavelength) and B being the resolution bandwidth of the ASE measurement.

$$\frac{1}{\text{SNR}_{\text{Lin}}} = \sum_{i=1}^{n+1} \frac{hf(G_i - 1)NF_iB}{P_i} \tag{3.3}$$

Power evolution along the OMS i.e., P_i can be computed to include Inter-channel Stimulated Raman Scattering (ISRS) effect along the fiber by solving the continuous-wave Raman equations using the triangular approximation proposed in Eq 4 of [22] in addition to the fiber loss and compensating amplifier's gain. The lightpath's non-linear noise power η at the end of each OMS is dependent on the channel frequency and is calculated as a sum of the SPM and XPM effects that include the impact of the powers of the M co-propagating signals on the OMS. They can be calculated using XPM as Eq 17 and SPM as Eq 18 of [23].

$$\frac{1}{\text{SNR}_{\text{NL}}} = \sum_{j=1}^{M} (\eta_{\text{SPM}} + \eta_{\text{XPM}})_j P_j^2 \tag{3.4}$$

Now from Eq (3.3) and Eq (3.4) we can compute the linear and the non-linear components of the lightpath's SNR for each OMS. When calculating the total SNR for a lightpath that crosses various OMSs, we must aggregate both the linear and non-linear components of the SNR from each OMS. Additionally, the BtB SNR, derived from experimental characterization, must be incorporated into this total (Eq 3.2). Given that the lightpath navigates through multiple OMSs, the noise from the ROADM filters must also be accounted for. Unlike the previous effects, in-line filtering introduces coloured ASE noise causing inter-symbol-interference (ISI). The influence of this filtering penalty has been analytically modelled using the estimation theory proposed by W. Yu et al in Eq 2 of [54].

3.3.2 Integration of the NT, RWA and Physical Layer Impairements in one tool

In Fig. 3.4 we explain how the three modules have been integrated to a single tool for network planning. Once we have calculated the lightpath's SNR on the identified path and for a specific wavelength, we check if the SLA for the required connection request is

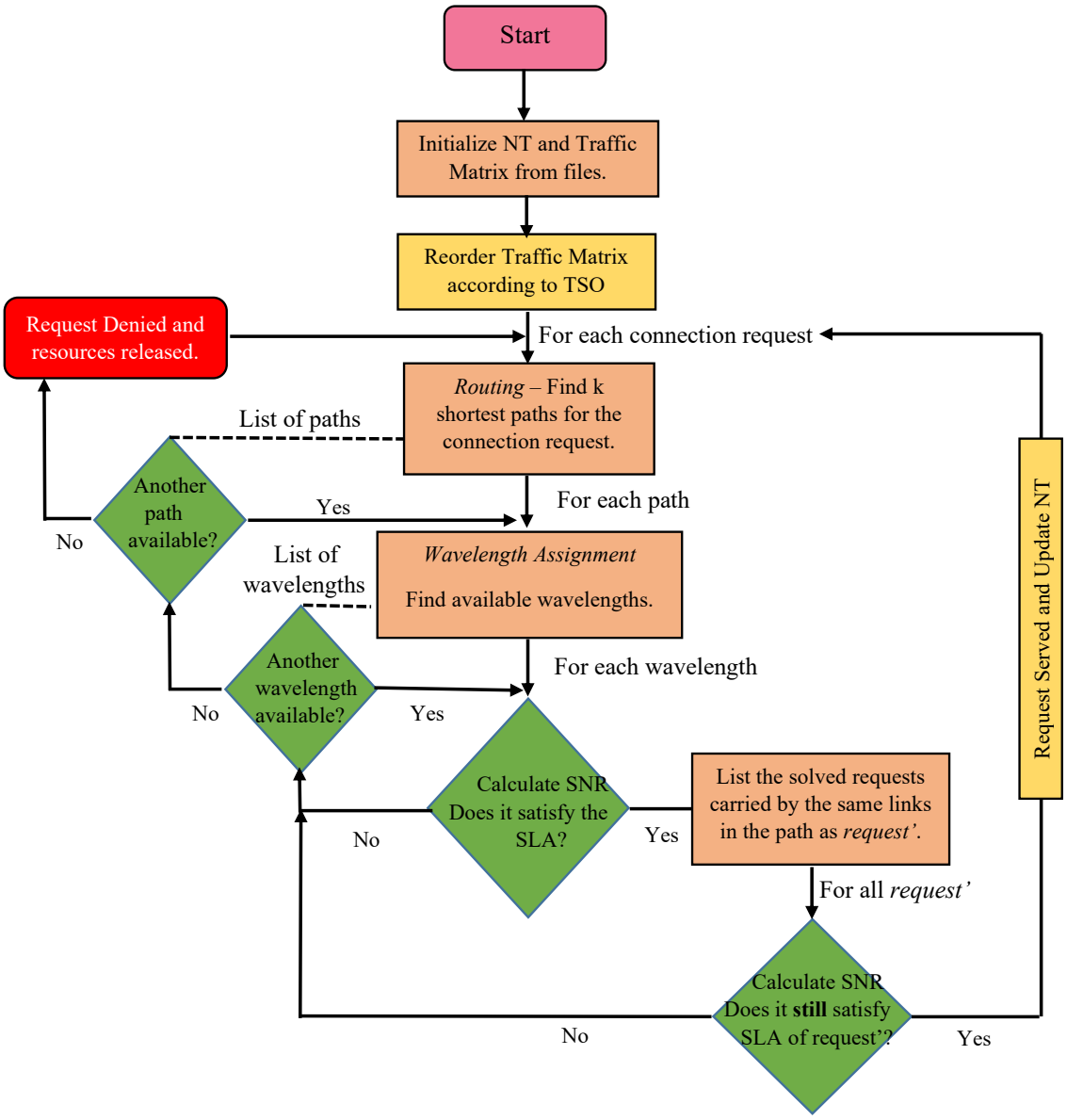

Figure 3.4: Network Planning flowchart with proposed ON Simulator

met or not. Apart from this, if we are performing the offline/online network planning, we do also check if this new connection request does share any of the OMSs on which other connection requests have been previously served. We gather the newly collected SNR of these requests and verify with their SLAs (Fig. 3.4). We then proceed to establish the new connection if and only if it does not break the SLAs of the old connection requests. For example, in Fig. 3.3, for the red lightpath connection request we can observe that it shares the link between the nodes D and E with an already existing green lightpath. In such a case, the simulator calculates the SNR of the green lightpath along with the new SNR of the red lightpath. This way we make sure that serving a new demand does not degrade the SLA of an already established link.

This information of the shared links is readily available in the NT module, making the simulator aware that it has solved a previous connection request on the same OMS and that solving the new connection request might change the SNR of the previous request, hence making network planning more reliable than simply considering WDM channels to be independent. The same procedure would be followed for the online network planning simulations, by reusing the RWA and the physical layer impairments modules to establish a lightpath connection and report performance metrics such as blocking probability, spectral occupancy of each link, etc. We can include the update of the NT based on the scheduled releases of the connection requests to precisely model the departures and arrivals of new demands.

For any network operation, such as optimization or the integration of OFs, the simulator functions as a "digital twin" of the network. A digital twin is a virtual model of a physical system that mirrors its real-time state, behavior, and performance. This approach ensures that the simulator maintains an up-to-date and detailed representation of the network, incorporating all current configurations, performance metrics, and operational parameters. Before implementing any new changes, the simulator evaluates their potential impact on the existing network state. This stateful simulation allows users to foresee the implications of their actions on network performance, thereby enabling informed and proactive decision-making.

To maintain this accurate digital representation, the simulator utilizes a comprehensive database that records all relevant parameters, including power levels, channel allocations, SNR values, and equipment configurations. This database is continuously updated with real-time data from the network, ensuring that the digital twin accurately reflects the actual conditions of the network. By mirroring the network in real-time, the digital twin allows for continuous monitoring and dynamic adjustment of the network's operation, thus optimizing performance and reliability.

This approach parallels the capabilities of commercial NMSs, which also track and manage network states. However, the integration of a digital twin offers a more dynamic and interactive simulation environment. Unlike traditional NMSs that primarily focus on monitoring and alerting, the digital twin simulates the impact of potential changes in a predictive and proactive manner. This enhanced capability enables more precise optimization and integration strategies, ultimately leading to improved network performance and reliability.

3.3.3 Merits of the proposed simulator

The proposed simulator integrates physical layer knowledge with network operations, enabling network engineers to make realistic and informed decisions. By choosing the closed-form ISRS GN model [23] over the QoT model proposed in [20], it provides a more accurate

estimation of physical layer impairments. This model accounts for the nonlinear interference (NLI) evolution along the fiber span for arbitrary values of fiber losses, considering wavelength-dependent fiber parameters, variable modulation formats, and launch power profiles. These formulas accurately assess performance over wideband optical transmission systems, allowing the simulator to incorporate future technological advancements. In particular [20] assumes flat power profiles at the beginning of the OMS's/links that the lightpath has to traverse along its path to reach the destination contrast to the reality. Our simulator uses the arbitrary powers obtained at the last amplifier of the previous OMS and propagates to the next one. Hence mimicking the real transmission system without over optimizing the performance. Additionally, to facilitate the extensive study of OFs such as QKD and evaluate their impact on existing WDM networks, our simulator is highly adaptable. While QKD channels require significantly lower power compared to WDM channels and are fundamentally different from classical channels, the simulator's design allows for extensions to handle QKD. This capability will be demonstrated in detail in Chapter 4, showcasing how the simulator can be used to model and analyze the integration of QKD into wideband systems with arbitrary launch powers.

3.3.4 Modular Design and Extensibility

The simulator is designed with modularity and extensibility in mind, which allows for easy modification and addition of new features as required. Python was chosen as a flexible language that allows us to use good existing open-source building blocks (NetworkX, GNPy or ISRS GN).

The code is organized into a Network class, which encapsulates the optical network behaviour and data related to it. The Network class is the central element of the code. Its methods are organized around different aspects of network operation, including initialization, capacity calculation (spectral occupancy of each link), path & wavelength finding, connection establishment and performance reporting. The path & wavelength finding method can import the external module SNR calculator if the network engineer plans to include the physical layer impairments into the network study. Otherwise, it would perform the RWA without the knowledge of the physical layer impairments. Since the data handled by the SNR calculation method is decoupled from the rest of the class, new network-optimisation algorithms can be implemented without impacting the SNR calculator code, and vice versa, facilitating the development process.

Likewise, the data handled by each method in the Network class are relatively separated from each other. Each method takes in only the data it needs to perform its function, and the class's instance variables (like network topology, occupied slots and wavelengths in each link, and traffic matrix) store the state of the network. New optimization algorithms can be written, and their impact can be studied by using the different methods integrated

in the main Network class.

Performing network functions such as transponder upgrades can be seamlessly handled with the simulator. When an upgrade occurs, the network topology is re-initialized to include all relevant information about the new transponders. Following this, we recompute the SNR for all previously served connection requests associated with the upgraded nodes. This ensures that the impact of the transponder upgrade is accurately reflected in the network's performance metrics. For new connection requests arriving in the traffic matrix, the simulator takes the transponder upgrade into account and calculates the SNR accordingly. At the same time, we perform a check on the existing connections' SLA, updating their SNR values as well. This approach allows us to study the impact of transponder upgrades without stopping the network, by dynamically recalculating SNR values.

Furthermore, to extend the simulator to Intensity Modulation/Direct Detection (IM/DD) systems, we can integrate new devices into the network topology, such as dispersion compensating fibers for CD or PMD compensators. These devices can be modeled in the external SNR calculator to accurately reflect their impact on network performance. By incorporating these elements, the simulator provides a comprehensive tool for evaluating a wide range of network upgrades and modifications.

The simulator's structure can handle different numbers of slots (flexible/fixed grid), wavelengths, and topologies. It also can handle a variety of connection requests (random traffic, Poisson traffic, etc.), different modulation formats and symbol rates, enabling to implement various network scenarios and assess their impact on performance. With the SLA for each connection request, we can extensively study the networks for metro, core, and datacentres. In addition, the aim of the designed simulator is to study the integration's impact of different OFs such as WC, all-optical packet switching, QKD, etc. on the overall network performance.

3.4 Simulation Results & Discussion

To test and validate our proposed tool, we conduct simulations on different network topologies. Unless otherwise specified we use the simulation parameters highlighted in Fig. 3.5 for the different simulations on the different network topologies. From the physical parameters listed in Fig. 3.5 we can observe the heterogeneity of the mesh network. The use of the high data rate 400 Gbps DP-16QAM and 200 Gbps DP-QPSK transponder demonstrates the simulator's capability to solve the non-linearities for the higher order modulations. We assume a fixed grid with total spectrum of 1.6 THz available on each link with a slot bandwidth of 80 GHz. Hence, the total number of WDM channels (=slots) on each link would be 20. The wavelength allocation for each slot is done based on the first-available wavelength from the C-Band (10 wavelengths from 1571–1567 & 10 wavelengths

from 1529–1523 nm). The reasoning behind the two extreme spectrums is to exploit the wavelength dependency of the SNR calculations and move certain requests to operate near the SLA to show the advantage of our simulator. From the node and link information as explained earlier we can construct the OMSs as shown in Fig. 3.4.

For the amplifier parameters, we have adopted a transparent design approach. This means that for an 80 km segment of SSMF with an attenuation coefficient of 0.2 dB/km, resulting in a total loss of 16 dB, we use an amplifier with an average gain of 16 dB. To incorporate wavelength dependency, we use a tilt of 2 dB, with the gain varying linearly from 17 dB for longer wavelengths to 15 dB for shorter wavelengths. A typical noise figure of 4.5 dB is chosen for all amplifiers, and the wavelength dependency of the NF is not considered at this stage.

To achieve more accurate modeling, we need to consider the gain ripple of amplifiers. Gain ripple refers to the quasi-periodic variations in the gain spectrum of an amplifier with wavelength. While our simulation initially assumes a smooth gain profile with tilt but no ripple, in reality, gain ripple can be influenced by various factors, including the number of active channels traversing the amplifier.

We propose learning the gain ripple experimentally, using physical experiments. This involves adding active optical channels and probing the input and output power spectra of each amplifier. The collected experimental data on gain ripple can then be incorporated into the amplifier's description in the network topology module. By updating the gain values based on actual measured ripple characteristics under different loading conditions, we can more accurately calculate the SNR. Currently, our simulator does not include gain ripples, but there is feasibility to incorporate them into the simulator. By integrating these experimentally measured ripple characteristics, we can enhance the accuracy and realism of the simulations.

Additionally, 0 dBm of per-wavelength optical power is assigned to the active lightpaths in our simulation which is the typical choice for the channel power.

Node	OADM	**Finisar** BW = 80 GHz
	Transponder	**Cisco NCS 1004** Baudrate = 69.43 Gbaud 200 Gbps DP-QPSK MinOSNR = 14 dB 400 Gbps DP-16QAM MinOSNR = 22 dB
Link	Fiber	**SSMF** Attn coeff = 0.2 dB/km Dispersion coeff = 17 ps/(nm.km) Dispersion slope = 0.061 ps/nm^2.km)
		PSCF Attn coeff = 0.17 dB/km Dispersion coeff = 21 ps/(nm.km) Dispersion slope = 0.059 ps/nm^2.km)

Figure 3.5: Simulation: Physical and technological parameters

3.4.1 Simple Network Planning

For the network planning, we use the topology shown in Fig. 3.6 (a) which is a fictitious mesh network with 5 nodes and 9 unidirectional links. We generate 100 connection demands that would request to carry a given amount of traffic between the specified source-destination pairs. Each demand requests a bitrate between 120 & 1200 Gbit/sec. The traffic demands have been meticulously designed to evaluate the significance of our tool and hence do not account for any statistical significance. By carefully designing a subset of traffic requests, we can illustrate the dynamic interactions within the network. Each new request must be evaluated in the context of the existing traffic, ensuring that the network can accommodate the new demand without degrading the QoT for existing connections. This approach highlights the simulator's ability to manage and optimize the network effectively, taking into account factors such as bandwidth, latency, and interference.

The careful design of these traffic demands allows us to demonstrate the simulator's capabilities in a controlled environment. This setup shows how the simulator handles complex scenarios, ensuring that each new connection maintains the required QoT while efficiently utilizing network resources. By addressing each traffic request in the context of existing demands, our simulator provides a realistic and robust solution for network planning and optimization. At the same time, the choice of very few traffic requests is to demonstrate sequentially how the QoT evolve under various network loads and their inter-dependency.

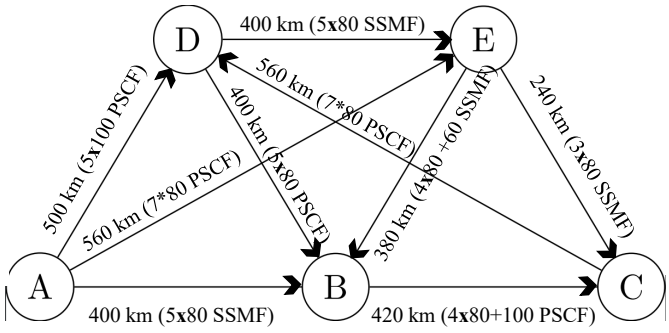

Figure 3.6: Network Topology with 5 nodes

For each traffic request, we allocate a path based on the k-shortest path algorithm with k=5. Given the small size of our network, using k=5 provides a good balance between computational efficiency and the flexibility to find alternative paths. We then select the modulation format based on the distance such that higher order modulations are assigned for longer reaches, since they would yield higher SNR as seen in the experiments of [37]. However, the simulator allows for flexibility in modulation-format heuristics. Users can specify the modulation format in the SLA, enabling the assignment of specific modulations based on the available transponders. Additionally, custom algorithms can be integrated

into the simulator to determine the modulation format, providing further adaptability to meet diverse network requirements.

Following, we allocate a slot, or multiple slots if required to satisfy the large request's bandwidth. There is no traffic grooming at this point, hence we allocate the slots completely for the demand. If multiple slots are required, provisioning is performed to assign the same path and consecutive slots, if they are available. Alternatively, if such slots are not available, provisioning will assign slots on a different path. The idea behind allocating consecutive slots was to purposefully block traffic requests earlier than usual by consuming the slots on some links (to show the advantage of our simulator with few traffic requests only). Once the modulation format is allocated, based on the available SNR threshold limits (6.2 dB for the 200 Gbps DP-QPSK and 12 dB for the 400 Gbps DP-16QAM) we define these limits as the SNR threshold (SLA). So, every connection request to be fulfilled should have an SNR greater than or equal to the threshold.

(a)

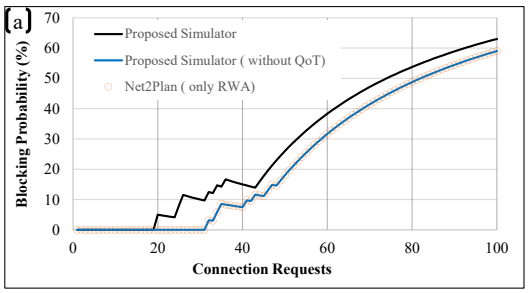

(b)

Links	Occupied Slots						
AB	0	2	4	12	12	12	12
AD	0	0	2	17	17	17	17
AE	0	5	8	13	20	20	20
BC	0	5	6	6	6	6	6
DE	0	7	15	15	15	15	15
DB	0	7	10	13	16	20	20
EC	0	0	6	12	20	20	20
EB	0	0	4	4	13	20	20
CD	0	10	18	18	18	18	18
Connection Requests	0	10	20	30	40	50	100

Figure 3.7: (a) Blocking Probability (%) vs Connection Requests (b) Spectral Slot Occupancy

In Fig. 3.7 (a) we report the blocking probability defined as the ratio of the requests blocked to the total connection requests being offered. Looking at the blocking probability we can observe that the amount of traffic being blocked is higher when we use our proposed simulator compared to the Net2Plan simulator with no QoT algorithm. To understand more about the results let's focus a particular attention starting from the 20th connection request: we can see from Fig. 3.7 (b) that the spectral slot allocation at this instance is not full but there has been a connection request that was blocked.

Fig. 3.8 shows the performance plot of the connection requests and help us understand this phenomenon. In the Fig. 3.8 (a) and (b) we have summarised the SNR evolution during the processing of the 20th connection request. From the plots in Fig. 3.8 we can observe that the SNR of the previously served requests (3, 6, 9, 10, 12, 16) has been changed while solving the 20th request, this is the core of our SNR module: when there are shared links from the old connection requests when serving a new connection request, we update the SNR of the old connection requests and compare it with the SLA to check if it is still respecting the threshold.

Consequently, the 20th request which requires a connection between the nodes C and

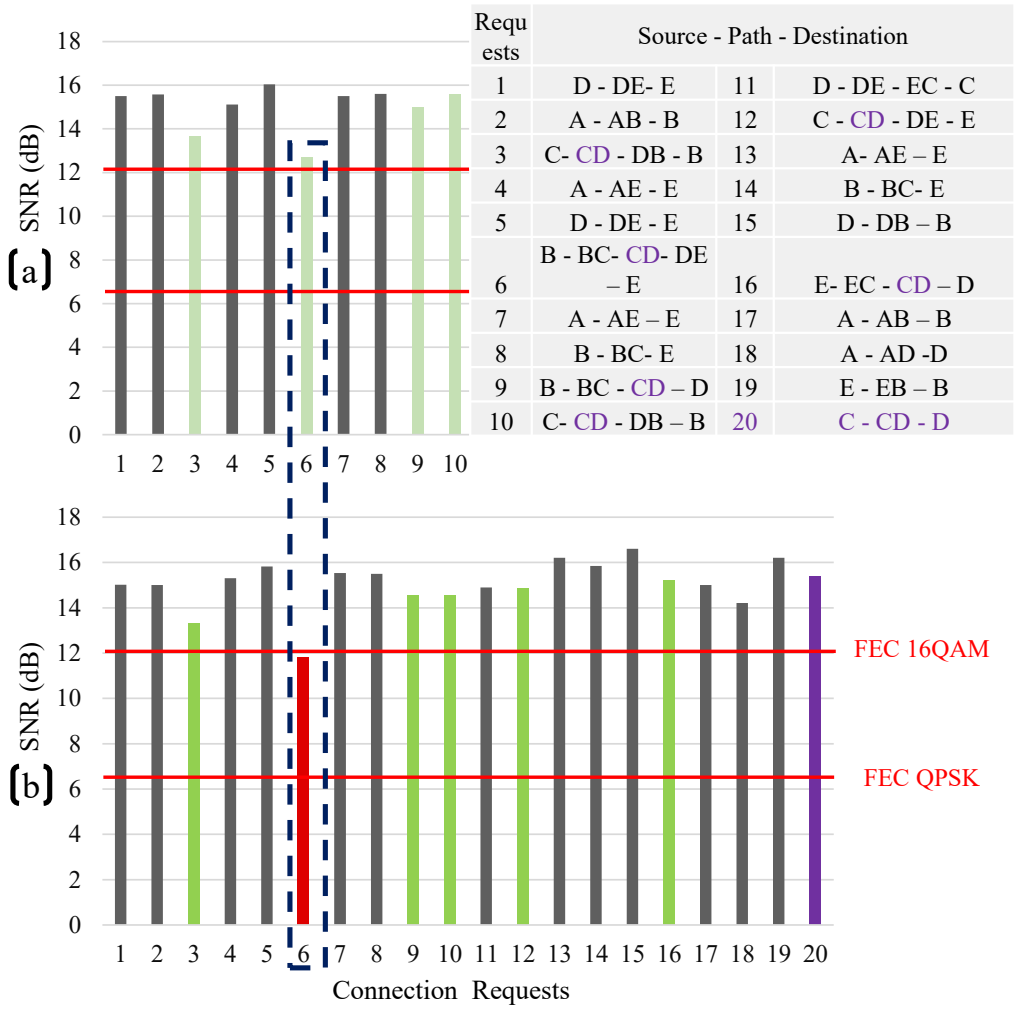

Requests	Source - Path - Destination		
1	D - DE- E	11	D - DE - EC - C
2	A - AB - B	12	C - CD - DE - E
3	C- CD - DB - B	13	A- AE – E
4	A - AE - E	14	B - BC- E
5	D - DE - E	15	D - DB – B
6	B - BC- CD- DE – E	16	E- EC - CD – D
7	A - AE – E	17	A - AB – B
8	B - BC- E	18	A - AD -D
9	B - BC - CD – D	19	E - EB – B
10	C- CD - DB – B	20	C - CD - D

Figure 3.8: (a) QoT evolution after solving the 10th request (b) QoT evolution after solving the 20th connection request

D would share the link CD with the served requests 3, 6, 9, 10, 12 and 16 and hence these SNRs would also be updated. But if we look at the Fig. 3.8 (b) request 6's SNR has been degraded below the threshold (red line), violating the SLA. Because of this, the new request will not be served abiding to the fact that there is no alternate path available.

Also, if we look at Fig. 3.7 (b) the number of slots occupied by the links BC, DE and CD have remained the same from 20th request till the 100th request. This is obvious since the 6th request, which is on these links, has a SNR close to the threshold hence any request that would share the path would degrade the SNR of the existing request on this path. Similar explanations can be drawn for the links AB and AD after solving 30 connections. For the remaining links, we can observe that after the 50th connection there is no available spectrum on the remaining links. Consequently, any subsequent request would be blocked.

From Fig. 3.7 (a), it becomes apparent that network planning with our tool, when conducted without accounting for physical layer impairments, aligns with the blocking

probabilities obtained with Net2Plan. The increasing pattern of blocked connection requests following the 50th request can be attributed to the unavailability of wavelength slots. This is further compounded by the design of the traffic requests that call for higher bandwidth requirements.

3.4.2 Complex Network Planning

We continue to explore network planning and optimization strategies within the context of a synthetic but realistically modeled optical network. The network topology and traffic matrices are designed to mimic a fictitious mesh network connecting the seven most populated cities in Spain. This topology taken from Net2Plan comprises of 7 nodes interconnected by 16 unidirectional links, simulating the primary communication pathways between these urban centers (Fig. 3.9). The model incorporates 42 distinct traffic demands, each representing a specific need to transport a given volume of data—termed "offered traffic"—between pairs of origin and destination nodes within the network. These demands range from 6.95 to 1815 Gbit/s, cumulating in a total offered traffic of 10 Tbit/s across the network. The average length of the links is around 273 kilometers, reflecting a realistic geographical spread akin to the distances between major Spanish cities.

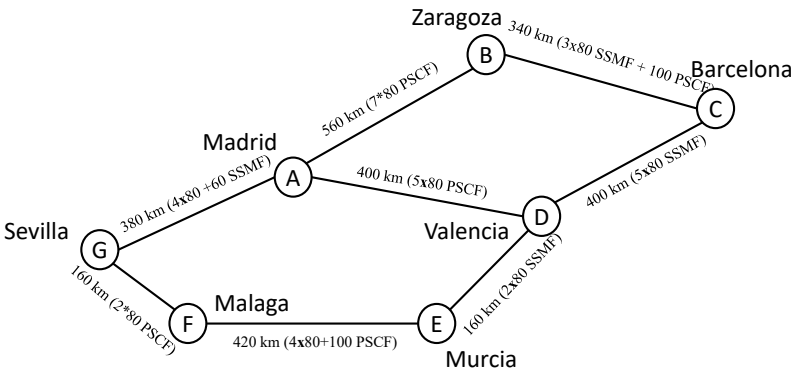

Figure 3.9: Network Topology with 7 nodes and 8 bi-directional links

For our simulations, we allocated 40 wavelengths within the C band, spanning from 1529.55 nm to 1560 nm with a spacing of 80 GHz. Given the allocation of 40 wavelengths per link and a bandwidth-spacing of 80 GHz per wavelength, each individual link in the network boasts a theoretical capacity of 40×80 Gbit/s, considering the frequency bandwidth to data rate conversion in the optical domain under fixed grid circumstances. With a total of 16 unidirectional links composing our network topology, the cumulative theoretical capacity of the entire network can be calculated as 16×40×80 Gbit/s. This translates to a substantial aggregate capacity of 51.2 Tbit/s across the network, underscoring the high data throughput potential inherent in DWDM optical networks.

In the implemented RWA, lightpaths are established directly from the origin to the destination node, maintaining the same WDM channel across all links of the path, adhering

to the wavelength continuity principle. Each node is assumed to function as a perfectly flexible ROADM, capable of dynamically managing wavelengths. In this network, each node is equipped with a degree 2 ROADM, suitable for bidirectional links. The ROADM introduces an estimated loss of around 15 dB ([55]) due to insertion losses from the WSS and other optical components. To maintain signal integrity, this loss is compensated by an EDFA, placed at the beginning of the OMS, operating in gain-constant mode.

Each lightpath is allocated a single WDM slot and is designated to carry a fixed traffic volume (R = slot bandwidth). Our strategy does not specifically ensure that multiple lightpaths serving extensive demands follow identical routes or use contiguous WDM slots, focusing instead on a more simplified yet effective allocation mechanism. Demands are prioritized and served in descending order based on the volume of traffic yet to be allocated. During this process, we evaluate the k=5 shortest paths for feasibility, ensuring that:

- A WDM slot is uniformly available across the intended path,
- The QoT requirements are satisfied, meaning that the SNR margins exceed predefined thresholds, and
- The establishment of a new lightpath does not adversely affect the SNR margins of existing lightpaths.

We compare the network planning with our tool against the existing baseline (Net2Plan) and the results are reported in Fig. 3.10. We observe the blocking probabilities of two network simulators — the Proposed Simulator, which integrates QoT-aware planning, and Net2Plan, which operates without QoT considerations. Similar to the earlier scenario, the Proposed Simulator exhibits a higher blocking probability across nearly all offered traffic levels compared to Net2Plan. For instance

1. At an offered traffic of 2.8×10^{12} bits/s, the blocking probability of the Proposed Simulator is around 18.265%, while Net2Plan shows 0%. This suggests that even at relatively low traffic levels, the Proposed Simulator is rejecting a higher percentage of demands due to QoT constraints.
2. At 1×10^{13} bits/s, the Proposed Simulator's blocking probability rises to 31%, whereas Net2Plan is still at 0%, indicating that Net2Plan is still able to find suitable paths without considering SNR margins.
3. As the offered traffic reaches 1×10^{14} bits/s, proposed simulators approaches 100% blocking probability, but the Net2Plan does so at very slower rate (at 1×10^{15} bits/s), showing its ability to handle a greater amount of traffic before reaching full saturation.

For the Proposed Simulator, which integrates QoT-aware planning, the blocking probability reaches 100% at an offered traffic level of 4.3×10^{13} bits/s. Interestingly, at this point,

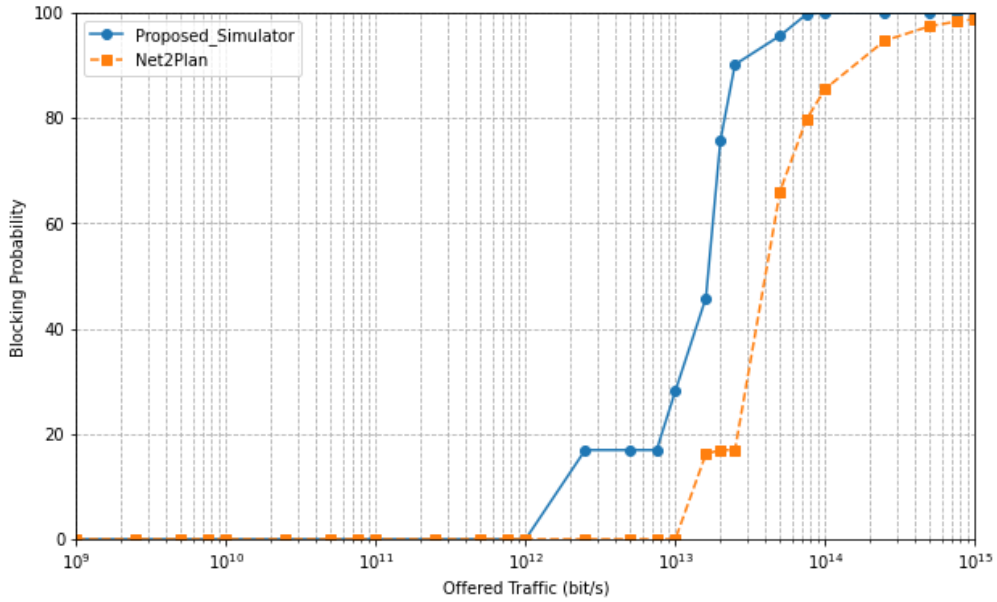

Figure 3.10: Blocking Probability vs Offered Traffic

the average link utilization was identified to be 57.8%. This suggests that while there is remaining physical capacity within the links, the QoT requirements prevent further allocations. The high SNR margins needed for maintaining the QoT mean that beyond this traffic threshold, additional demands cannot be accommodated without violating QoT constraints. Hence, the simulator enforces a conservative approach, prioritizing transmission quality over capacity maximization.

In contrast, Net2Plan, which operates without QoT constraints, shows a more gradual increase in blocking probability, only reaching 100% at 1×10^{15} bits/s. Correspondingly, link utilization under Net2Plan continues to reach 100%, full capacity utilization. This demonstrates the RWA tool's focus on optimizing capacity usage, allocating as many demands as possible until the network is saturated. The absence of QoT requirements allows Net2Plan to utilize available resources more aggressively.

The findings illustrate a trade-off between capacity utilization and transmission quality. The Proposed Simulator, adhering to QoT requirements, ensures high-quality transmissions at the cost of underutilized network capacity. Net2Plan, meanwhile, capitalizes on the available bandwidth to its fullest extent but may do so at the potential expense of reduced transmission quality, which is not factored into its allocation mechanism.

This disparity in approaches underscores the critical role of QoT in network planning. While QoT-aware planning may lead to lower utilization rates, it is essential for scenarios where the fidelity of data transmission is crucial. Conversely, maximizing link utilization may be preferred in high-capacity, cost-sensitive environments where quality constraints are more relaxed.

These observations can be attributed to the stringent QoT requirements imposed by the

Proposed Simulator, which considers the SNR margins before provisioning new lightpaths. These considerations inherently restrict the number of requests that can be accommodated, as some potential lightpaths are rejected to maintain the quality standards of the existing network, leading to a higher blocking probability.

3.4.3 Transponder Upgrade and Impact

We continue to use the similar topology as in the earlier scenario, but now we look at the average SNR margins of the traffic requests computed using the proposed simulator. The SNR margins at a traffic of 1×10^{13} bits/s are reported in the Fig. 3.11 where the blocking probability was 29%. Bound to our RWA strategy we might have demands that are only partially served and others which are completely served. As we look at the margins plot (Fig. 3.11) the number of occurrences sum to 42 indicating that all the demands are served either partially or totally. Also from the Fig. 3.11 it is evident that we have SNR margins greater than 5 dB, which can allow us to upgrade the transponder i.e we use 400 Gbps DP-16QAM modulation format for the services that require larger bandwidth and hence allowing more free slots and wavelengths for other demands.

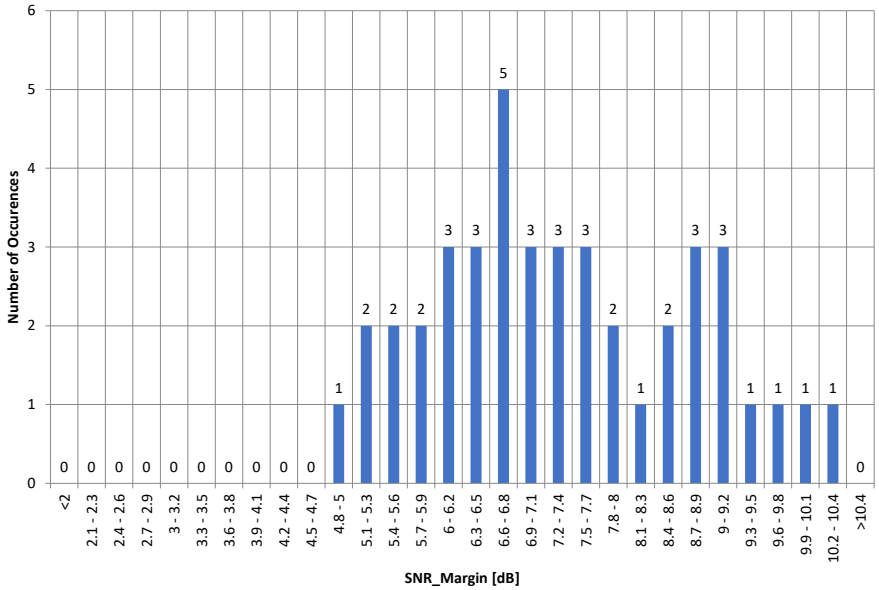

Figure 3.11: Available SNR margins in the network

This upgrade results shown in Fig. 3.12, indicate an improvement of the blocking probability. The increase can be attributed to the amount of traffic capabilities increased. The integration of the QoT into the RWA has helped us to test out the transponder upgrade with their impact on the physical layer impairments.

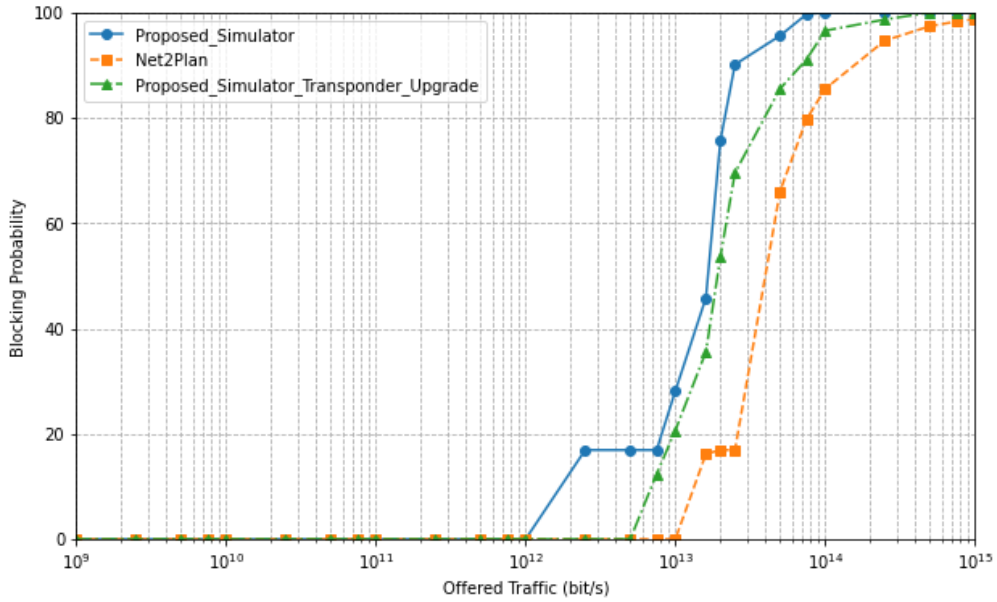

Figure 3.12: Blocking Probability vs Offered Traffic (After upgrading the transponders)

3.4.4 Computational Time Analysis

The efficiency of a network simulator is critically gauged by its computational performance, specifically the time it takes to simulate different levels of network traffic. Our evaluation assesses the computational time required by the Proposed Simulator under the earlier scenario i.e. for the 7-node topology, including the baseline simulator performance, the transponder upgrade, and comparative analysis against the established Net2Plan simulator.

Our results, as illustrated in Fig. 3.13, demonstrate the computational time scalability with respect to the offered traffic within the network. The Proposed Simulator shows higher computational time efficiency comparable to Net2Plan under all traffic loading conditions. This is due to the additional QoT calculations required by the Proposed Simulator, which are not a consideration for Net2Plan.

For example, at a traffic volume of 1×10^{13} bits/s, the computational time of the Proposed Simulator is approximately 300 seconds, which increases to around 800 seconds at 1×10^{15} bits/s. In contrast, with the Net2Plan which increases from 1 sec (at 1×10^{13} bits/s) only to 7 secs (at 1×10^{15} bits/s). Implementation of the transponder upgrade, we observe an increased computational time, particularly at higher traffic levels. This indicates that the enhancements introduced with the upgrade even though improve blocking probabilities, as discussed previously, also contribute to the increase in the computational overhead.

In summary, the integration of QoT considerations into the simulation does entail a computational overhead, yet it is justified by the gains in transmission quality and the potential for future-proofing the network against increasing data loads. The computational burden stems from the real-time routing and wavelength allocation based on the SNR and

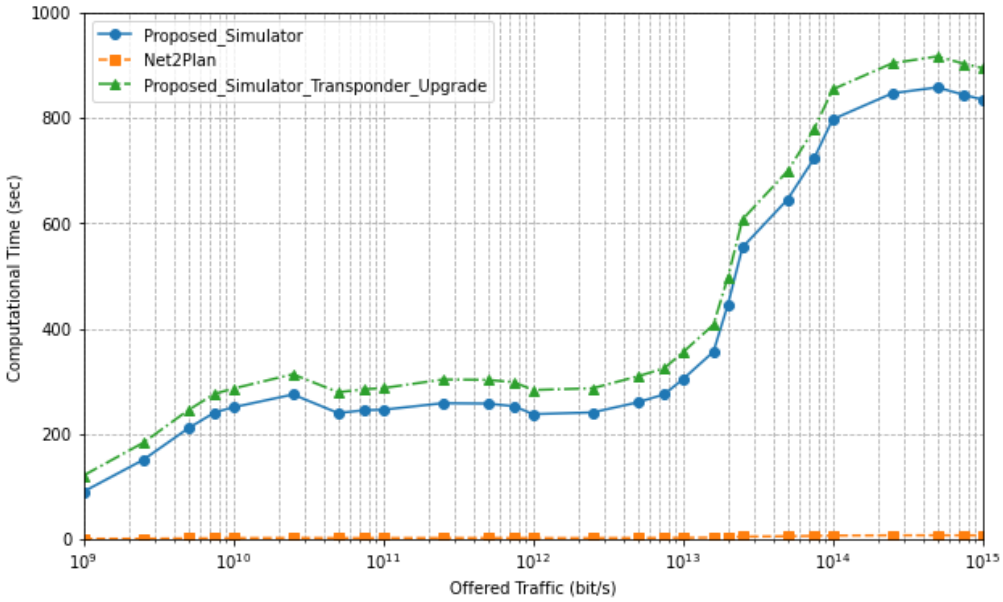

Figure 3.13: Computational time vs. Offered Traffic for different simulation scenarios.

processes that would require re-calculation of the existing connection's SNR to safeguard them from breaking. This necessitates a more detailed investigation to accurately quantify the computation time for each module involved.

3.4.5 Simple OF: Wavelength Converter (WC)

In this scenario, we seek to showcase the extensibility of our simulator by integrating wavelength conversion as an OF example. We start by placing a WC at the node C and evaluate the blocking probability.

We continue with the same traffic structure described in scenario 1. When allocating the wavelength on the OMSs involving node C, the wavelength finding method would have a new function of wavelength conversion that can allocate a different wavelength for the request on its OMSs compared to the other OMSs in its path. Adding this new function would not disturb the basic functionality of the Network class but only functions as an additional feature. We start by re-initializing the network topology to include the change of state of the ON. The change is embedded in the OMS information built from the nodes and the links, then along with the OMS information we associate a flag to indicate the presence of an OF at that node and associated links. We have implemented the functionality of the WC on the links that include WC-enabled nodes. It allows to change the wavelength to the unused wavelength available on those links. In the path & wavelength finding module we then use this functionality to select the wavelength for the request that traverses these links and calculate the SNR. This illustrates the modularity and extensibility potential of the proposed simulator.

The WC used in the simulation is an all-optical wavelength converter that switches

from one wavelength to another without converting the signal to the electrical domain (O-E-O). While no explicit approximation of the conversion efficiency is made, an OSNR degradation of 1 dB is arbitrarily considered in the simulations to account for potential losses inherent in the all-optical wavelength conversion process. This degradation is applied when the signal undergoes wavelength conversion, reflecting the minor but present losses that might occur.

Since we know that the 6^{th} connection is the bottle-neck service in the network because of its low SNR, 16-QAM modulation was allocated to this request (because of its reach). Since the higher wavelengths on the two links CD, DE that are required to serve the request have been consumed by the earlier requests, we can now allocate only lower wavelengths.

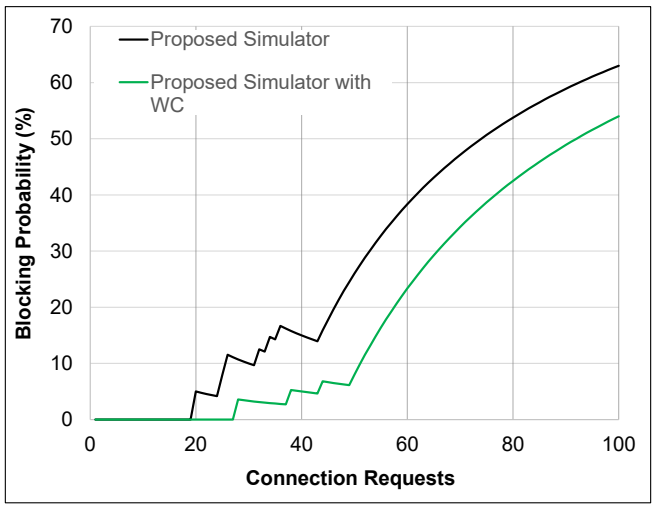

Figure 3.14: Blocking Probability in presence of WC

From [37] we know that having higher order modulations on the lower wavelengths would impact their performance adversely. Hence, relocating this wavelength on a higher value would improve the performance of the request. Since we have placed the WC only at a single node, the impact of the cumulative SNR would not be very much significant. The results are reported in Fig. 3.14 where we can observe that a single WC converter placed at C has improved the number of connections being served while retaining the performance of the connections.

3.5 Conclusion

In this chapter, we have demonstrated the dual purpose of our proposed simulator: managing network planning while accounting for physical layer impairments. Our simulator's modular design enables the easy integration of new functionalities, ensuring that network performance is optimized both in terms of resource allocation and Quality of Transmission (QoT).

From our initial simple network simulations with a topology of 5 nodes and 9 unidirectional links, we observed that our simulator's blocking probability was higher compared to Net2Plan. Specifically, at an offered traffic of 2.8×10^{12}, bits/s, the blocking probability of our simulator was around 18.265%, while Net2Plan showed 0%. This pattern continued as traffic increased, with our simulator reaching a 100% blocking probability at 4.3×10^{13}, bits/s, compared to Net2Plan's 100% blocking probability only at 1×10^{15}, bits/s.

These results underscore our simulator's strict adherence to QoT requirements. We serve connection requests only if the QoT for all existing and new connections is maintained. This conservative approach ensures high transmission quality but at the cost of higher blocking probabilities compared to Net2Plan, which does not consider QoT constraints.

However, this approach allowed us to upgrade transponders effectively. By being aware of the available SNR margins, we could allocate 400 Gbps DP-16QAM modulation formats to services requiring larger bandwidths, thus freeing up more slots and wavelengths for other demands. This upgrade reduced the blocking probability significantly, illustrating the simulator's capacity to optimize network resources while maintaining QoT. Specifically, the transponder upgrade brought down the blocking probability from 29% to approximately 18% at 2.8×10^{12}, bits/s.

In the more complex network simulations, involving a topology of 7 nodes and 8 bidirectional links, the same trend was observed. Our simulator consistently demonstrated higher blocking probabilities due to its stringent QoT checks. For example, as the offered traffic reaches 1×10^{14} bits/s, our simulator approaches 100% blocking probability, but the Net2Plan does so at very slower rate (at 1×10^{15} bits/s) indicating our careful consideration of SNR margins.

One of the significant advantages of our simulator is its modularity and ease of integration of new optical functionalities. For example, we integrated a wavelength converter at a specific node and evaluated its impact on blocking probability. The inclusion of the WC at one of the nodes in the 5-node topology has improved the number of connections served while maintaining the SNR of existing connections. Specifically, the blocking probability was reduced from 31% to 24%. This integration was straightforward and demonstrated the simulator's ability to adapt to new requirements and study their effects at the network level.

Having established the effectiveness of our simulator in managing network planning along with the physical layer impairments, including the integration of a simple optical functionality like the wavelength converter, we now turn our attention to integrating more complex optical functionalities for security. In the next chapter, we will explore the incorporation of quantum key distribution into our simulator. We will study its impact on network performance and security, highlighting how our simulator can be used to assess the feasibility and effects of advanced security mechanisms in optical networks. The the-

oretical modeling and integration of QKD presents additional challenges compared to the wavelength converter, and we will delve into these complexities to ensure accurate and effective implementation.

CHAPTER 4

Integrating QKD as a Functionality in Optical Networks: Simulation and Impact Analysis

4.1 Introduction

Quantum Key Distribution (QKD) has been proposed as a secure solution for the next generation of optical communication networks. Traditional encryption techniques, utilizing public-key cryptography, offer defense against cyber threats [56, 57]. The degree of security provided by these techniques depends on the computational complexity of the applied mathematical functions. Nevertheless, the emergence of faster electronic processing units threatens to compromise the security ensured by public-key cryptography.

Furthermore, the advent of quantum computers [58–64] demands the need for QKD to protect information carried via communication networks, as existing encryption techniques will be ineffective in the era of quantum computing. [65–67]

In the broader discourse on quantum computing, Shor's algorithm [68] represents a pivotal breakthrough, highlighting the profound implications quantum technologies have on modern cryptography. Introduced by Peter Shor in 1994, this quantum algorithm can efficiently perform prime factorization—previously deemed a computationally hard problem—by reducing it to a polynomial time complexity relative to the number of digits. This advancement poses a significant threat to cryptographic systems like the RSA (Rivest–Shamir–Adleman) algorithm, which rely on the difficulty of prime factorization to ensure security. As quantum computers become more feasible and accessible, they could decrypt data secured by RSA within a manageable timeframe, rendering such encryption obsolete. This underscores the urgent need for quantum-resistant cryptographic methodologies in the face of advancing quantum computing capabilities.

Traditionally, optical fiber, due to its guided medium for optical signal transmission, has been viewed as a secure transmission method. Nevertheless, advancements in hacking techniques and the increasing sophistication of cyber-attacks, including jamming, eaves-

dropping, and data interception [26, 69, 70], have exposed vulnerabilities in optical fiber communications. These developments underscore the necessity for enhanced security measures. It is within this context that QKD emerges as a promising enhancement to bolster the security of optical networks.

As we navigate these challenges, the integration of Quantum Key Distribution (QKD) into existing optical network infrastructures becomes crucial. QKD is feasible through both free space [71–73] and optical fiber [74–76] mediums. Initially, QKD experiments were conducted using isolated dark fibers, which are optical fibers specifically allocated for quantum communication, separate from those used for classical data transmission. However, the scarcity of dark fibers makes them an impractical foundation for widespread quantum communication, just as constructing a separate global optical network for QKD is not economically viable. Given that optical fibers currently carry the bulk of global internet traffic and have a broad deployment worldwide in various networks—including access, metro, terrestrial backbone, and submarine—it is broadly agreed upon that QKD needs to be integrated into existing optical networks.

Yet, the integration poses challenges since quantum signals, which consist of only a few photons per pulse, are significantly weaker than classical signals. For example, at 1550 nm, 0 dBm, and 50 Gbaud, classical signals can have around 1.5×10^5 photons per symbol. (This value is derived by first calculating the energy of a single photon using $E = \frac{h \cdot c}{\lambda}$ [77], where h is Planck's constant, c is the speed of light, and λ is the wavelength. The energy per symbol is then found by dividing the optical power by the symbol rate, and the number of photons per symbol is obtained by dividing the energy per symbol by the energy of a single photon). This discrepancy in photon numbers makes the coexistence of quantum and classical data within the same optical fiber challenging. Moreover, quantum signals not only are inherently weaker but also have a much shorter transmission range compared to classical communications. Any interaction between quantum and classical signals can compromise the integrity of the quantum signals and modify their quantum states. Furthermore, the RWA procedure, which includes establishing optimal pathways and wavelength assignments for lightpaths, must be modified to account for the Quantum Key Distribution and Wavelength Division Multiplexing (QKD-WDM) integrated network's particular limits and requirements.

When QKD channels are propagated alongside the WDM channels, several technical challenges arise due to the coexistence of these channels in the same fiber. Some of the challenges are:

1. Crosstalk: The close proximity of QKD and WDM channels within the same fiber can result in crosstalk, which is the unwanted coupling of signal power from one channel to another. Crosstalk can cause interference and degrade the performance of both QKD and WDM channels. This is particularly relevant when the channel

spacing between the QKD and WDM channels is narrow. While crosstalk cannot be completely eliminated, it can be reduced through the use of advanced filtering techniques [7]. The effectiveness of these techniques, however, also depends on the power differential between the channels, which means that practical implementation may require careful optimization of channel powers and spacing.

2. Raman scattering: As intense classical signals travel through the optical fiber, noise photons of different wavelengths may arise due to a range of nonlinear optical interactions. If these noise photons share the same wavelength as the quantum signals, it becomes impossible to separate them at the receiver's end, resulting in the addition of in-band noise. Spontaneous Raman Scattering, a predominant nonlinear effect in optical fibers, poses a significant limitation to the integration of QKD systems within classical optical networks [8, 78].

3. Power level differences: QKD channels and WDM channels typically operate at different power levels. QKD systems, especially those based on single-photon transmission, require very low power levels to ensure secure communication. In contrast, WDM channels operate at higher power levels to maintain signal quality over long distances. When QKD and WDM channels coexist in the same fiber, power fluctuations and leakage from WDM channels can affect the QKD channel's performance, increasing the Quantum Bit Error Rate (QBER) and reducing the Secure Key Rate (SKR). QBER is a critical performance metric in QKD systems, defined as the ratio of erroneous bits to the total number of key bits received over the quantum channel. Mathematically, it is expressed as:

$$\text{QBER} = \frac{N_{\text{error}}}{N_{\text{total}}}$$

where N_{error} is the number of bits that were received incorrectly, and N_{total} is the total number of bits transmitted [79]. If the QBER exceeds a certain threshold, the security of the QKD system is compromised, as it may indicate potential eavesdropping or a high level of noise. SKR, is another key performance metric in QKD systems, representing the rate at which usable, secure cryptographic key bits are distilled from the raw key bits after accounting for error correction and privacy amplification. It is typically measured in bits per second (bps) and is given by:

$$\text{SKR} = R_{\text{raw}} \times (1 - H(Q_{\text{BER}})) - R_{\text{EC}} - R_{\text{PA}}$$

where R_{raw} is the raw key generation rate, $H(Q_{\text{BER}})$ is the binary entropy function of the QBER, R_{EC} is the rate reduction due to error correction, and R_{PA} is the rate reduction due to privacy amplification [79].

4. Modulation format compatibility: QKD systems may use different modulation formats than WDM systems. For instance, discrete-variable QKD systems employ qubits encoded in various quantum states, while continuous-variable QKD systems use coherent or squeezed states of light. These differences in modulation formats can complicate the integration process and may require additional hardware or signal processing techniques to ensure compatibility.

5. Spectral efficiency limitations: The introduction of QKD channels can consume a portion of the available spectrum for the QKD itself and some guard bands. These guard bands are essential to prevent crosstalk and maintain necessary channel spacing between QKD and WDM channels, which are crucial for preserving the integrity of signals across the network. However, the inclusion of guard bands results in further reductions in spectral efficiency by limiting the number of additional WDM channels that can be accommodated. This constraint significantly impacts the network's capacity to handle dense traffic loads, posing a substantial challenge in network design and operation.

6. Dispersion effects: Chromatic and polarization-mode dispersion can influence the performance of both QKD and WDM channels. When integrating QKD channels into a WDM network, it is essential to account for these dispersion effects to maintain the stability and synchronization of the quantum channel.

7. Four-wave mixing: In optical fibers, the $\chi^{(3)}$ nonlinearity induces a third-order nonlinear effect when two or three more pump waves are present, known as Four-wave mixing (FWM). For FWM to occur efficiently, a phase-matching condition must be met. While FWM might constitute a significant source of noise over very short distances, it is considerably less impactful than Raman scattering over the lengths typical of practical fibers. Additionally, FWM can be significantly mitigated by optimizing the channel configuration or employing polarization multiplexing [76, 78].

After examining the various challenges posed by the coexistence of QKD and WDM channels, another pivotal issue is that: QKD systems cannot pass through standard optical amplifiers, which are essential components in extending the reach of communication signals over long distances. Quantum signals are inherently delicate, and the process of amplification can disrupt the quantum information they carry, thereby rendering the quantum keys useless. This limitation is particularly impactful because it restricts the length of fiber over which secure quantum communication can be achieved without signal degradation. Addressing this issue is crucial for the practical deployment of QKD in broader optical network infrastructures and requires innovative solutions to maintain signal integrity over extended distances.

Additionally, tackling the challenges of interference and RWA optimization is essential for the successful and secure integration of QKD with WDM networks. The interplay between QKD and existing WDM channels presents both technical hurdles and opportunities for innovation. This chapter aims to explore the mutual impact of incorporating QKD into WDM networks, focusing on identifying the technical barriers, understanding the root causes of these interactions, and formulating strategies for harmonious and secure coexistence. While several challenges such as crosstalk, FWM, and dispersion effects limitations exist, this discussion will predominantly concentrate on Raman scattering, given its significant and pervasive influence on QKD performance. Moreover, it seeks to refine RWA strategies to ensure efficient channel allocation, critical for maximizing network performance and security.

In this pursuit, the chapter delves into the mutual influences of QKD integration within WDM-based optical networks, scrutinizing the technical nuances and the repercussions of such integration. To address these challenges effectively, we use a accurate Raman noise model and add to that a RWA strategy that serves and protects the QKD traffic while still monitoring the impact on the blocking probability of the classical WDM channels. Furthermore, we developed targeted heuristics aimed at optimizing the placement of WDM and QKD channels to specifically minimize Raman noise, which is a significant concern. Our network simulation's results show that by adopting the right RWA method and adjusting channel placement with our heuristics, and accepting minor compromises on the QKD SKR, we can bring down the blocking probability for the WDM classical traffic to a level comparable to cases without the presence of QKD. This demonstrates that with strategic planning, system adjustments, and precise channel management, it is feasible to integrate QKD into existing WDM networks without significantly compromising the network performance.

4.2 Literature Survey

We commence by exploring the fundamentals of QKD, providing a foundational understanding of its role as a paradigm shift in secure communication. We will further explore detailed literature to enhance our understanding of QKD's transformative role in secure communications.

4.2.1 A basic QKD system's components and functionalities

A typical QKD system operates by utilizing two distinct channels: the Quantum Secret Channel (QSCh) and the Public Information Channel (PICh). Together, these channels, along with the QKD protocol and encryption/decryption units, form the backbone of a QKD communication system (Figure 4.1).

- The QSCh facilitates the transfer of quantum information, typically in the form of photon states, between two parties (commonly referred to as Alice and Bob). This channel handles the secure exchange of quantum bits (qubits) that are fundamental to key generation.
- The PICh, in contrast, is responsible for non-quantum communication between Alice and Bob. It is primarily used to share information related to the measurement bases used during the transmission of qubits and for post-processing tasks such as key validation and error correction. After these processes, Alice and Bob are able to generate a final shared secret key.

The QKD protocol orchestrates the entire process by ensuring a secure connection between the two nodes. It handles the generation of secret keys and guarantees the integrity and security of the exchanged information during key establishment. The protocol also verifies the correctness of data through mutual communication between the parties, ensuring the security of the distributed keys. Finally, the encryption and decryption modules play a critical role in maintaining confidentiality. Once the secret keys are established, they are employed to encrypt sensitive data. The corresponding decryption process ensures that only the intended recipient, who holds the secret key, can retrieve the original information.

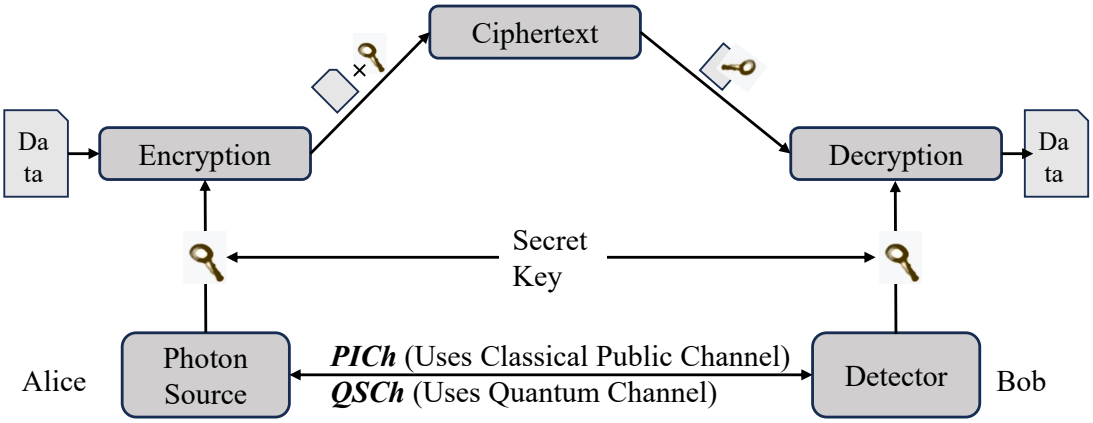

Figure 4.1: Basic QKD System

There are two foundational approaches for implementing Quantum Key Distribution (QKD) protocols: the Prepare and Measure (P&M) method and the Entanglement-Based (EB) method [56, 80, 81]. Within these approaches, QKD protocols are generally categorized into three broad families: Discrete Variable QKD (DV-QKD), Continuous Variable QKD (CV-QKD), and Distributed Phase Reference QKD (DPR-QKD) [80]. Table 4.1 provides a summary of these QKD protocols. These families encompass various techniques, each offering specific strengths and tailored applications. CV-QKD leverages continuous-variable quantum states, such as those produced by coherent or squeezed light, enabling it to interface smoothly with the components used in traditional telecom networks. This

characteristic makes it an excellent candidate for integration with existing optical systems. In contrast, DV-QKD utilizes discrete quantum states, typically referred to as qubits, and serves as the foundation for well-established protocols like BB84, which has become a cornerstone in the field of quantum cryptography [82]. Moreover, DPR-QKD adds further robustness by employing decoy states, which enhance its resistance against sophisticated attacks such as photon number splitting.

Table 4.1: Overview of QKD Protocols by Family [80]

Protocol Family	**Protocols (Year)**	**Key Features and Principles**
DV-QKD	BB84 (1984), B92 (1992), SSP (1998/1999), SARG04 (2004)	All are P&M protocols based on Heisenberg's Uncertainty Principle. BB84 is the pioneering protocol, B92 simplifies BB84 with two non-orthogonal states, SSP extends BB84 with six polarization states, and SARG04 differs in classical phase processing.
	E91 (1991), BBM92 (1992)	Both are EB protocols based on Quantum Entanglement. E91 is the first entanglement-based QKD protocol, while BBM92 is an entangled version of BB84.
CV-QKD	Squeezed-State BB84 (2000), Gaussian Protocol (2001)	Both are P&M protocols using Heisenberg's Uncertainty Principle. Squeezed-State BB84 introduces squeezed-state with discrete modulation, while the Gaussian protocol employs Gaussian modulation.
DPR-QKD	DPS (2003), COW (2004)	Both are P&M protocols leveraging Heisenberg's Uncertainty Principle. DPS uses weak coherent sources with delay circuits, and COW uses coherent pulses with sequences of non-empty and empty pulses.

One of the key reasons CV-QKD is attractive for deployment in modern optical networks is its inherent compatibility with contemporary telecommunications equipment, including coherent receivers and continuous-wave lasers. This compatibility ensures that CV-QKD can be integrated seamlessly into network infrastructures that utilize Wavelength Division Multiplexing (WDM) and other optical technologies. Additionally, CV-QKD has the potential to operate at higher repetition rates, providing more efficient synchroniza-

tion with conventional communication systems and improving overall system performance. However, CV-QKD also faces significant challenges, particularly in managing noise and defending against coordinated attacks. To safeguard the integrity of the quantum keys generated, it is crucial to implement effective error correction and privacy amplification mechanisms. These processes are essential for reducing the amount of information available to potential eavesdroppers and ensuring that the shared secret keys remain uncompromised.

While CV-QKD shows promise for integration with classical optical networks, significant challenges arise due to the coexistence of quantum and classical signals within the same fiber infrastructure. One of the main issues is the generation of noise from classical signals (seen in 4.1, which can degrade the performance of the quantum channel. To address these challenges, advanced techniques must be implemented, such as dynamic power control for the classical signals, strategic wavelength spacing, and the use of optical filters to suppress unwanted noise.

Another critical aspect to consider when implementing QKD is the SNR or QBER, as quantum signals tend to degrade more rapidly than classical ones, which restricts their effective transmission range. Among the various QKD protocols, DV-QKD typically supports longer transmission distances compared to CV-QKD. This is because DV-QKD can handle greater levels of signal loss, making it more suited for long-distance fiber links. In contrast, CV-QKD is more vulnerable to noise and attenuation, which limits its operational range, especially in scenarios where signal degradation becomes a significant concern.

Ultimately, selecting the most appropriate QKD protocol for a given network depends on several factors, including the network's architecture, the performance requirements, and the specific security needs. Each protocol comes with its own set of advantages and limitations, and a thorough evaluation is required to determine which is best suited for a particular application.

4.2.2 Integration of QKD with WDM-based optical networks

Numerous studies have examined the performance implications of integrating QKD systems. We first discuss the research works investigating the effects on ***point-to-point optical transmission systems***.

In [83], the authors develop a theoretical model to analyze the physical layer performance of what is effectively a point-to-point link rather than a complete network within the UK national quantum network (UKQNtel) context. This analysis utilizes COW-QKD in the O band integrated with 500 Gb/s encrypted data in the C band across a 121 km stretch between BT Labs and the University of Cambridge. While the model is fitted with real-world experimental data to study the impact on the QBER and the achievable SKR, it does not address the broader network implications, such as the cost increase due to the use of two different transmission bands.

In [84], the authors report on the achievable QBER and SKR when a quantum channel in the O Band (1310 nm) of a QKD system co-propagates with DWDM data channels carrying a total power of 17dBm in the C Band (1550 nm range) over 50 km of standard single-mode fiber (SSMF). Implementing these dual-band strategies effectively reduces quantum noise interference, which is crucial for preserving the integrity of quantum keys across long distances. Nevertheless, the deployment of such integrated systems entails significant financial outlays. The necessity for new infrastructure, including ROADMs and advanced transponders, leads to substantial CAPEX. Furthermore, they predominantly focuses on improving QKD performance without considering its impact on classical WDM systems, particularly in blocking probability.

In [85], the authors focus on identifying optimal coexisting classical light wavelengths that could be used alongside C band quantum networks to minimize interference from spontaneous Raman scattering. This study specifically investigates the effects of introducing quantum channels in the C Band, contrasting to other approaches that might use different bands. The main results show that particular wavelengths can significantly reduce the impact of Raman scattering, facilitating better coexistence within the same C band. However, the research does not extend to studying the overall impact of integration on network performance. Specifically, while the paper underscores the importance of managing Raman noise for coexistence in the same band, it does not explore how this integration affects the operational aspects of classical WDM systems.

In [86] authors have integrated their in-house designed CV-QKD technology with existing optical infrastructure and a point-to-point WDM link in the same band. They evaluated the CV-QKD system's resistance to spontaneous Raman scattering noise, which is the most prevalent degradation in a WDM co-existence environment for QKD. They specifically evaluated the influence of a WDM 10X10 Gb/s ON-OFF-keying signal on generated spontaneous Raman scattering noise in the QKD channel through experimentation. The effect of spontaneous Raman scattering noise is evaluated for several transmission circumstances, i.e., for different optical launch powers of the WDM signal and for different transmission links of 20, 40, 60, and 80 km. Based on the experimental data and on the measured system's parameters, they estimated the key rates and reach capabilities of the proposed CV-QKD system. The scheme supports a key rate of 90 kbit/s over 20 km, for an ideal QKD system multiplexed with 2-mW optical power.

So far, we have been reporting the papers on the networks consisting of single point-to-point links, when we proceed further to the ***mesh networks***, we will encounter the new networking challenges for which the conventional methods (such as routing, resource allocation, network resilience) are not suitable. A variety of proposals have been made for different networking challenges that have been reported in Table 4.2.

Table 4.2: Summary of Key Networking Challenges and Related Works [82]

Networking Challenge	**Year(s) and Reference(s)**	**Summary of Related Works**
RWTA	2017 [87], 2017 [67]	Proposed a QKD-secured optical network architecture using SDN, addressing the RWTA problem with a static RWTA strategy. Additionally, an Integer Linear Programming (ILP) model along with a heuristic was developed for RWTA, providing dual security-level solutions.
	2017 [88]	Introduced the concept of Knowledge of Demand (KoD) for efficient network resource provisioning, utilizing the Quantum Knapsack Problem (QKP) technique.
	2018 [89], 2018 [90]	Developed an RWTA algorithm with flexible key update periods in dynamic traffic scenarios, using the concept of Time-Slot Windows (TSW) to reduce time conflicts. A secret key generation scheme was proposed and experimentally verified over a 200 km fiber loop, providing physical layer security based on optical channel feature extraction.
	2019 [91], 2019 [92]	Proposed an Auxiliary Graph-based RWTA (AG-RWTA) algorithm to optimize quantum key resource usage. Additionally, a new node structure was designed for distributing global quantum keys to secure multicast services.
Network Resiliency	2019 [93], 2019 [94]	Focused on protecting secret keys against network failures by developing two new survivable schemes. A Security Knowledge Flow Model (SKFM) was constructed to enhance the resiliency of QKD networks by strengthening Security Knowledge Resilience Systems (SKRS).
	2019 [95]	Introduced a novel Shared Backup Path Protection (SBPP) scheme, leveraging dynamic time windows for TDM-based QKD-secured optical networks.

Networking Challenge	Year(s) and Reference(s)	Summary of Related Works
	2020 [96], 2020 [97]	Developed a dynamic algorithm for mixed/hybrid resource allocation in backup QKD-secured optical networks. Additionally, a novel quantum node structure with bypass capabilities was designed for scenarios where node distances are within a specific range.
Trusted Repeater Node Placement and Key Recycling Approach	2020 [98, 99], 2021 [100]	Proposed a hybrid trusted/untrusted relay-based QKD network architecture that incorporates both Trusted Relay Nodes (TRNs) and Untrusted Relay Nodes (UTRNs).
	2019 [101]	Addressed the cost-minimization challenge by constructing a cost-oriented model and designing cost-efficient algorithms for QKD networking.
	2020 [102]	Proposed key recycling mechanisms, including partial, full, and mixed recycling, to increase the availability of secure keys in QKD systems.

The outlined articles explored the details of mesh network designs, with a specific focus on the routing and wavelength time assignment (RWTA) strategies needed to incorporate Quantum Key Distribution (QKD) systems. These studies extensively cover different routing strategies to improve network resiliency and integrate trusted nodes for extending QKD over longer distances. However, they often don't delve into detailed considerations on channel allocation. When discussing wavelength allocation, the focus is mainly on different bands, showing a careful approach to optimizing network resources. Emphasizing routing over channel allocation highlights the importance of establishing reliable and secure paths for quantum communication within the broader network infrastructure. However, it also suggests a need for further comprehensive study on optimal wavelength and channel management.

Contrary to the earlier reported papers the authors in [103] have proposed a first analysis of CV-QKD integration in a classical WDM network. They applied a simplified noise model when coexistence occurs and studied the impact on the classical WDM traffic's blocking probability —the ratio of traffic requests denied to total requested traffic.

The literature reveals that the impact on QKD channels has been thoroughly investigated across different fiber lengths and fiber launch powers, with performance metrics typically measured by QBER or the SKR. However, there are limited studies that have

examined the integration effects on the classical WDM signals due to the co-existence. Furthermore, while existing research into networking challenges has led to enhanced network orchestration, these studies primarily focus on the performance of QKD networks in isolation. Consequently, there is a notable gap in understanding how QKD channels might affect the performance, routing, and resource allocation of existing classical channels at the network level, highlighting a critical area for further research.

The work that we propose here gauges the effects of QKD channel integration on the physical layer and impairment-aware network planning of WDM channels. We rigorously examine various network performance parameters, positioning the SKR as the primary Quality of Protection (QoP) metric for QKD. This study places a particular emphasis on modeling Raman noise for QKD channels, which significantly influences SKR and thereby impacts the overall security efficacy of the quantum network.

In parallel, for classical WDM systems, SNR and blocking probability are analyzed as crucial Quality of Transmission (QoT) parameters. These metrics are essential for understanding how the integration of quantum channels affects traditional optical network operations, particularly in terms of channel capacity and overall network efficiency.

To address these complex challenges, our methodology integrates theoretical analysis with numerical simulations, utilizing the custom-developed network simulator to explore the bidirectional impacts of QKD-WDM integration. This includes a detailed examination of capacity, Raman noise, power levels, SNR and SKR. By developing optimization algorithms for RWA, the study not only seeks to minimize the impact of Raman noise on QoP but also strives to maintain the QoT for classical channels. This approach aims to ensure that the coexistence of QKD and WDM channels within the network meets both high performance and security standards.

4.3 Modeling Secure Key Rate and Noise Contributions in QKD Systems

A precise model of QKD functionality is paramount in the endeavor to integrate QKD with classical optical networks. This model must account for the complexities introduced by the presence of classical WDM signals. As mentioned earlier, we will focus on the integration of the CV-QKD due to its compatibility with telecommunication technologies and potential integration capabilities into existing networks.

The system architecture depicted in Fig. 4.2 illustrates the integration of QKD within a WDM network, designed to facilitate the simultaneous transmission of quantum and classical data. At the heart of this integration are multiplexers (MUX) and demultiplexers (DEMUX), strategically deployed to manage multiple data channels. These include standard WDM signals for classical data transmission alongside dedicated channels for

quantum-encrypted communications. To safeguard the integrity of these signals, the QKD pathway is meticulously engineered to circumvent any optical amplifiers (OA) that would completely destroy the QKD signal. The integration employs two critical types of optical filters to achieve this. Optical Filter 1 is strategically placed immediately after the multiplexer at the transmission end, serving as a notch filter. Its primary role is to sift through the ASE noise from the classical WDM channels, effectively preventing this common source of interference from contaminating the quantum signals. This filter is crucial for keeping the quantum channel pure at its inception, avoiding the introduction of noise elements that could otherwise lead to errors in key distribution.

Optical Filter 2, situated just before the demultiplexer at the reception end, is tailored as a bandpass filter designed specifically for the quantum frequency. This filter performs the critical function of isolating the incoming quantum signals from any residual classical noise or adjacent channel crosstalk. By precisely filtering out all non-relevant wavelengths, Optical Filter 2 ensures that only quantum information reaches CV-QKD Bob.

While optical filters effectively mitigate issues like out-of-band ASE noise, they are insufficient to address all noise concerns in quantum key distribution systems. Particularly, nonlinear noise sources such as FWM and Raman scattering present substantial challenges in the integration of QKD within WDM networks. These nonlinear phenomena arise due to the interactions between different wavelengths within the fiber, influenced by the fiber's material properties and the high power of classical channels.

FWM, for instance, can generate new frequencies that interfere with the quantum channels, potentially leading to erroneous detections and compromised security. Similarly, Raman noise, caused by the scattering of photons off the vibrational modes of the optical fiber, can lead to background noise that significantly degrades the quantum signal. Such effects are exacerbated in high-power environments typical of dense WDM systems and cannot be eliminated simply by filtering.

The focus on these nonlinear noise sources is driven by their pervasive impact on the fidelity and security of the transmitted quantum keys. The proposed system design incorporates advanced filtering techniques to handle ASE and out-band leakage noise, but it also emphasizes the meticulous analysis and mitigation of nonlinear noise phenomena, such as Raman noise and FWM. Achieving high isolation levels is crucial to this approach. The system aims for isolation well above the typical 30 dB provided by multiplexers, targeting operational efficiencies in the realm of 80 dB or greater. This high level of isolation is essential to ensure that the quantum channel remains free from the influence of classical channels, despite the inherent limitations of optical filtering against nonlinear noise.

Therefore, a detailed investigation into the nonlinear Raman scattering effect is pursued to develop robust strategies that enhance the resilience of QKD systems against these challenging noise sources, ensuring the secure and efficient transmission of quantum keys

across integrated quantum-classical communication networks.

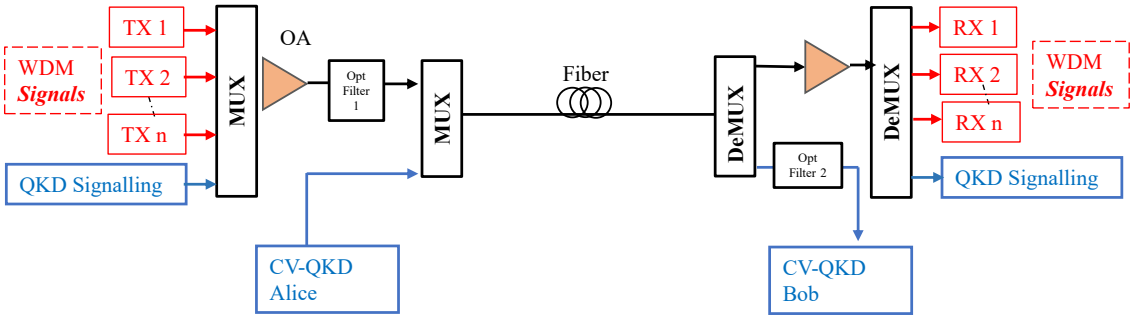

Figure 4.2: Typical Schematic for the co-existence of the WDM and QKD signals

4.3.1 SKR Model for Quantum Channels

The secure-key rate, denoted as $K = f_{\text{sym}} \cdot r$, is derived from the quantum channel's symbol rate (f_{sym}) and the secret fraction (r, in bits per symbol), where the secret fraction's optimal value is determined numerically based on the channel's transmissivity(T), the excess noise (ξ) measured at the channel output, the efficiency of information reconciliation (β), and the detection type (μ) [104], assuming an ideally efficient receiver. For a given link length (L) with n classical WDM signals, the SKR can be calculated as a function of the channel's transmissivity (T) and excess noise (ξ), where transmittivity is given by:

$$T = 10^{-\frac{\alpha_{\text{dB}}}{10}}, \tag{4.1}$$

$$\alpha_{\text{dB}} = \alpha_0 + \alpha_L \cdot L, \tag{4.2}$$

with α_0 representing a fixed insertion loss, and α_L denoting the fiber's attenuation coefficient. The excess noise is modeled using a simple linear approach that aggregates various impairments arising from classical channels:

$$\xi = \xi_0 + \xi_{\text{Raman}} + \xi_{\text{FWM}} + \xi_{\text{crosstalk}}. \tag{4.3}$$

In this equation, ξ represents the total excess noise, which is composed of the detection noise (untrusted) ξ_0, the Raman noise contribution ξ_{Raman}, the four-wave mixing noise ξ_{FWM}, and the crosstalk noise $\xi_{\text{crosstalk}}$ (all of them in shot noise units (SNU)). Shot noise units are a measure of noise relative to the quantum noise limit of the system, which is the inherent noise due to the quantum nature of light. Each component contributes to the overall excess noise in the system, thereby affecting the performance of quantum communication channels.

For our study, we focus on Raman noise because the literature identifies it as the most significant source of excess noise in quantum channels. Raman noise, generated by the interaction of photons with the vibrational modes of the optical fiber, can severely

degrade the quantum signal. While other noise sources, such as FWM, can be mitigated through techniques like appropriate channel spacing, Raman noise is more challenging to manage. Therefore, understanding and mitigating Raman noise is crucial for enhancing the performance and security of QKD systems.

4.3.2 Raman Noise Model Integration

Raman scattering occurs when light interacts with the molecules of a material, causing the energy of the light to shift as it scatters. While most of the light scatters without changing its frequency, a small portion undergoes inelastic scattering, where the energy changes due to interactions with the vibrational modes of the molecules. This process creates light at new frequencies that are different from the original. These shifts in frequency, called Raman scattered light, are a direct result of how the light transfers energy to or from the molecular vibrations, offering valuable information about the material's molecular structure. If the scattered light has less energy than the incoming light, we observe a *Stokes shift*, indicating that energy has been transferred to the molecules. Conversely, if the scattered light gains energy from the molecules, it produces an *anti-Stokes shift*, where the light is scattered at a higher frequency than the original.

Raman scattering can occur in two primary forms: spontaneous and stimulated. Spontaneous Raman scattering happens naturally and randomly, with only a small fraction of light undergoing this process. However, when conditions are favorable, such as when a high-powered laser (pump) is introduced, *stimulated Raman scattering (SRS)* can take place. In this scenario, energy from the pump beam is transferred to a weaker signal beam, causing the scattered light to become amplified. This interaction creates a coherent process where the signal is strengthened, and additional energy is absorbed by the molecular vibrations of the medium, leading to an intensified output of scattered light. If both the signal and pump light travel in the same direction through the medium, the process is referred to as **forward or co-pump**. In contrast, when the signal and pump beams enter from opposite directions, it is called **backward or counter-pump**.

While SRS enhances the signal, it also generates noise. Managing this noise is critical, as excessive buildup can degrade the quality of the transmitted information. This form of noise, commonly known as amplified spontaneous emission (ASE), is an inevitable by-product in any optical amplification process. In the context of Raman amplifiers, ASE is specifically generated through *spontaneous Raman scattering*, and its presence must be carefully monitored to ensure the integrity of the transmission system.

According to Eq. 6 of [105], the generation and amplification of ASE obeys

$$\frac{dP_{ASE}^{+}}{dz} = -\alpha_{ASE} P_{ASE}^{+} + C_R(\lambda_{ASE}, \lambda_p) P_p P_{ASE}^{+} + C_R(\lambda_{ASE}, \lambda_p) \left[1 + \eta(T)\right] h\nu_{ASE} B_{\text{ref}} P_p \tag{4.4}$$

where P_{ASE}^{+} denotes the ASE power in one polarization component within a bandwidth of B_{ref}. Here, P_p represents the total depolarized pump power at position z. One notable distinction between this equation and the gain equation referenced in [105] for the signal is the presence of an additional inhomogeneous source term in the differential equation. This source term incorporates a phonon occupancy factor

$$\eta(T) = \frac{1}{\exp\left(\frac{h\Delta\nu}{k_B T}\right) - 1} \tag{4.5}$$

where is h Planck's constant, k_B is Boltzmann's constant, T is the temperature of the fiber in kelvins, and $\Delta\nu$ is the frequency separation between the pump and signal [105]. At $25°C$, η is approximately 0.14 at the Raman gain peak ($\Delta\nu = 13$ THz), and so it is a small correction factor. If precision is required, however, it needs to be considered, particularly for broad-band amplifiers where $\Delta\nu$ can be small when short wavelength channels are close to long-wavelength pumps . Another distinction between the mathematical description of ASE and signals is the boundary conditions, which for ASE are typically $P_{ASE}^{+}(0) = 0$.

In the Eq. 4.4, the first term α represents the attenuation of the fiber, the second term $C_R(\lambda_{ASE}, \lambda_p) P_p P_{ASE}^{+}$ represents the SRS between pump and ASE signals, the third term $C_R(\lambda_{ASE}, \lambda_p) \left[1 + \eta(T)\right] h\nu_{ASE} B_{\text{ref}} P_p$ represents the spontaneous Raman scattering of pump waves.

According to the model developed in the GNPy [20], we have ASE noise as the

$$\frac{dP_{ASE}^{+}}{dz} = C_R(\lambda_{ASE}, \lambda_p) \left[1 + \eta(T)\right] h\nu_{ASE} B_{\text{ref}} P_p \tag{4.6}$$

Compared to Eq. 4.4 the first part corresponding to the SRS is absent. The assumption to use only the second part of the Eq. 4.4 likely stems from the following reasoning: *By imposing the condition ($df > 0$), they ensure that the Raman gain effect occurs only when the pump frequency is higher than the signal frequency (Stokes shift), accounting for both polarization modes.*

4.3.2.1 ASE generation with polychromatic pumping and WDM signals

Utilizing the spectral flexibility of Raman amplification to shape the gain spectrum by combining multiple pump wavelengths and to create a polychromatic pump spectrum. Broadband Raman fiber amplifiers can be modeled using ordinary differential equations, which are suitable for polychromatic pump spectra and WDM signals. The average optical power of a pump or signal component at wavelength λ_i traveling in the positive z-direction can be denoted as P_i^{+}, and it follows (similar to the Eq. 1 of [105])

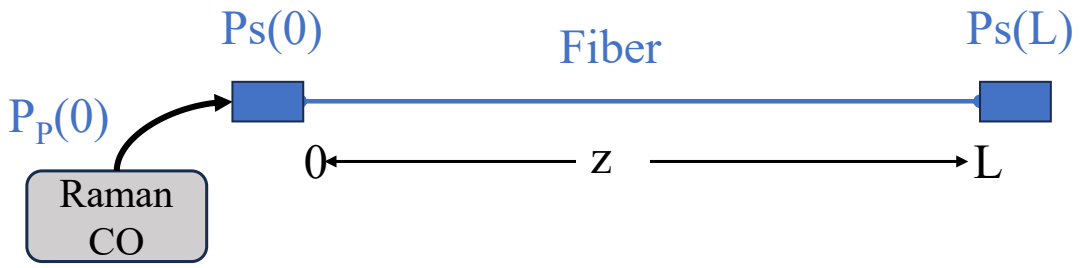

Figure 4.3: Schematic of a simple Raman fiber amplification

$$\frac{dP_i^+}{dz} = \left(\gamma_{st,i}^{em} - \gamma_{st,i}^{ab} - \alpha_i\right) P_i^+ \tag{4.7}$$

where $\gamma_{st,i}^{em}$ and $\gamma_{st,i}^{ab}$ are stimulated emission and absorption factors, respectively, given by (Eq. 20 of [105])

$$\gamma_{st,i}^{em} = \sum_{\lambda_j<\lambda_i} C_R(\lambda_i,\lambda_j)\left[P_j^+\right], \tag{4.8}$$

and

$$\gamma_{st,i}^{ab} = \sum_{\lambda_j>\lambda_i} C_R(\lambda_i,\lambda_j)\left[P_j^+\right]\left(\frac{\lambda_j}{\lambda_i}\right), \tag{4.9}$$

where P_j^+ are the average powers of pumps and signals at other wavelengths, λ_j.

The equation governing the growth of ASE power $P_{ASE,i}^+$ in one polarization (multiply by 2 for the dual polarization) component and in a bandwidth $B_{\text{ref},i}$ (in Hz) is

$$\frac{dP_{ASE,i}^+}{dz} = \left(\gamma_{st,i}^{em} - \gamma_{st,i}^{ab} - \alpha_i\right) P_{ASE,i}^+ + \left(\gamma_{sp,i}^{em} - \gamma_{sp,i}^{ab}\right) \tag{4.10}$$

The factor $\gamma_{sp,i}^{ab}$ accounts for Raman spontaneous absorption, and is given by (Eq. 21 of [105])

$$\gamma_{sp,i}^{ab} = \sum_{\lambda_j>\lambda_i} C_R(\lambda_i,\lambda_j) 2\eta_{ij}(T) h\nu_j B_{\text{ref},j} P_j^+ \tag{4.11}$$

and the phonon occupancy factor is given by (Eq. 22 of [105])

$$\eta_{ij}(T) = \frac{1}{\exp\left(\frac{h\Delta\nu_{ij}}{k_B T}\right) - 1} \tag{4.12}$$

where $\gamma_{sp,i}^{em}$ is a spontaneous emission factor, given by (Eq. 24 of [105])

$$\gamma_{sp,i}^{em} = \sum_{\lambda_j<\lambda_i} C_R(\lambda_i,\lambda_j)\left[1+\eta_{ji}(T)\right] h\nu_i B_{\text{ref},i} P_j^+ \tag{4.13}$$

4.3.2.2 ASE as the Raman noise (SpRS) for the co-existence of the classical and QKD systems

The interaction between classical and QKD signals is similar to the process in Raman amplifiers, where SpRS creates ASE. We use a similar approach to understand how classical signals affect QKD. In this comparison, the classical signals act as the polychromatic pump, while the QKD channel experiences effects similar to ASE due to SpRS induced by these classical signals. Therefore, we use Eq. 4.10 to calculate the amount of the SpRS noise based on co-propagating WDM signals.

Solution for the Eq. 4.10:

We start by solving the Eq. 4.10 using mathematical techniques suitable for first-order differential equations. The differential equation can be rearranged as follows:

$$\frac{dP^{+}_{SpRS,i}}{dz} + \left(\alpha_i + \gamma^{ab}_{st,i} - \gamma^{em}_{st,i}\right) P^{+}_{SpRS,i} = \gamma^{em}_{sp,i} - \gamma^{ab}_{sp,i} \tag{4.14}$$

Let $\beta_i = \alpha_i + \gamma^{ab}_{st,i} - \gamma^{em}_{st,i}$. The integrating factor is $e^{\int \beta_i z}$, and applying it gives:

$$\frac{d}{dz}\left(e^{\int \beta_i z} P^{+}_{SpRS,i}\right) = \left(\gamma^{em}_{sp,i} - \gamma^{ab}_{sp,i}\right) e^{\int \beta_i z} \tag{4.15}$$

Integrating both sides with respect to z:

$$e^{\int \beta_i z} P^{+}_{SpRS,i} = \int \left(\gamma^{em}_{sp,i} - \gamma^{ab}_{sp,i}\right) e^{\int \beta_i z} dz + C \tag{4.16}$$

Applying the initial condition $P^{+}_{SpRS,i}(0) = P_{0,i}$:

$$P^{+}_{SpRS,i}(z) = e^{-\int \beta_i z}\left(P_{0,i} + \int_0^z \left(\gamma^{em}_{sp,i} - \gamma^{ab}_{sp,i}\right) e^{\int \beta_i z'} dz'\right) \tag{4.17}$$

4.3.2.3 Validation of the SpRS calculation

To rigorously assess the reliability of our model, we undertook a validation study by comparing our results with those reported in existing literature. This comparative analysis not only corroborates our findings but also pinpoints areas where our model introduces new insights or improvements over established models.

The validation process relies on a research study outlined in [106]. The study explores a 40-channel dense WDM system that adheres to the ITU standard 100GHz grid in the C-band (1530-1565 nm). This system covers a wavelength range from 1529.55 nm (Channel 1) to 1560.61 nm (Channel 40). Within this range, a specific number of n channels are designated for quantum communications, while the remaining channels are utilized for classical data transmission.

The simulations were conducted using SSMF with the following characteristics: an attenuation coefficient of 0.2 dB/km, a dispersion coefficient of 17 ps/(nm·km), and a

dispersion slope of 0.061 ps/(nm^2·km). Additionally, the Raman gain coefficient of the SSMF fiber, which quantifies the strength of Raman scattering, was incorporated into the model to accurately simulate the interactions between quantum and classical channels from [105].

We duplicated this setup exactly to validate and make a direct comparison. Our simulations were carried out over a 40 km point-to-point connection, with all conventional channels operating at a consistent power level of 0 dBm, mirroring the arrangement outlined in the [106]. The choice of a 40 km point-to-point link is strategic, as it aligns with the typical transmission limit for CV-QKD systems. This distance ensures that the simulation captures the critical effects of signal degradation and Raman scattering, which are pivotal in determining the feasibility and performance of QKD over existing fiber infrastructure. Moreover, the use of a 40-channel dense WDM system is representative of a typical metropolitan area network, where such hybrid quantum-classical systems are expected to be implemented. Metropolitan networks are a key focus area for QKD deployment due to their relatively short link distances and the high density of data traffic, making them ideal for demonstrating the practical integration of QKD with classical channels. The decision to confine the simulation to the C-band is equally important. The C-band is the most commonly used wavelength range in optical communications, and demonstrating the successful integration of QKD within this band is crucial for proving that quantum and classical signals can coexist without the need for additional band (S/L/O) allocation.

We use a different modeling approach compared to the reference study. While the reference study uses Eq 5 of [106] to simulate the Raman noise effects from the co-propagating WDM on QKD channels, we employ our SpRS model obtained in Eq. 4.17 for this purpose. This difference in methodologies is essential because it involves a more dynamic calculation of power variations along the propagation distance 'z' and includes the impacts of stimulated Raman scattering on the classical channel powers due to their interactions among themselves.

The results of our simulations are illustrated in Fig. 4.4, where we observe a close match between our data and those from [106]. The minor discrepancies noted can be attributed to our model's more nuanced approach to power dynamics and Raman scattering effects, unlike the assumptions of constant power levels used in the reference study. This not only validates our model but also highlights its enhanced capability to handle complex interactions within quantum-classical hybrid systems.

The computational time required for simulating the Raman noise in the system differs significantly between our model and that of [106]. The primary reason for this difference lies in the complexity of the models employed. In [106], the Raman noise is calculated using an algebraic equation, which provides a rapid estimation but does not account for the dynamic variations in power propagation along the fiber length. This approach, while efficient,

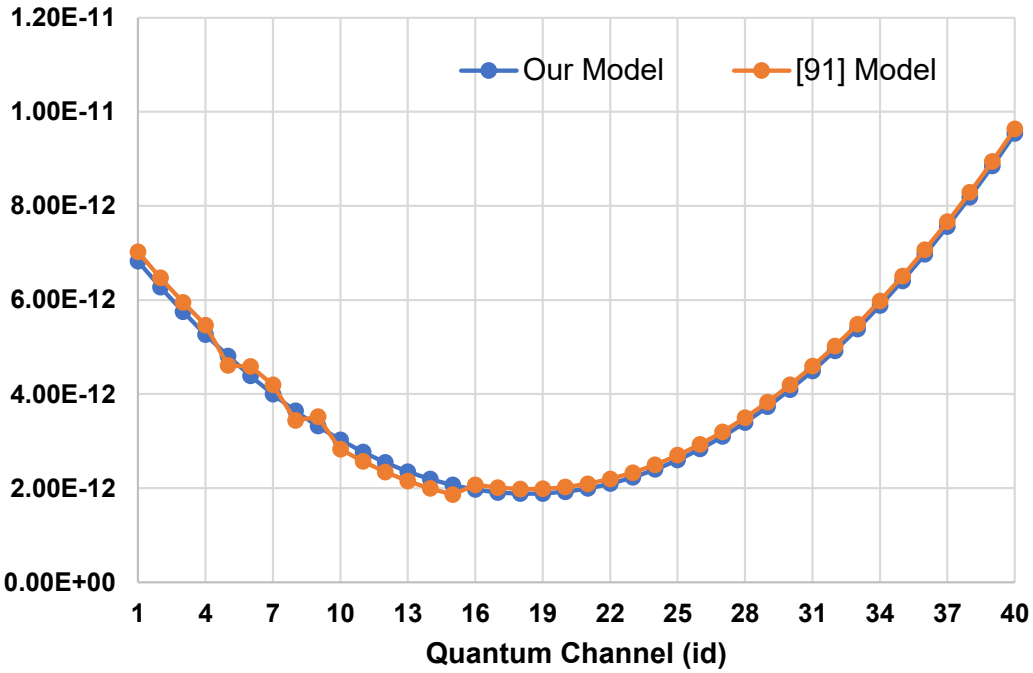

Figure 4.4: SpRS noise calculations for different placements of the quantum channel for a 40 km link

results in a computation time of approximately 1.064×10^{-5} seconds per simulation with 39 active classical channels co-propagating with 1 QKD channel. The computational time values provided were measured by running both simulation models under identical conditions, ensuring a fair comparison between the two approaches. Both models were executed on the same machine to avoid any discrepancies in hardware performance affecting the results. Specifically, the simulations were performed on a machine equipped with an Intel i7 processor, 16 GB RAM, and running Windows operating system.

In contrast, our model, as described in Eq. 4.17, employs a more sophisticated approach using first-order differential equations to solve for the Raman noise along with the power propagation dynamics. This method involves solving the differential equations iteratively, allowing for a more accurate representation of the interactions between classical and quantum channels along the entire propagation distance. Consequently, this increased computational complexity results in a longer computation time of approximately 2.78×10^{-5} seconds per simulation. Despite the additional computational overhead, the enhanced accuracy of our model provides a more realistic and detailed analysis of Raman scattering effects in hybrid quantum-classical systems.

4.4 Integrating the Raman noise model to calculate the SKR

We integrate the Raman scattering noise from the neighboring WDM signals into the SKR model of the QKD signals. For example, if we have a set of WDM channels with frequencies from 193.5 to 194 THz spaced by 50 GHz and suppose that we are interested in placing a quantum channel at the mid-frequency, say at 193.75 THz, the most straightforward approach to calculate the Raman noise from the neighboring active WDM (classical) channels would be to compute the ASE power using the above-formulated equations.

The SpRS noise power collected using the ODE equations is in power units. In our model for the QKD integration to calculate the SKR for the quantum channel, we use the calculated SpRS noise but in the units of the shot noise, i.e. SNU. The conversion to the SNU units is detailed below.

Let us consider the coexistence transmission shown in Fig. 4.2. In [107] authors have described the theoretical analysis on integrating the noise contribution from different sources such as

1. Leakage from the classical channels into the QKD channels at CV-QKD Bob
2. Spontaneous Raman Scattering Noise at the CV-QKD's receiver (Bob)
3. Four-wave mixing

We only focus on the Raman noise (SpRS) theoretical model. The SpRS noise power within a bandwidth of $\Delta\lambda$ measured at the output of the fiber in Fig. 4.2 is called as P_{SpSRS}. Given that the insertion loss of the DEMUX is η_{DMU} the in-band SpSRS photon number (per spatiotemporal mode) measured at the output of DEMUX (CV-QKD Bob in Fig. 4.2) is given by

$$\langle N^{(C)}_{\mathrm{SpSRS}} \rangle = \frac{\lambda^3}{hc^2} \frac{P_{\mathrm{SpRS}}}{\Delta\lambda} \eta_{DMU} \tag{4.18}$$

Finally, when we are using a homodyne detection-based scheme with Gaussian-modulated coherent state (GMCS) the excess noise contributed by noise photons in matched mode is given by (modeled as output from a chaotic source with Bose-Einstein photon statistics in shot noise units)

$$\epsilon_{\mathrm{out}} = 2\eta_{\mathrm{Bob}} \langle N^{\mathrm{in}}_{\mathrm{GMCS}} \rangle \tag{4.19}$$

where N_{GMCS} is the number of noise photons in matched mode arrived at Bob (CV-QKD Bob in Fig. 4.2) and is equal to the $\frac{1}{2} N^{(C)}_{\mathrm{SpSRS}}$

Hence, we have the final expression for the excess noise at Bob as follows:

$$\epsilon_{\mathrm{out}} = \eta_{\mathrm{Bob}} \frac{\lambda^3}{hc^2} \frac{P_{\mathrm{SpRS}}}{\Delta\lambda} \eta_{DMU} \tag{4.20}$$

The SKR model developed by us does require the excess noise at the end of the channel. So, to obtain the excess noise we divide Eq. 4.20 by the efficiency of the Bob and the insertion loss of the DEMUX.

Finally, the excess noise in SNU at the end of the channel is given as

$$\epsilon_{\text{ch}} = \frac{\lambda^3}{hc^2} \frac{P_{\text{SpRS}}}{\Delta\lambda} \tag{4.21}$$

4.4.1 Validation of SpRS as excess noise in SNU

Authors in [108] have used the Eqns. [4.18-4.21] to compute the SpRS in the SNU units for a simple system with the classical channel at 1550.12 nm and QKD channel at 1531.12 nm. The power of the classical channel is set at 0 dBm over the fiber length of 25 km SMF. The excess noise reported in [108] was 1.3e-3 SNU.

We perform the simulation with the same settings using the SpRS model proposed earlier. The obtained Raman noise is equal to 3.23×10^{-11} W, in a 0.5 nm bandwidth. The equivalent excess in the SNU units using the Eq. 4.21 is 1.92×10^{-3} SNU. Despite a small discrepancy, the close agreement demonstrates that our SpRS model is still valid and reliable for estimating excess noise in QKD systems.

Having established a robust model for the functionality of QKD within WDM networks, we now turn our attention to define the network parameters and pospose different scenarios. The following section, titled 'Wavelength Allocation Strategy for Co-existence', delves into our systematic approach to identifying optimal spectral regions for QKD channels amid the congested C-Band spectrum. This method not only assesses the Spontaneous Raman Scattering noise across various load conditions but also fine-tunes the placement of quantum channels to achieve the lowest possible interference in a fully loaded WDM network. By exploring the dynamics of SpRS noise in different operational scenarios, we illustrate how wavelength management underpins the effective coexistence of quantum and classical channels, ensuring that the integrity and security of quantum communications are maintained in a densely populated optical spectrum.

4.5 Wavelength Allocation Strategy for the co-existence of classical-quantum

Across the C-Band spectrum, our approach seeks to systematically identifies regions of minimal SpRS noise under full spectral load to determine the ideal placement for the QKD channel. We also verify our approach amidst varying load conditions.

Case Study: 40 channel 100 GHz ITU Grid C-band spectrum optimization: In Fig. 4.5, we simulate the placement of one QKD channel among 40 possible wavelengths ranging

from 1529.55 nm to 1560.61 nm, with 39 classical channels simultaneously active at 0 dBm on a standard SMF fiber with a 0.2 dB/km loss coefficient with C_R defined as in [8]. We analyze SpRS noise levels for link lengths of 40 km (green line) and 20 km (blue line), revealing consistently low SpRS noise in the window 1541.35 nm - 1543.73 nm,identifying this spectral bandwidth as the optimal placement for the QKD channel.

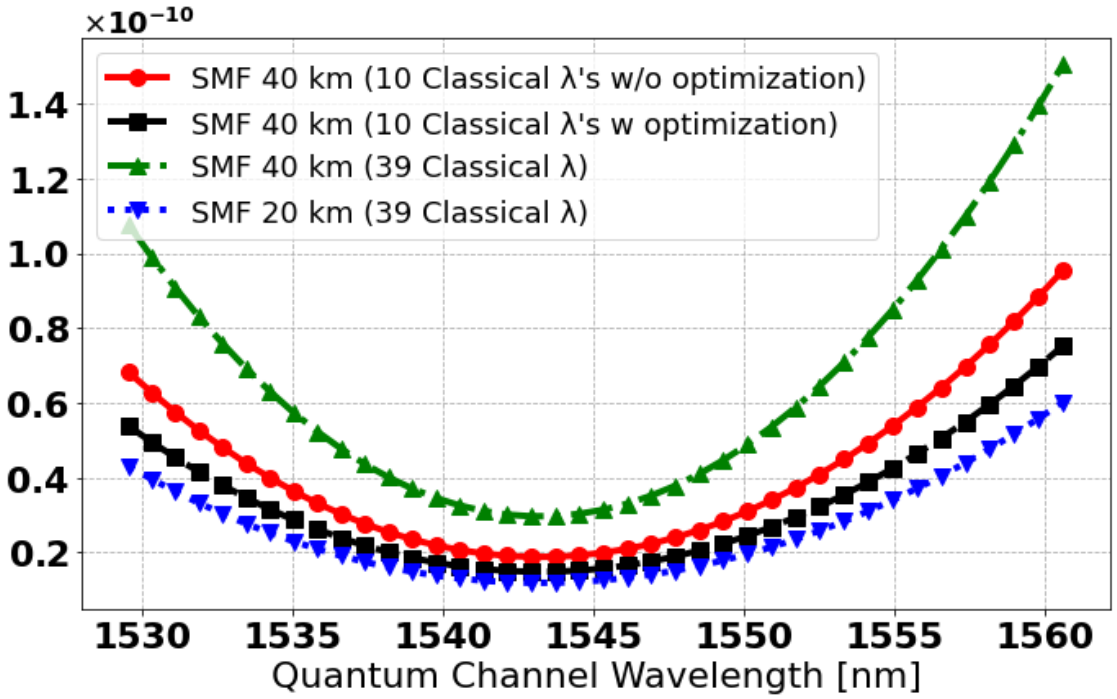

Figure 4.5: Quantum Channel Placement and SpRS for a 40 channel ITU-T grid with 100 GHz channel spacing

As an example for varying load, for a 40 km link with only 10 classical channels, we systematically explore two configurations by first presetting the QKD channel at each of the 40 potential wavelengths: a) allocating the 10 classical channels using the 'first-fit' method (red line); and b) calculating the placement of classical channels to achieve the lowest Raman noise at the preset QKD channel (black line). The latter configuration yields the lowest magnitude of SpRS noise in the same region 1541.35 nm - 1543.73 nm. This systematic wavelength optimization for quantum-classical channels' coexistence, fundamental to our heuristic strategies, helps us establish optimum network assumptions. We refer to this approach as 'Quantum Aware Wavelength Assignment' (QAWA).

4.6 Simulations and Discussion

We perform simulations on a fictious mesh network to analyze the impact of the QKD integration into the classical QoT-aware WDM routing and wavelength assignment. Our simulator integrates the earlier mentioned SKR model as a Quality of Protection (QoP)

indicator for QKD and an SNR derived from the ISRS-GN model as the QoT indicator for classical traffic.

4.6.1 Network Description

Fig. 4.6 represents a 7-node mesh network with 16 unidirectional (8 bidirectional links) links with 42 traffic demands (taken from the Net2Plan "example 7 node network with traffic demands of Spain") ranging from 6.95 to 1815 Gbit/s, totaling 10 Tbit/s. We maintained a consistent traffic matrix for classical and QKD traffic, uniformly scaling to maximum loads of 1000 Tbit/s and 1 Tb/s to vary the load. The links average 273 km each; however, since CV-QKD is usually limited to ranges up to tens of km, we rescaled all the links by using scale factors Λ. We report the results at the two specific values of Λ 0.01 and 0.1 representing the campus-scale network and metropolitan network respectively. The simulation parameters are reported in Table. 4.3.

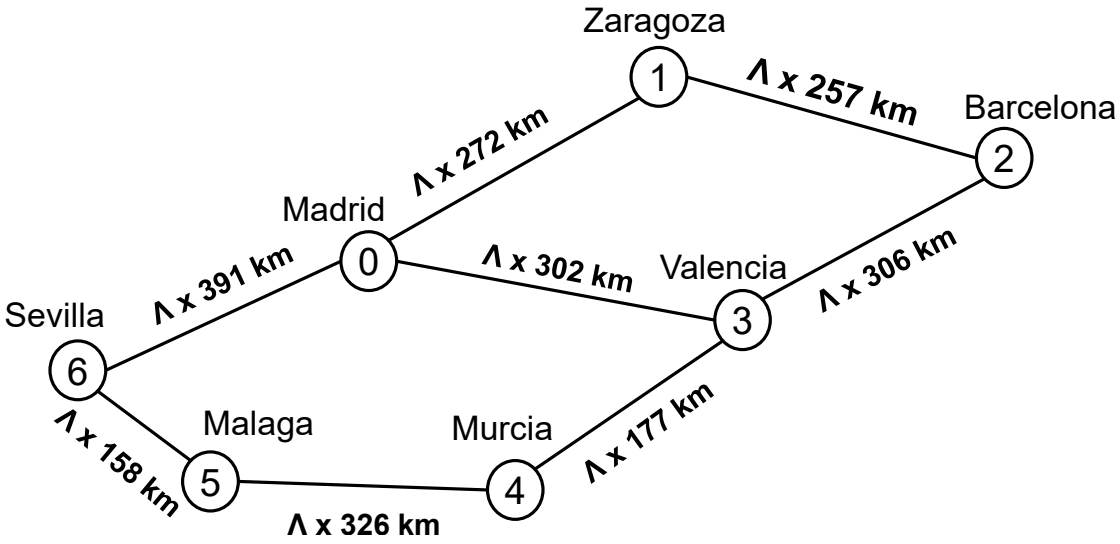

Figure 4.6: Network Topology

4.6.2 Routing and Wavelength Assignment

4.6.2.1 CV-QKD Traffic

In our approach, CV-QKD demands are managed as in an opaque network, considering the range limitations inherent to CV-QKD. We avoid any optical bypasses, which would otherwise extend the paths and diminish the overall capacity. Each node within the network is treated as a trusted relay, aggregating traffic from all CV-QKD demands destined for the same link. Initially, the CV-QKD capacity of each link is assessed based on the maximum key rate (SKR) achievable in the absence of Raman noise, assuming no classical traffic interference.

Table 4.3: CV-QKD and WDM Simulation Parameters

Parameter	**Value**
Maximum classical WDM channels per fiber	40 wavelengths (1529.55 nm to 1560.61 nm)
Channel spacing	100 GHz
Classical data rate per WDM channel	100 Gbit/s [32 Gbaud DP-QPSK]
Classical optical power per WDM channel	0 dBm/ -10 dBm
Optical fiber attenuation	0.2 dB/km
Insertion loss on quantum channel	2 dB
CV-QKD symbol rate	1 Gbaud
CV-QKD reconciliation efficiency	0.95
CV-QKD detection type	Heterodyne
CV-QKD receiver fixed noise	10^{-3} SNU
Maximum paths per node pair in RWA	5

Subsequently, we prioritize the demands by focusing on those with the largest volumes of unallocated traffic. For each of these demands, we evaluate the k shortest possible paths, selecting the path that offers the highest remaining capacity. A route is then established to carry as much of the demand's traffic as possible, ensuring that the aggregated traffic on any link does not exceed its calculated capacity. This process is repeated iteratively until all CV-QKD demands have been accommodated or no additional routes can be established.

For the quantum channel, a comprehensive analysis of the available wavelength spectrum is conducted to preemptively secure the optimal placement for the QKD channel, a critical step that precedes the introduction of classical traffic. We identify and designate the wavelength exhibiting the lowest Raman noise as the primary QKD channel. To further safeguard against cross-talk and FWM noise, adjacent channels are reserved as guard bands. This meticulous strategy helps to protect the quantum communications within the network.

4.6.2.2 Classical Traffic

In our network configuration, a Routing and Wavelength Assignment (RWA) heuristic is utilized to manage classical traffic demands as in a transparent network. In this model, lightpaths are directly established from the origin to the destination node, maintaining wavelength continuity across all links in the path. This assumes that each node functions as a perfectly flexible ROADM. Given the manageable short ranges (after scaling the network), all paths are considered classically feasible without the necessity for signal regeneration.

Each lightpath occupies a single WDM slot and is designated to carry a fixed traffic rate (R), 100G.

No specific arrangements are made to ensure that multiple lightpaths required to fulfill large demands follow identical routes or occupy contiguous WDM slots. Instead, demands are processed in decreasing order of their yet-unallocated traffic volumes. During this process, the k shortest possible paths are assessed for each demand to confirm the availability of a WDM slot across the entire path. Additionally, it is verified that the inclusion of a new slot does not compromise any link's ability to support its existing CV-QKD traffic, ensuring no reduction in the CV-QKD capacity below its current load. A lightpath with a capacity of 100 Gbit/s is then established on the shortest path that meets these criteria.

This procedure is iteratively repeated until all classical demands are accommodated or no additional lightpaths can be established. Our classical channel allocation strategy employs a refined heuristic that considers the k-shortest paths (where k=5) to efficiently fill WDM slots. This approach is meticulously designed to ensure that Raman noise remains below the threshold that would impact the QoP of the QKD channels while maintaining the required QoT for classical WDM channels.

Moreover, the algorithm dynamically optimizes wavelength placement to minimize the Raman noise affecting the QKD channel. This adaptive strategy enhances the system's resilience to traffic fluctuations and the introduction of new channels, ensuring robust and reliable network performance under varying operational conditions.

4.6.3 Simulations on an example Metropolitan Network ($\Lambda = 0.1$)

As we allocate the CV-QKD traffic first, we start by looking at the blocking probabilities of the CV-QKD traffic. Additionally, in some simulations, we have implemented a conservative strategy where the total CV-QKD traffic on each link is deliberately kept below the link's maximum CV-QKD capacity by a set margin. This conservative allocation has shown a significant impact on system performance and reliability.

Fig 4.7 shows the relationship between the offered QKD traffic and the resulting blocked QKD traffic, with different margins applied. The x-axis represents the offered QKD traffic in bits per second, ranging from 10^6 to 10^{12} bits per second, while the y-axis represents the percentage of blocked QKD traffic.

At a lower traffic level of 10^7 bits per second, the blocking probability is minimal across all margin levels (No Margins, 5%, 12%, and 14%). The system can handle the offered traffic effectively without significant blocking, indicating sufficient network capacity for low traffic levels.

As the offered QKD traffic increases to 2.8×10^8 bits per second, we observe distinct differences in blocking probability depending on the margin applied. For the scenario with no margins (Green Line), blocking starts to become noticeable around this traffic level,

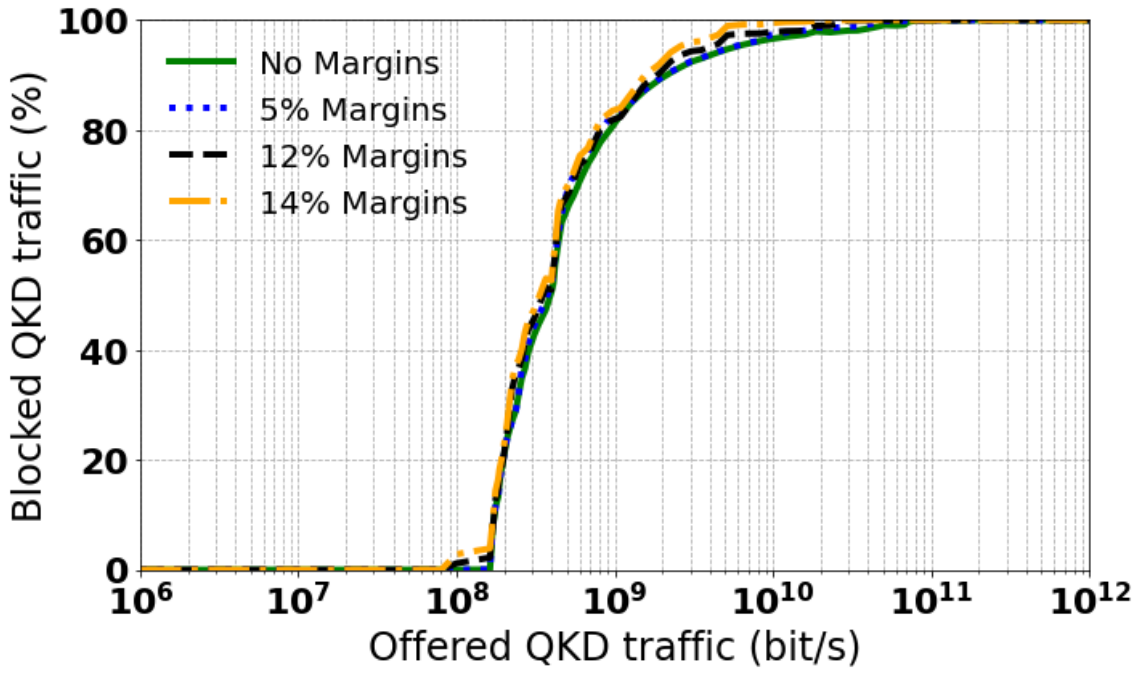

Figure 4.7: Blocking Probability of the CV-QKD Traffic w and w/o margins

but it is still manageable. When a 5% margin (Blue Dashed Line) is applied, the system starts blocking QKD traffic slightly earlier compared to the no margins case, indicating a minor increase in blocking probability. With a 12% margin (Black Dashed Line), blocking becomes significant, starting earlier than both the no margins and 5% margins cases, highlighting the impact of higher margins. At a 14% margin (Orange Dashed Line), the blocking probability curve is quite similar to the 12% margin case, showing early onset of blocking, indicating that increasing margins leads to more frequent blocking of QKD traffic.

At a higher traffic level of 4.5×10^9 bits per second, the system experiences a sharp rise in blocking probability across all margin levels. For the no margins scenario (Green Line), the blocking probability approaches 100%, indicating that the network capacity is overwhelmed at this traffic level. With 5% margins (Blue Dashed Line), blocking reaches nearly 100%, slightly earlier than in the no margins case, demonstrating the impact of applying a 5% margin. The 12% margin scenario (Black Dashed Line) sees the blocking probability quickly rise to near 100%, starting earlier than both the no margins and 5% margins cases, showing significant blocking due to higher margins. Similarly, in the 14% margin case (Orange Dashed Line), the blocking probability reaches close to 100% early, confirming that higher margins lead to an increased likelihood of blocking at high traffic levels.

To describe in a nutshell, we observe that maintaining a margin of 5%-15% on the total CV-QKD traffic below the link's capacity slightly increases the blocking probability of the

CV-QKD traffic. However, this increase is minimal, and importantly, it demonstrates a significant effect when allocating classical traffic.

Classical Traffic Blocking Probability (@ CV-QKD traffic $= 4.5\times10^9$ bit/sec)

We evaluated the blocking probability using our proposed heuristics. In the case of 'Heuristics 'a'', we consider only the calculated Raman noise to decide whether a light-path satisfies the QoP and QoT requirements. 'Heuristics 'b'' adds to that a wavelength optimization placement. Additionally, we benchmark against both the Low Raman and High Raman extreme cases developed in [103]. For the Low Raman scenario, the Raman noise of each channel is fixed to a lower bound of 10^{-12} SNU/W, whereas in the High Raman scenario, the Raman noise is fixed at 10 SNU/W. These fixed values replace the need for calculating the Raman noise dynamically. Lastly, we compare these results with the blocking probability of classical traffic in the absence of any QKD signals ('No QKD').

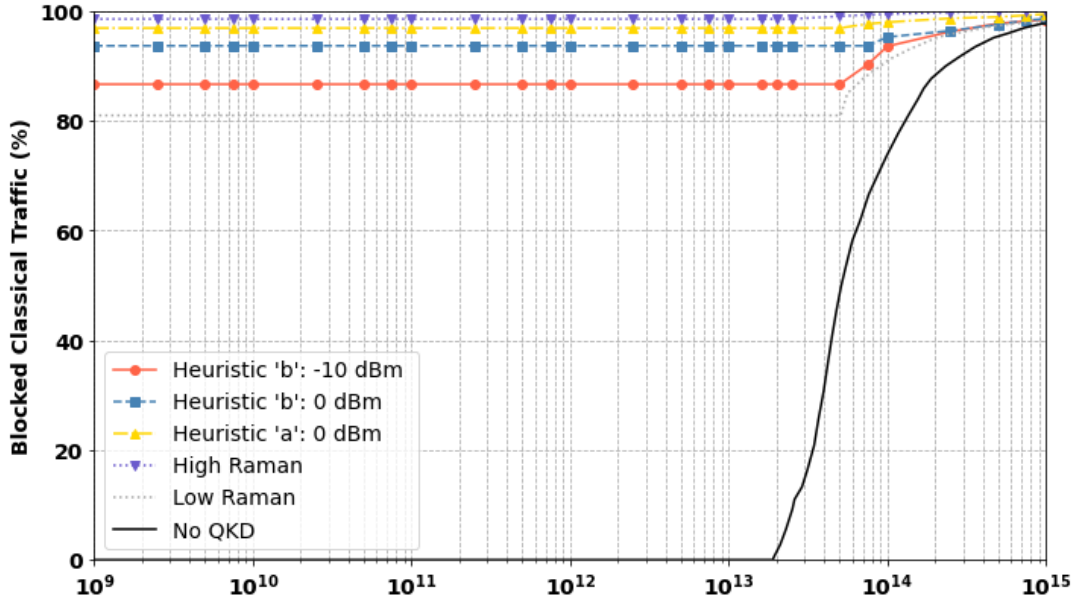

Figure 4.8: Classical Traffic Blocking Probability for a CV-QKD traffic of 4.5×10^9 bit/s at (no margins)

In Fig 4.8 'High Raman' represents the upper extreme, resulting in a high blocking floor of 98% at low classical traffic levels. 'Heuristic a: 0 dBm' lowers this to 96.4% due to high Raman noise levels of 3×10^{-1} SNU against tolerable limits near 0 SNU. 'Heuristic b: 0 dBm' further reduces the blocking floor to 94%, comparable to 'Low Raman,' (at 82%) which underestimates Raman noise we are still performing worse. However, none matches the 'No QKD' scenario, which could concern network operators because of the high blocking floors.

For the 4.5×10^9 bit/s CV-QKD traffic, as we can see from Fig 4.9, the tolerable Raman noise values for most of the links is at 0 SNU for the case of no margins because of high CV-QKD traffic. Also bound to the fact that we are dealing with high CV-QKD traffic, at

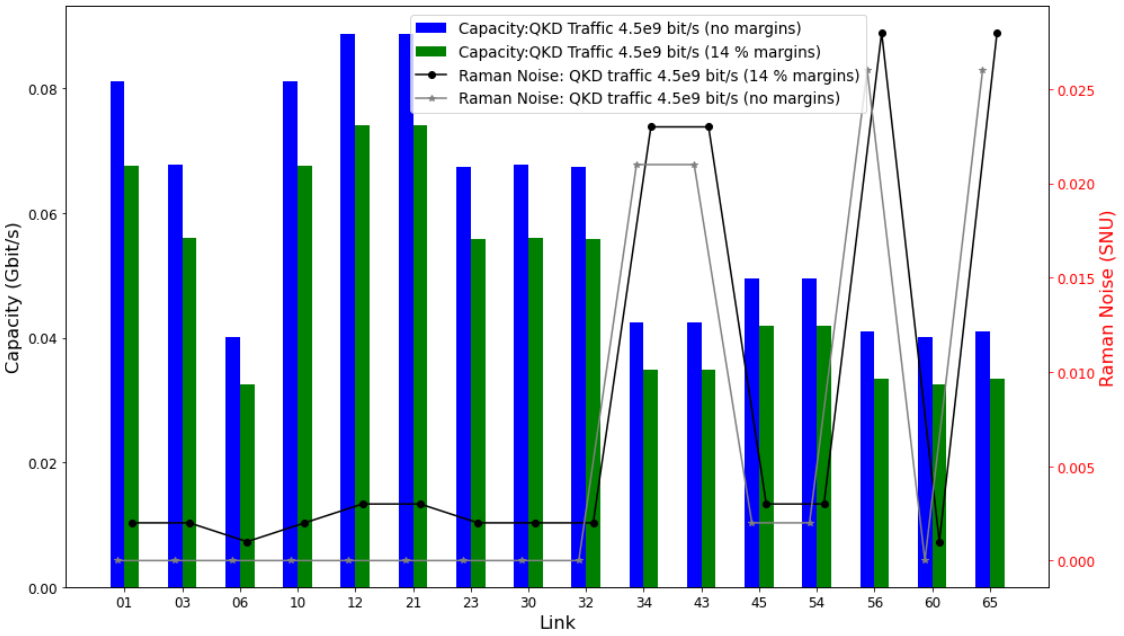

Figure 4.9: Tolerable Raman Noise and CV-QKD Link Capacities at CV-QKD traffic of 4.5×10^9 bit/s

the no margin case itself we have a blocking probability of 76% (Fig 4.7). As we can see from Fig 4.9 adding the constraint with 14% margins has significantly (improvement by 0.001 SNU of Raman noise would be enough to decrease the blocking probability similar to the low Raman case) increased the tolerable Raman noise.

The increase in tolerable Raman noise by availing margins can help us to solve the blocking floor of the classical traffic. Before allocating the classical traffic, we look back at the CV-QKD blocking probability plot(Fig 4.7). The plot indicates that adding margins up to 14% causes a minimal increase in blocking probability. Hence, now we allocate the classical traffic and analyze the obtained blocking probabilities shown in Fig 4.10

The first significant observation would be the match between the no QKD and the lower extreme Raman noise modeling ('Low Raman') case since we have the minimum tolerable amount of the Raman noise being non-zero (green bar-black line in Fig 4.9 (b)).

It even markedly improves the blocking floor (to 37.5%) with 'High Raman' itself (Fig 4.10). Using 'Heuristic a' we do reduce the blocking floor greatly to 1.5%. Now using 'Heuristic 'b' we have the better performance since the blocking floor has e=been reduced to 0% at the low classical traffics resembling the 'No QKD' line. But at the high amounts of the classical traffic, we still would have slightly higher blocking probability than the 'Low Raman' and the 'No QKD'. Additionally, reducing classical power by 10 dB ensuring the QoT for classical signals, closely aligning blocking probability with the 'No QKD' line even at the higher amounts of the classical traffic because of the reduction of the Raman noise.

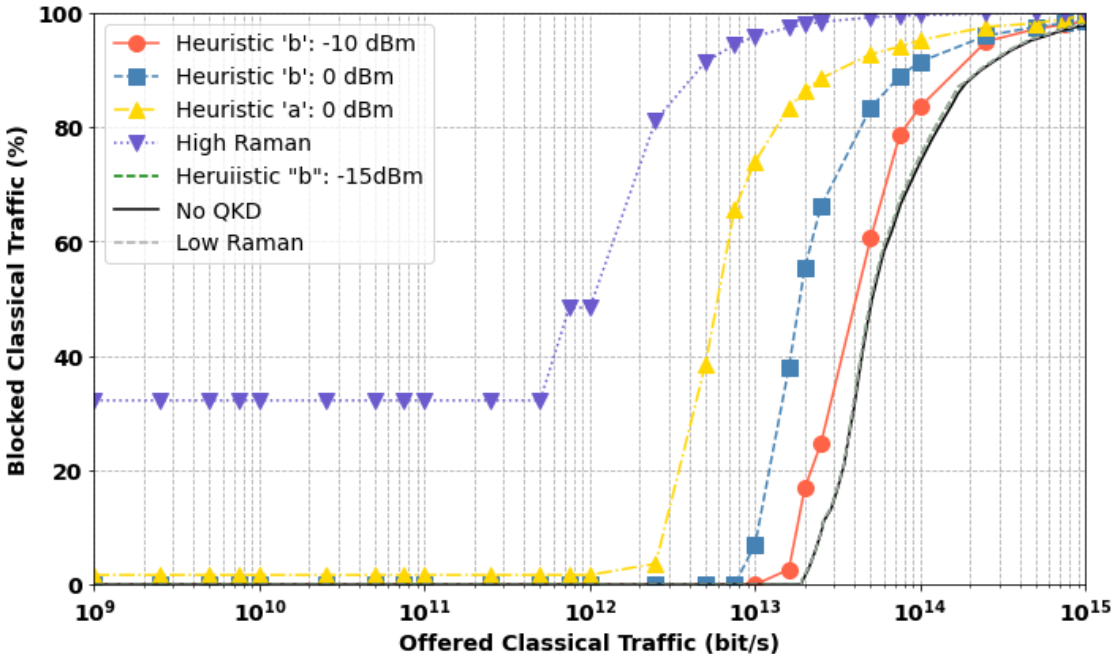

Figure 4.10: Classical Traffic Blocking Probability for a CV-QKD traffic of 4.5×10^9 bit/s (14% margins)

Hence by utilizing the margins on the CV-QKD links with a minimal impact on the blocking the CV-QKD traffic along with the optimized wavelength placement of the classical and quantum channels, we have significantly improved the blocking probabilities of the classical traffic.

Classical Traffic Blocking Probability (@ CV-QKD traffic $= 2.8 \times 10^8$ bit/sec)

Now we relax the amount of the CV-QKD traffic on the network by reducing it to 2.8×10^8. In Fig 4.11, 'High Raman' indicates the upper extreme, resulting in an 84.6% BP floor even at low traffic. 'Heuristic a: 0 dBm' reduces this to 28.8%, with Raman noise ranging from 1.5×10^{-2} SNU to 2.1×10^{-1} SNU across an average link length of 26 km, accommodating 4 to 37 classical channels. These levels exceed the tolerable limits, which are set by QKD traffic at approximately 10^{-3} SNU, and at 0 SNU on some links due to high QKD traffic. 'Heuristic b: 0 dBm' lowers the low traffic blocking floor to 17%, bringing the Raman noise between 9.2×10^{-6} SNU and 1.1×10^{-3} SNU, akin to 'Low Raman'. For a classical traffic load between 1 and 5 Tbit/s, we can bring the BP to 17% by decreasing the power of the classical WDM channels by 10 dB, while still maintaining the needed QoT. Although these first configurations lower the BP floor around 20%, we still do not match the 'No QKD' scenario.

As we can see from Fig 4.12, the tolerable Raman noise values for a few links are at 0 SNU for the case of no margins, hence resulting in high blocking floors. With 12% of margin, we do see some improvement in the tolerable Raman noise. The amount of CV-

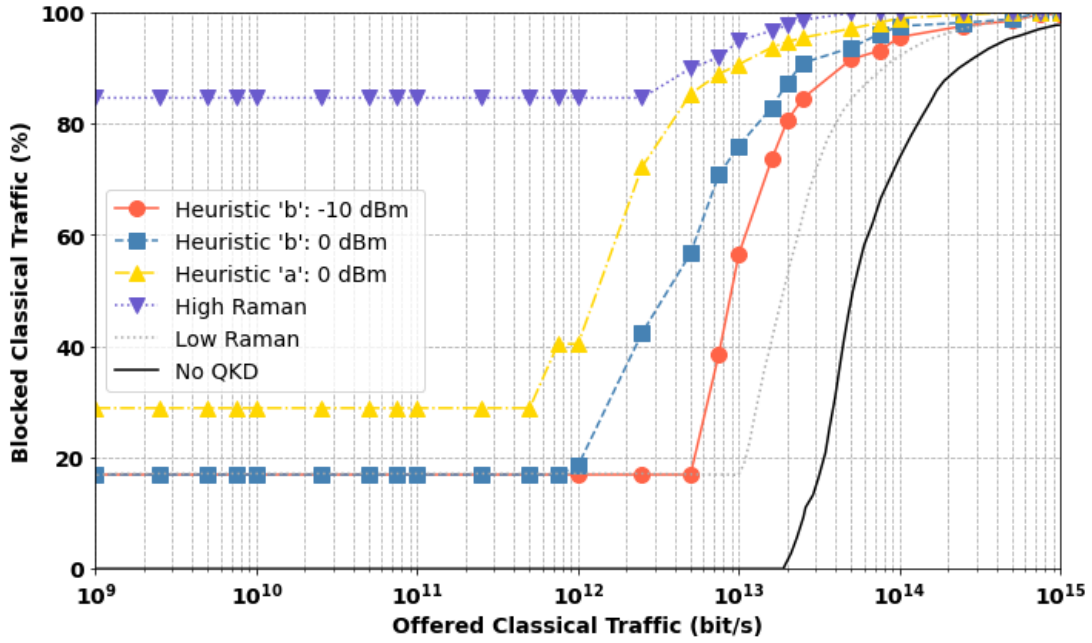

Figure 4.11: Classical Traffic Blocking Probability for a CV-QKD traffic of 2.8×10^8 bit/s (no margins)

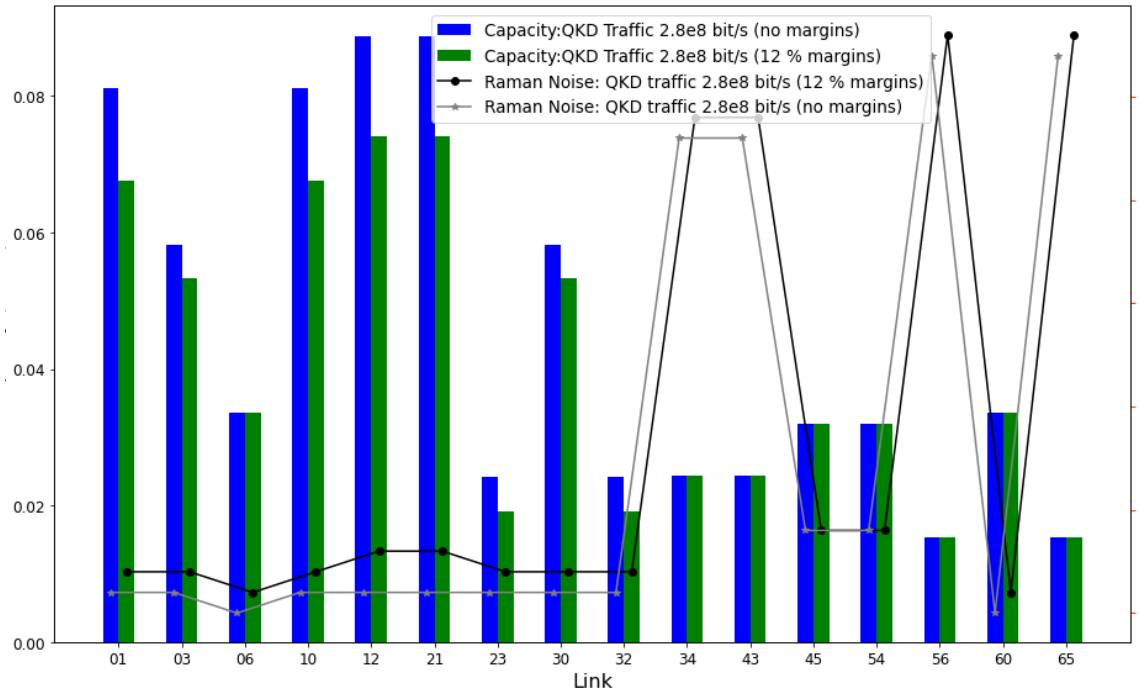

Figure 4.12: Tolerable Raman Noise and CV-QKD Link Capacities at CV-QKD traffic of 2.8×10^8 bit/s

QKD traffic that would be blocked, with a 12% margin, shows only a small increase in Fig 4.7.

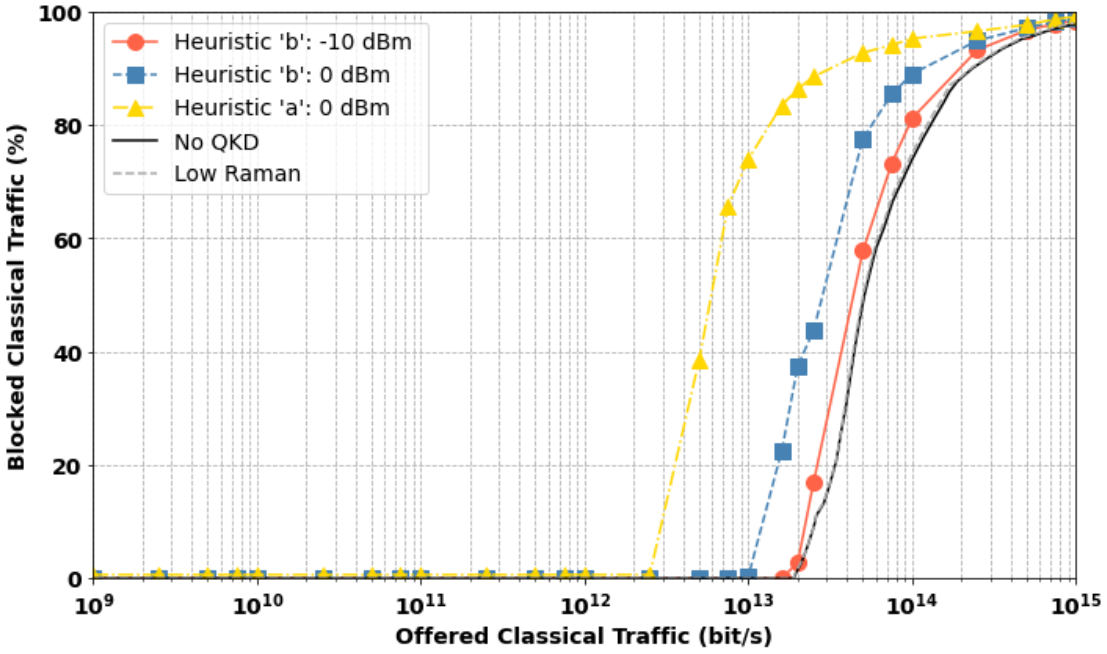

Figure 4.13: Classical Traffic Blocking Probability for a CV-QKD traffic of 2.8×10^8 bit/s (12% margins)

We start now looking at the case with a 12% margin, the blocking probabilities obtained in this case are summarised in Fig 4.13. Using 'Heuristic a', we determine that a 12% margin is enough to eliminate the BP floor of the classical traffic and bring it to a "No-QKD" level for low traffic loads (Yellow line). This result is achieved with a minimal increase of the CV-QKD's blocking probability (Fig 4.7). Using 'Heuristic b', we not only reduce the blocking floor but also enhance the classical network capacity from 1 Tbit/s to 10 Tbit/s, with a 280 Mbit/s network-wide QKD key exchanges. For high traffic loads, blocking probability remains a bit higher than in 'No QKD' conditions. This can be addressed by using 'Heuristic b' and reducing classical channels' power by 10 dB. We ensure that the QoT for classical signals in these conditions is still satisfied. As shown in Fig 4.13, the 'Heuristic b: -10 dBm' curve shows a near identical performance as the 'No QKD' results.

Classical Traffic Blocking Probability (@ CV-QKD traffic $= 1 \times 10^7$ bit/sec)

Finally, we further reduce the CV-QKD traffic to 1×10^7 bit/s. As we can see from Fig 4.15 without using any margins, tolerable Raman noise of the links is considerably high because of the very low amount of CV-QKD traffic. In the same Fig 4.15 we can see that none of the links are filled to half of at least a quarter of their maximum tolerable capacity (blue bars).

Fig 4.14 shows that 'Heuristic a' lowers the blocking floor floor with a 5% margin while 'Heuristic b', without any margin, reaches a higher capacity of 10.5 Tbit/s without a

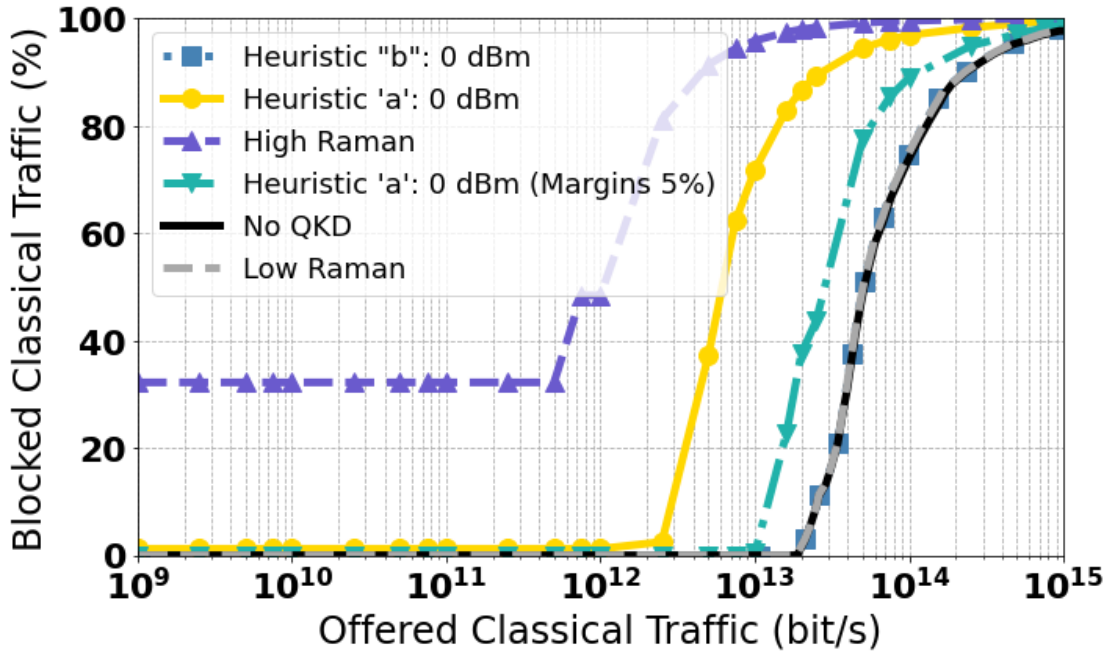

Figure 4.14: Classical Traffic Blocking Probability for a CV-QKD traffic of 1×10^7 bit/s

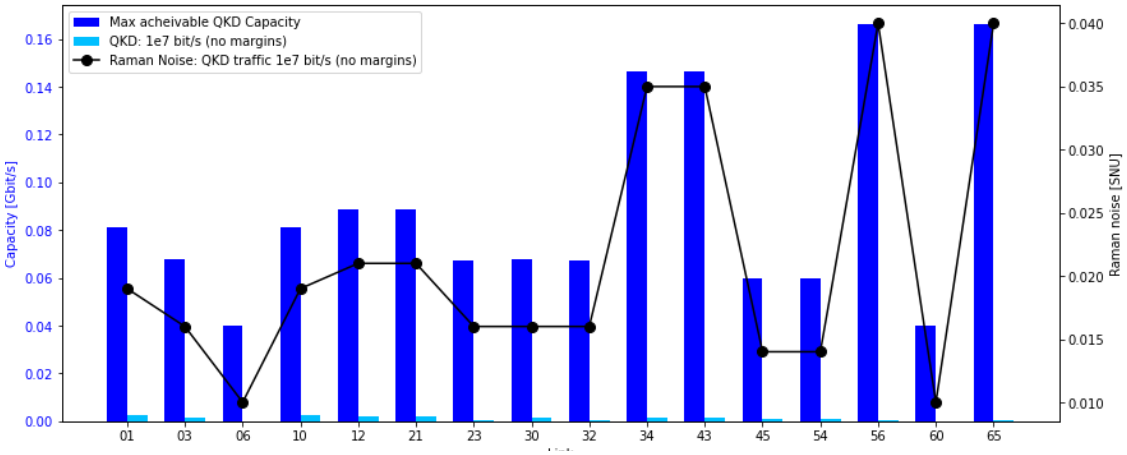

Figure 4.15: Tolerable Raman Noise and CV-QKD Link Capacities at CV-QKD traffic of 1×10^7 bit/s

blocking floor. These two approaches may offer network operators a choice between using 'Heuristic a' with margins or implementing 'Heuristic b'.

4.7 Summary

In this chapter, we have effectively utilized the simulator developed in Chapter 3 to integrate QKD functionality within classical optical networks, aiming to enhance the security of these networks.

We began by exploring the fundamental components and functionalities of a basic QKD

system, followed by a detailed literature survey examining the integration of QKD with WDM-based optical networks. This survey highlighted the various technical challenges associated with such integration, including crosstalk, Raman scattering, power level differences, modulation format compatibility, and nonlinear noise sources such as FWM and Raman noise.

A detailed investigation into the nonlinear Raman scattering effect was conducted, leading to the development of a robust Raman noise model. This model was validated against existing literature, demonstrating its reliability in estimating excess noise in QKD systems. We incorporated this model into our SKR calculations to evaluate the impact of Raman noise on the performance and security of QKD channels.

Furthermore, we developed a wavelength allocation strategy for the coexistence of classical and quantum channels, optimizing the placement of QKD channels to minimize Spontaneous Raman Scattering noise. Our network simulations showed that by adopting appropriate RWA methods and optimizing channel placement, we could significantly reduce the blocking probability for classical WDM traffic, even in the presence of high QKD traffic.

We evaluated the coexistence of a QKD channel with classical WDM channels in a meshed network. Our 'heuristic a' accurately calculated Raman noise, while the 'Quantum Aware Wavelength Assignment' (QAWA) approach applied wavelength placement optimization to minimize Raman noise. With 'QAWA,' we aligned the blocking probability of classical channels with 'No-QKD' conditions at network-wide QKD key exchange rates of 10 Mbit/s. Additionally, by applying a 12% margin or reducing the power of classical channels, we successfully managed classical traffic without blocking up to 20 Tbit/s for 280 Mbit/s QKD rates.

Conclusions and Future Directions

Conclusions

This thesis has examined impairment-aware optical network planning, addressing the pressing need for high-capacity, reliable, and cost-effective optical networks. By incorporating physical layer impairments into the planning process, our research has demonstrated significant improvements in addressing the data crunch, enhancing reliability through margins, and increasing security with new optical functionalities such as QKD.

The benefits of impairment-aware network planning are manifold. It allows for the optimization of existing infrastructure, thereby reducing the need for immediate upgrades and minimizing costs. Our work on SNR aware channel power optimization highlights this approach's potential. We developed and validated strategies for per-channel power allocation, focusing on both capacity and margin optimization. These strategies were experimentally validated on tandem networks, showing significant improvements in capacity and SNR margins compared to baseline methods like LOGO. For instance, in a tandem network scenario, our approach increased capacity by up to 0.2 bps/Hz and improved SNR margins by 2.8 dB, addressing the capacity crunch without incurring additional CAPEX.

Following the success of SNR-aware equalization, we proposed a extended network simulator for impairment-aware planning. This modular and extensible simulator integrates Network Topology, routing and wavelength assignment, and physical layer impairments into a cohesive tool. By bridging the data and control planes, the simulator offers a holistic view of network performance. Our simulations, conducted on an example 5-node topology, revealed that stringent QoT requirements could lead to higher blocking probabilities compared to traditional simulators like Net2Plan. Specifically, the blocking probability increased by approximately 15% under high traffic loads when QoT requirements were enforced. However, these stringent QoT standards ensure that transmission quality is consistently met, resulting in more reliable network performance overall.

Additionally, the simulator facilitates easy and feasible equipment upgrades by evaluating QoT requirements and leftover SNR margins. For example, during a transponder upgrade, the simulator can identify instances where SNR margins are sufficient to support

higher-order modulation formats without degrading QoT. This capability allows network operators to upgrade transponders incrementally as margins become available, minimizing disruptions and ensuring smooth transitions. It also allows them to address capacity crunch without incurring additional CAPEX.

Furthermore, the integration of optical functionalities like wavelength converters demonstrated a significant reduction in blocking probability, enhancing overall network efficiency. In our 5-node topology simulation, the use of wavelength converters reduced the blocking probability by up to 25%, showcasing their effectiveness in optimizing network resource utilization and maintaining high QoT standards.

Through these capabilities, the impairment-aware network simulator not only ensures robust and efficient network performance but also provides a practical approach to network planning and management, accommodating both current needs and future upgrades.

Finally, the feasibility of integrating Quantum Key Distribution (QKD) within existing optical networks was another critical aspect of this research. Simulation results demonstrated that with appropriate noise management, QKD channels can coexist with classical channels without significantly impacting overall network performance. This integration enhances network security, providing robust defense against quantum attacks.

The findings of our work have significant implications for the future of optical network design and operation. By considering physical layer impairments during the planning process, networks can achieve higher efficiency, optimizing both capacity and reliability without substantial increases in CAPEX or OPEX. This approach not only addresses current network demands but also prepares the infrastructure for the integration of advanced optical functionalities such as optical packet switching, flexible grid systems, and other emerging technologies. The integration of Quantum Key Distribution provides a significant enhancement to network security, ensuring robust protection against emerging quantum threats. Additionally, the proposed network simulator, with its modular and extensible design, supports the incorporation of future optical functionalities. For instance, it can simulate the impact of new technologies like space-division multiplexing, etc. on network performance, allowing for proactive planning and optimization. The developed tools and methodologies offer scalable and flexible solutions that can adapt to varying network demands and technological advancements, ensuring that optical networks remain at the forefront of technological innovation and continue to meet the evolving needs of the digital era.

In conclusion, this thesis has demonstrated the feasibility and benefits of impairment-aware network planning and the integration of QKD with classical WDM systems. The proposed methodologies and findings enhance the security, efficiency, and reliability of optical networks, laying the groundwork for future advancements in quantum communication technologies. By addressing both theoretical and practical aspects, this work paves

the way for the widespread adoption of quantum-secure communication in modern optical networks, ensuring robust protection against emerging cybersecurity threats.

Future Directions

Building on the findings of this thesis, several areas for future research are identified. To further validate and enhance the proposed SNR-aware per-channel power optimization strategies, it is essential to extend simulations and experiments to more complex network topologies. This will ensure the scalability and robustness of our algorithms in diverse and real-world scenarios. Similarly, investigating the performance of QKD-integrated optical networks in more complex topologies will provide deeper insights into the practical challenges and benefits of such integrations.

Additionally, investigating the impact of environmental factors, such as temperature variations and physical disturbances, on the performance of QKD systems in integrated networks is crucial. Developing more sophisticated noise mitigation techniques, particularly for managing nonlinear noise sources such as Four-Wave Mixing (FWM), will further enhance network performance and reliability.

Making the network simulator more generic is another critical future direction. This involves enhancing its capability to include a broader range of optical functionalities, such as optical packet switching, flexible grid systems, and space-division multiplexing, etc. By doing so, the simulator can provide a comprehensive tool for network planning and optimization that remains relevant as new technologies emerge.

One emerging area in the field of optical networks is Optical Spectrum as a Service (OSaaS). In this model, the optical spectrum is managed as a service, and users may not have detailed knowledge of the underlying equipment, treating it more like a black box. Our impairment-aware network planning tool can play a pivotal role in this context by managing power allocations and ensuring QoT standards for the different services that would share the spectrum. This includes integrating QKD to enhance security within the OSaaS framework, ensuring that even in a black-box environment, robust security and optimal performance are maintained.

Finally, exploring hybrid network architectures that combine the strengths of both QKD and classical encryption methods will achieve optimal security and performance. This approach can leverage the unique advantages of quantum and classical technologies, providing a versatile and future-proof framework for secure optical communication networks.

Bibliography

[1] Peter J Winzer, David T Neilson, et al. "Fiber-optic transmission and networking: the previous 20 and the next 20 years". In: *Optics express* 26.18 (2018), pp. 24190–24239.

[2] J Gill. *Future-proofing your network with infinera C + L*. URL: www.infinera.com/blog/future-proofing-your-network-with-infinera%02c-l/tag/innovation/.

[3] Victor Lopez, Benyuan Zhu, et al. "Optimized design and challenges for C&L band optical line systems". In: *Journal of Lightwave Technology* 38.5 (2020), pp. 1080–1091.

[4] André Souza, Bruno Correia, et al. "Cost analysis of ultrawideband transmission in optical networks". In: *Journal of Optical Communications and Networking* 16.2 (2024), pp. 81–93.

[5] Avishek Nag, Massimo Tornatore, et al. "Power Management in Mixed Line Rate Optical Network". In: *Photonics in Switching*. Optica Publishing Group. 2010, PTuB4.

[6] Adel A. M. Saleh and Jane M. Simmons. "All-Optical Networking—Evolution, Benefits, Challenges, and Future Vision". In: *Proceedings of the IEEE* 100.5 (2012), pp. 1105–1117.

[7] Yingqiu Mao, Bi-Xiao Wang, et al. "Integrating quantum key distribution with classical communications in backbone fiber network". In: *Optics express* 26.5 (2018), pp. 6010–6020.

[8] TE Chapuran, P Toliver, et al. "Optical networking for quantum key distribution and quantum communications". In: *New Journal of Physics* 11.10 (2009), p. 105001.

[9] Telegeography. url: https://blog.telegeography.com/total-international-bandwidth-now-stands-at-1217-tbps.

[10] Ericsson. Url: https://www.ericsson.com/en/reports-and-papers/mobility-report/dataforecasts/mobile-traffic-forecast.

[11] Joseph Berthold, Adel AM Saleh, et al. “Optical networking: Past, present, and future”. In: *Journal of lightwave technology* 26.9 (2008), pp. 1104–1118. URL: https://doi.org/10.1109/JLT.2008.923609.

[12] GFiber:[online] https://fiber.google.com/blog/2022/09/fast-forward-future-is-multi-gig.html.

[13] Miquel Garrich Alabarce and Pablo Pavón Mariño. “Optical network design and analysis tools: A test of time”. In: *Optical Switching and Networking* 44 (2022), p. 100651. URL: https://doi.org/10.1016/j.osn.2021.100651.

[14] Seiji Okamoto, Kyo Minoguchi, et al. “A study on the effect of ultra-wide band WDM on optical transmission systems”. In: *Journal of Lightwave Technology* 38.5 (2019), pp. 1061–1070. URL: https://doi.org/10.1109/JLT.2019.2962178.

[15] K. Christodoulopoulos, I. Tomkos, et al. “Elastic Bandwidth Allocation in Flexible OFDM-Based Optical Networks”. In: *Journal of Lightwave Technology* 29.9 (2011), pp. 1354–1366. URL: https://doi.org/10.1109/JLT.2011.2125777.

[16] David F. Welch, Fred A. Kish, et al. “The Realization of Large-Scale Photonic Integrated Circuits and the Associated Impact on Fiber-Optic Communication Systems”. In: *Journal of Lightwave Technology* 24.12 (2006), pp. 4674–4683. URL: https://doi.org/10.1109/JLT.2006.885769.

[17] Daniel King, Adrian Farrel, et al. “The role of SDN and NFV for flexible optical networks: Current status, challenges and opportunities”. In: *2015 17th international conference on transparent optical networks (ICTON)*. IEEE. Budapest, Hungary, 2015, pp. 1–6. URL: https://doi.org/10.1109/ICTON.2015.7193447.

[18] David J. Ives, Hou-Man Chin, et al. “Single Channel Probe Utilizing the EGN Model to Estimate Link Parameters for Network Abstraction”. In: *2017 European Conference on Optical Communication (ECOC)*. 2017, pp. 1–3.

[19] P. Poggiolini, G. Bosco, et al. “The GN-Model of Fiber Non-Linear Propagation and its Applications”. In: *Journal of Lightwave Technology* 32.4 (2014), pp. 694–721.

[20] Vittorio Curri. “GNPy model of the physical layer for open and disaggregated optical networking (*Invited*)”. In: *J. Opt. Commun. Netw.* 14.6 (2022), pp. C92–C104. URL: https://opg.optica.org/jocn/abstract.cfm?URI=jocn-14-6-C92.

[21] Alberto Bononi, Jean-Christophe Antona, et al. “The generalized droop formula for low signal to noise ratio optical links”. In: *Journal of Lightwave Technology* 38.8 (2020). doi: 10.1109/JLT.2020.2966145, pp. 2201–2213.

[22] Daniel Semrau, Eric Sillekens, et al. “Modeling and mitigation of fiber nonlinearity in wideband optical signal transmission”. In: *Journal of Optical Communications and Networking* 12.6 (2020), pp. C68–C76.

[23] H. Buglia, M. Jarmolovičius, et al. “A Closed-Form Expression for the Gaussian Noise Model in the Presence of Inter-Channel Stimulated Raman Scattering Extended for Arbitrary Loss and Fibre Length”. In: *Journal of Lightwave Technology* 41.11 (2023), pp. 3577–3586. URL: https://doi.org/10.1109/JLT.2023.3256185.

[24] Cédric Ware, Mounia Lourdiane, et al. “Can software-defined networks turn impractical optical functionalities into network-savers?” In: *2014 16th International Conference on Transparent Optical Networks (ICTON)*. IEEE. 2014, pp. 1–4. URL: https://doi.org/10.1109/ICTON.2014.6876566.

[25] Shun Yao, Biswanath Mukherjee, et al. “Advances in photonic packet switching: An overview”. In: *IEEE Communications Magazine* 38.2 (2000), pp. 84–94.

[26] Mable P Fok, Zhexing Wang, et al. “Optical layer security in fiber-optic networks”. In: *IEEE Transactions on Information Forensics and Security* 6.3 (2011), pp. 725–736.

[27] OptSim Application Notes and Examples, Rsoft Design Group, Inc. URL: https://www.synopsys.com/photonic-solutions/optsim/single-mode-network.html.

[28] OptiSystem. URL: https://optiwave.com/optisystem-overview/.

[29] OMNET++. URL: https://omnetpp.org/.

[30] GF Riley and TR Henderson. “The ns-3 Network Simulator”. In: *Wehrle, K., Güneş, M., Gross, J. (eds) Modeling and Tools for Network Simulation*. Springer Berlin Heidelberg, Berlin, Heidelberg, 2010. URL: https://doi.org/10.1007/978-3-642-12331-3%5C_2.

[31] Pablo Pavon-Marino and Jose-Luis Izquierdo-Zaragoza. “Net2plan: an open source network planning tool for bridging the gap between academia and industry”. In: *IEEE Network*. Vol. 29. 5. IEEE, 2015, pp. 90–96. URL: https://doi.org/10.1109/MNET.2015.7293311.

[32] Huawei. *OSNR Loss Equalization*. Available online. URL: https://info.support.huawei.com/network/ptmngsys/Web/WDMkg/en/83_osnr_loss_box.html.

[33] Ian Roberts, Joseph M Kahn, et al. “Convex channel power optimization in nonlinear WDM systems using Gaussian noise model”. In: *Journal of Lightwave Technology* 34.13 (2016), pp. 3212–3222.

[34] Ian Roberts, Joseph M Kahn, et al. “Channel power optimization of WDM systems following Gaussian noise nonlinearity model in presence of stimulated Raman scattering”. In: *Journal of Lightwave Technology* 35.23 (2017), pp. 5237–5249.

[35] Jose Krause Perin, Joseph M Kahn, et al. “Importance of amplifier physics in maximizing the capacity of submarine links”. In: *Journal of Lightwave Technology* 37.9 (2019), pp. 2076–2085.

[36] Ramin Hashemi, H Beyranvand, et al. "Joint channel power and amplifier gain optimization in coherent DWDM systems". In: *Optics Communications* 475 (2020), p. 126212.

[37] Venkata Virajit Garbhapu, Alessio Ferrari, et al. "Network-wide SNR-based channel power optimization". In: *2021 European Conference on Optical Communication (ECOC)*. IEEE. 2021, pp. 1–4. URL: https://doi.org/10.1109/ECOC52684.2021.9605942.

[38] Alessio Ferrari, Venkata Virajit Garbhapu, et al. "Demonstration of AI-Light: an Automation Framework to Optimize the Channel Powers Leveraging a Digital Twin". In: *2022 Optical Fiber Communication Conference (OFC)*. Optica Publishing Group. San Diego, CA, USA, 2022, pp. 1–3.

[39] Ivan Fernandez de Jauregui Ruiz, Amirhossein Ghazisaeidi, et al. "An accurate model for system performance analysis of optical fibre networks with in-line filtering". In: *45th European Conference on Optical Communication (ECOC 2019)*. 2019, pp. 1–4.

[40] Venkata Virajit Garbhapu, Cédric Ware, et al. "Physical-layer-aware network simulator for future optical functionalities". In: *2023 14th International Conference on Network of the Future (NoF)*. IEEE. 2023, pp. 28–36.

[41] VPIplayer. *VPIplayer*. URL: https://www.vpiphotonics.com/Tools/OpticalSystems/Demos/.

[42] Ori Gerstel, Masahiko Jinno, et al. "Elastic optical networking: A new dawn for the optical layer?" In: *IEEE communications Magazine* 50.2 (2012), s12–s20. URL: https://doi.org/10.1109/MCOM.2012.6146481.

[43] Bijoy Chand Chatterjee, Nityananda Sarma, et al. "Routing and spectrum allocation in elastic optical networks: A tutorial". In: *IEEE Communications Surveys & Tutorials*. Vol. 17. 3. IEEE, 2015, pp. 1776–1800.

[44] Cisco. *Cisco Annual Internet Report (2018–2023) White Paper*. URL: https://www.cisco.com/c/en/us/solutions/collateral/executive-perspectives/annual-internet-report/white-paper-c11-741490.html.

[45] Alessio Ferrari, Antonio Napoli, et al. "Assessment on the achievable throughput of multi-band ITU-T G. 652. D fiber transmission systems". In: *Journal of Lightwave Technology* 38.16 (2020), pp. 4279–4291.

[46] Andrea D'Amico, Bruno Correia, et al. "Scalable and disaggregated GGN approximation applied to a C+ L+ S optical network". In: *Journal of Lightwave Technology* 40.11 (2022), pp. 3499–3511.

[47] Jan Kundrát, Andrea Campanella, et al. “Physical-layer awareness: GNPy and ONOS for end-to-end circuits in disaggregated networks”. In: *2020 Optical Fiber Communications Conference and Exhibition (OFC)*. IEEE. 2020, pp. 1–3.

[48] Bob Lantz, Alan A Díaz-Montiel, et al. “Demonstration of software-defined packet-optical network emulation with mininet-optical and onos”. In: *Optical Fiber Communication Conference*. Optica Publishing Group. 2020, M3Z–9.

[49] Aric Hagberg, Pieter Swart, et al. “Exploring network structure, dynamics, and function using NetworkX”. In: *Proceedings of the 7th Python in Science Conference (SciPy2008), Gäel Varoquaux, Travis Vaught, and Jarrod Millman (Eds), (Pasadena, CA USA)*. 2008, pp. 11–18.

[50] David J Ives, Hou-Man Chin, et al. “Single channel probe utilizing the EGN model to estimate link parameters for network abstraction”. In: *2017 European Conference on Optical Communication (ECOC), Gothenburg, Sweden*. IEEE. 2017, pp. 1–3. URL: https://doi.org/10.1109/ECOC.2017.8345967.

[51] Hami Rabbani, Lotfollah Beygi, et al. “Quality of transmission aware optical networking using enhanced Gaussian noise model”. In: *Journal of Lightwave Technology* 37.3 (2019), pp. 831–838.

[52] John D Downie, Xiaojun Liang, et al. “SNR model for generalized droop with constant output power amplifier systems and experimental measurements”. In: *Journal of Lightwave Technology* 38.12 (2020), pp. 3214–3220.

[53] Daniel Semrau, Robert I Killey, et al. “A closed-form approximation of the Gaussian noise model in the presence of inter-channel stimulated Raman scattering”. In: *Journal of Lightwave Technology* 37.9 (2019), pp. 1924–1936. URL: https://doi.org/10.1109/JLT.2019.2895237.

[54] Wenbo Yu. “Investigation of Filtering Penalty Estimation Considering WSS Statistical Characteristics and Link Noise Distribution”. In: *2022 Asia Communications and Photonics Conference (ACP), Shenzhen, China*. IEEE. 2022, pp. 462–464. URL: https://doi.org/10.1109/ACP55869.2022.10088544.

[55] Xiaotian Zhu, Xiang Wang, et al. “Low-loss and polarization insensitive 32× 4 optical switch for ROADM applications”. In: *Light: Science & Applications* 13.1 (2024), p. 94.

[56] Nicolas Gisin, Grégoire Ribordy, et al. “Quantum cryptography”. In: *Reviews of modern physics* 74.1 (2002), pp. 145–195.

[57] Ronald L Rivest, Adi Shamir, et al. “A method for obtaining digital signatures and public-key cryptosystems”. In: *Communications of the ACM* 21.2 (1978), pp. 120–126.

[58] Shantanu Debnath, Norbert M Linke, et al. “Demonstration of a small programmable quantum computer with atomic qubits”. In: *Nature* 536.7614 (2016), pp. 63–66.

[59] Marcello Caleffi, Angela Sara Cacciapuoti, et al. “Quantum internet: From communication to distributed computing!” In: *Proceedings of the 5th ACM international conference on nanoscale computing and communication*. Reykjavik, Iceland, 2018, pp. 1–4.

[60] Angela Sara Cacciapuoti, Marcello Caleffi, et al. “Quantum internet: Networking challenges in distributed quantum computing”. In: *IEEE Network* 34.1 (2019), pp. 137–143.

[61] Marcello Caleffi, Daryus Chandra, et al. “The rise of the quantum internet”. In: *Computer* 53.6 (2020), pp. 67–72.

[62] Daniele Cuomo, Marcello Caleffi, et al. “Towards a distributed quantum computing ecosystem”. In: *IET Quantum Communication* 1.1 (2020), pp. 3–8.

[63] Angela Sara Cacciapuoti, Marcello Caleffi, et al. “When entanglement meets classical communications: Quantum teleportation for the quantum internet”. In: *IEEE Transactions on Communications* 68.6 (2020), pp. 3808–3833.

[64] Neel Kanth Kundu, Soumya P Dash, et al. “MIMO terahertz quantum key distribution”. In: *IEEE Communications Letters* 25.10 (2021). [Online]. Available: arXiv:2105.03642, pp. 3345–3349.

[65] N. Wolchover. “A tricky path to quantum-safe encryption”. to be published.

[66] Kent AG Fisher, Anne Broadbent, et al. “Quantum computing on encrypted data”. In: *Nature communications* 5.1 (2014), p. 3074.

[67] Yuan Cao, Yongli Zhao, et al. “Resource assignment strategy in optical networks integrated with quantum key distribution”. In: *IEEE/OSA Journal of Optical Communications and Networking* 9.11 (2017), pp. 995–1004.

[68] Peter W Shor. “Algorithms for quantum computation: discrete logarithms and factoring”. In: *Proceedings 35th annual symposium on foundations of computer science*. Ieee. 1994, pp. 124–134.

[69] Marija Furdek, Nina Skorin-Kapov, et al. “Vulnerabilities and security issues in optical networks”. In: *2014 16th International Conference on Transparent Optical Networks (ICTON)*. IEEE. Graz, Austria, 2014, pp. 1–4.

[70] Nina Skorin-Kapov, Marija Furdek, et al. “Physical-layer security in evolving optical networks”. In: *IEEE Communications Magazine* 54.8 (2016), pp. 110–117.

[71] WT Buttler, RJ Hughes, et al. “Practical free-space quantum key distribution over 1 km”. In: *Physical Review Letters* 81.15 (1998), pp. 3283–3286.

[72] Cheng-Zhi Peng, Tao Yang, et al. “Experimental free-space distribution of entangled photon pairs over 13 km: towards satellite-based global quantum communication”. In: *Physical review letters* 94.15 (2005), p. 150501.

[73] Sheng-Kai Liao, Hai-Lin Yong, et al. “Long-distance free-space quantum key distribution in daylight towards inter-satellite communication”. In: *Nature Photonics* 11.8 (2017), pp. 509–513.

[74] Richard J Hughes, George L Morgan, et al. “Quantum key distribution over a 48 km optical fibre network”. In: *Journal of Modern Optics* 47.2-3 (2000), pp. 533–547.

[75] Alberto Boaron, Gianluca Boso, et al. “Secure quantum key distribution over 421 km of optical fiber”. In: *Physical review letters* 121.19 (2018), p. 190502.

[76] NA Peters, P Toliver, et al. “Dense wavelength multiplexing of 1550 nm QKD with strong classical channels in reconfigurable networking environments”. In: *New Journal of physics* 11.4 (2009), p. 045012.

[77] Wikipedia contributors. *Photon energy — Wikipedia, The Free Encyclopedia*. [Online; accessed 4-September-2024]. 2024. URL: https://en.wikipedia.org/w/index.php?title=Photon_energy&oldid=1240575774.

[78] Patrick Eraerds, Nino Walenta, et al. “Quantum key distribution and 1 Gbps data encryption over a single fibre”. In: *New Journal of Physics* 12.6 (2010), p. 063027.

[79] Yuyuan Tian and Fengming Xin. “Establishment and performance evaluation of quantum-safe 5G fronthaul optical architecture”. In: *Computers and Electrical Engineering* 110 (2023), p. 108895. URL: https://www.sciencedirect.com/science/article/pii/S0045790623003191.

[80] Valerio Scarani, Helle Bechmann-Pasquinucci, et al. “The security of practical quantum key distribution”. In: *Reviews of modern physics* 81.3 (2009), pp. 1301–1350.

[81] Mhlambululi Mafu and Makhamisa Senekane. “Security of quantum key distribution protocols”. In: *Advanced Technologies of Quantum Key Distribution*. IntechOpen, 2018.

[82] Purva Sharma, Anuj Agrawal, et al. “Quantum Key Distribution Secured Optical Networks: A Survey”. In: *IEEE Open Journal of the Communications Society* PP (Aug. 2021), pp. 1–1.

[83] Xiao Duan, Joseph Pearse, et al. “Performance Analysis on Co-existence of COW-QKD and Classical DWDM Channels Transmission in UK National Quantum Networks”. In: *Journal of lightwave technology* (2023).

[84] P Gavignet, F Mondain, et al. “Co-propagation of 6 Tb/s (60* 100Gb/s) DWDM & QKD channels with˜ 17 dBm aggregated WDM power over 50 km Standard Single Mode Fiber”. In: *Optical Fiber Communication Conference*. Optica Publishing Group. 2023, Tu3H–2.

[85] Jordan M Thomas, Gregory S Kanter, et al. “Optimization of classical light wavelengths coexisting with c-band quantum networks for minimal noise impact”. In: *Optical Fiber Communication Conference*. Optica Publishing Group. 2023, Tu3H–3.

[86] Fotini Karinou, Hans H Brunner, et al. “Toward the integration of CV quantum key distribution in deployed optical networks”. In: *IEEE Photonics Technology Letters* 30.7 (2018), pp. 650–653.

[87] Yuan Cao, Yongli Zhao, et al. “Resource allocation in software-defined optical networks secured by quantum key distribution”. In: *2017 Opto-Electronics and Communications Conference (OECC) and Photonics Global Conference (PGC)*. IEEE. 2017, pp. 1–3.

[88] Yuan Cao, Yongli Zhao, et al. “Key on demand (KoD) for software-defined optical networks secured by quantum key distribution (QKD)”. In: *Optics express* 25.22 (2017), pp. 26453–26467.

[89] Hua Wang, Yongli Zhao, et al. “A flexible key-updating method for software-defined optical networks secured by quantum key distribution”. In: *Optical Fiber Technology* 45 (2018), pp. 195–200.

[90] Xiaokun Yang, Yajie Li, et al. “Demonstration of key generation scheme based on feature extraction of optical fiber channel”. In: *Asia Communications and Photonics Conference*. Optica Publishing Group. Hangzhou, China, 2018, pp. M2D–5.

[91] Kai Dong, Yongli Zhao, et al. “Auxiliary graph based routing, wavelength and timeslot assignment in metro quantum optical networks”. In: *2019 24th OptoElectronics and Communications Conference (OECC) and 2019 International Conference on Photonics in Switching and Computing (PSC)*. IEEE. Fukuoka, Japan, 2019, pp. 1–3.

[92] Kai Dong, Yongli Zhao, et al. “Auxiliary topology based global quantum key distribution for secure multicast service”. In: *2019 24th OptoElectronics and Communications Conference (OECC) and 2019 International Conference on Photonics in Switching and Computing (PSC)*. IEEE. Fukuoka, Japan, 2019, pp. 1–3.

[93] Hua Wang, Yongli Zhao, et al. “Protection schemes for key service in optical networks secured by quantum key distribution (QKD)”. In: *Journal of Optical Communications and Networking* 11.3 (2019), pp. 67–78.

[94] Hua Wang, Yongli Zhao, et al. "Resilient quantum key distribution (QKD)-integrated optical networks with secret-key recovery strategy". In: *IEEE Access* 7 (2019), pp. 60079–60090.

[95] Yuhui Wang, Xiaosong Yu, et al. "A novel shared backup path protection scheme in time-division-multiplexing based QKD optical networks". In: *Asia Communications and Photonics Conference*. Optica Publishing Group. Chengdu, China, 2019, pp. M4C–6.

[96] Lu Lu, Xiaosong Yu, et al. "Dynamic wavelength and key resource adjustment in WDM based QKD optical networks". In: *2020 Asia Communications and Photonics Conference (ACP) and International Conference on Information Photonics and Optical Communications (IPOC)*. IEEE. Beijing, China, 2020, pp. 1–3.

[97] Kai Dong, Yongli Zhao, et al. "Auxiliary graph based routing, wavelength, and time-slot assignment in metro quantum optical networks with a novel node structure". In: *Optics express* 28.5 (2020), pp. 5936–5952.

[98] Yuan Cao, Yongli Zhao, et al. "Mixed relay placement for quantum key distribution chain deployment over optical networks". In: *2020 European Conference on Optical Communications (ECOC)*. IEEE. 2020, pp. 1–4.

[99] Xingyu Zou, Xiaosong Yu, et al. "Collaborative routing in partially-trusted relay based quantum key distribution optical networks". In: *2020 Optical Fiber Communications Conference and Exhibition (OFC)*. IEEE. San Diego, CA, USA, 2020, pp. 1–3.

[100] Yuan Cao, Yongli Zhao, et al. "Hybrid trusted/untrusted relay-based quantum key distribution over optical backbone networks". In: *IEEE Journal on Selected Areas in Communications* 39.9 (2021), pp. 2701–2718.

[101] Yuan Cao, Yongli Zhao, et al. "Cost-efficient quantum key distribution (QKD) over WDM networks". In: *Journal of Optical Communications and Networking* 11.6 (2019), pp. 285–298.

[102] Xinying Li, Yongli Zhao, et al. "Key-recycling strategies in quantum-key-distribution networks". In: *Applied Sciences* 10.11 (2020), p. 3734.

[103] Cédric Ware, Raphaël Aymeric, et al. "Potential impact of CV-QKD integration on classical WDM network capacity". In: *IEEE Photonics Technology Letters* 34.18 (2022), pp. 957–960.

[104] Fabian Laudenbach, Christoph Pacher, et al. "Continuous-variable quantum key distribution with Gaussian modulation—the theory of practical implementations". In: *Advanced Quantum Technologies* 1.1 (2018), p. 1800011.

[105] J. Bromage. “Raman amplification for fiber communications systems”. In: *Journal of Lightwave Technology* 22.1 (2004), pp. 79–93.

[106] Rui Lin and Jiajia Chen. “Minimizing spontaneous Raman scattering noise for quantum key distribution in WDM networks”. In: *Optical Fiber Communication Conference*. Optica Publishing Group. 2021, F4E–6.

[107] Bing Qi, Wen Zhu, et al. “Feasibility of quantum key distribution through a dense wavelength division multiplexing network”. In: *New Journal of Physics* 12.10 (2010), p. 103042.

[108] Rupesh Kumar, Hao Qin, et al. “Coexistence of continuous variable QKD with intense DWDM classical channels”. In: *New Journal of Physics* 17.4 (2015), p. 043027.

ECOLE
DOCTORALE

Titre : Planification du réseau tenant compte des déficiences

Mots clés : Réseaux optiques, non-linéarités, QKD

Résumé : Les réseaux optiques sont l'épine dorsale de la communication mondiale de données, essentiels pour répondre à la demande croissante de réseaux rapides et fiables. Cette thèse aborde deux défis principaux : le besoin de capacité accrue et l'intégration de nouvelles fonctionnalités optiques. La demande incessante de capacité a poussé les limites de l'infrastructure actuelle, et bien que des solutions telles que l'ajout de fibres, l'extension du spectre ou l'utilisation de transpondeurs flexibles soient possibles, elles entraînent des dépenses en capital importantes. Nous proposons des heuristiques à l'échelle du réseau qui modélisent les dégradations linéaires et non linéaires et suggèrent des allocations de puissance par canal pour maximiser le SNR à l'échelle du réseau, augmentant ainsi la capacité. Le deuxième défi concerne l'intégration de nouvelles fonctionnalités optiques, ce qui nécessite de prendre en compte les interactions au niveau du réseau et de la couche physique. Les outils SDN traditionnels négligent souvent la couche physique, c'est pourquoi nous avons développé un simulateur de réseau optique qui intègre l'impact de la couche physique dans la planification du réseau. Nous démontrons l'intégration d'une fonctionnalité optique, la distribution quantique de clés (QKD), qui améliore la sécurité grâce aux principes de la mécanique quantique. En optimisant le placement des longueurs d'onde pour minimiser le bruit Raman, nous proposons des heuristiques à l'échelle du réseau qui améliorent la coexistence des signaux QKD et classiques dans la même bande. Relever ces défis souligne l'importance de la planification des réseaux sensibilisée aux impairments, formant le cœur de la conception des futurs réseaux optiques pour répondre aux demandes croissantes avec une efficacité, une capacité et une sécurité accrues.

Title : Impairment Aware Optical Networks

Keywords : Optical Networks, Non-Linearities, QKD

Abstract : Optical networks are the backbone of global data communication, essential for meeting the ever-growing demand for high-speed, reliable networks. This thesis addresses two key challenges: the need for higher capacity and the integration of new optical functionalities. The relentless demand for capacity has pushed the limits of current infrastructure, and while solutions like additional fibers, extended spectrum, or new flex-rate transponders are possible, they come with significant capital expenditure. We propose network-wide heuristics that model linear and nonlinear impairments and suggest per-channel power allocations to maximize network-wide SNR, thus enhancing capacity. The second challenge involves integrating new optical functionalities, which requires consideration of both network-level and physical-layer interactions. Traditional SDN tools often overlook the physical layer, so we developed an optical network simulator that incorporates physical layer impairments into network planning. We demonstrate the integration of an example optical functionality Quantum Key Distribution (QKD), that enhances security through quantum mechanics principles. By optimizing wavelength placement to minimize Raman noise, we propose network-wide heuristics that improve the coexistence of QKD and classical signals in the same band. Addressing these challenges underscores the importance of impairment-aware network planning, forming the core of future optical network design to meet growing demands with enhanced efficiency, capacity, and security.

Institut Polytechnique de Paris
91120 Palaiseau, France